

326
8/11/67
LA-3729

MASTER

LOS ALAMOS SCIENTIFIC LABORATORY
of the
University of California
LOS ALAMOS • NEW MEXICO

Measurements of Solar X-Ray Emission
from the Ions Carbon VI and Nitrogen VII

UNITED STATES
ATOMIC ENERGY COMMISSION
CONTRACT W-7405-ENG. 36

DISTRIBUTION OF THIS DOCUMENT IS UNLIMITED

DISCLAIMER

This report was prepared as an account of work sponsored by an agency of the United States Government. Neither the United States Government nor any agency Thereof, nor any of their employees, makes any warranty, express or implied, or assumes any legal liability or responsibility for the accuracy, completeness, or usefulness of any information, apparatus, product, or process disclosed, or represents that its use would not infringe privately owned rights. Reference herein to any specific commercial product, process, or service by trade name, trademark, manufacturer, or otherwise does not necessarily constitute or imply its endorsement, recommendation, or favoring by the United States Government or any agency thereof. The views and opinions of authors expressed herein do not necessarily state or reflect those of the United States Government or any agency thereof.

DISCLAIMER

Portions of this document may be illegible in electronic image products. Images are produced from the best available original document.

LEGAL NOTICE

This report was prepared as an account of Government sponsored work. Neither the United States, nor the Commission, nor any person acting on behalf of the Commission:

A. Makes any warranty or representation, expressed or implied, with respect to the accuracy, completeness, or usefulness of the information contained in this report, or that the use of any information, apparatus, method, or process disclosed in this report may not infringe privately owned rights; or

B. Assumes any liabilities with respect to the use of, or for damages resulting from the use of any information, apparatus, method, or process disclosed in this report.

As used in the above, "person acting on behalf of the Commission" includes any employee or contractor of the Commission, or employee of such contractor, to the extent that such employee or contractor of the Commission, or employee of such contractor prepares, disseminates, or provides access to, any information pursuant to his employment or contract with the Commission, or his employment with such contractor.

This report expresses the opinions of the author or authors and does not necessarily reflect the opinions or views of the Los Alamos Scientific Laboratory.

Printed in the United States of America. Available from Clearinghouse for Federal Scientific and Technical Information National Bureau of Standards, U. S. Department of Commerce

Springfield, Virginia 22151

Price: Printed Copy \$3.00; Microfiche \$0.65

LA-3729
UC-34, PHYSICS
TID-4500

CFSTI PRICES

H.C. \$3.00; MN .65

**LOS ALAMOS SCIENTIFIC LABORATORY
of the
University of California**

LOS ALAMOS • NEW MEXICO

Report written: June 1, 1967

Report distributed: July 27, 1967

**Measurements of Solar X-Ray Emission
from the Ions Carbon VI and Nitrogen VII***

by

W. Doyle Evans

*Also submitted as a thesis in partial fulfillment of the requirements for the degree of Doctor of Philosophy in Physics from the University of New Mexico

LEGAL NOTICE

This report was prepared as an account of Government sponsored work. Neither the United States, nor the Commission, nor any person acting on behalf of the Commission:

A. Makes any warranty or representation, expressed or implied, with respect to the accuracy, completeness, or usefulness of the information contained in this report, or that the use of any information, apparatus, method, or process disclosed in this report may not infringe privately owned rights; or

B. Assumes any liabilities with respect to the use of, or for damages resulting from the use of any information, apparatus, method, or process disclosed in this report.

As used in the above, "person acting on behalf of the Commission" includes any employee or contractor of the Commission, or employee of such contractor, to the extent that such employee or contractor of the Commission, or employee of such contractor prepares, disseminates, or provides access to, any information pursuant to his employment or contract with the Commission, or his employment with such contractor.

**THIS PAGE
WAS INTENTIONALLY
LEFT BLANK**

ABSTRACT

Two identical instrument packages containing x-ray crystal spectrometers were flown aboard Nike-Tomahawk sounding rockets launched from Kauai, Hawaii, on August 8 and 11, 1967. Each package contained eight curved crystal, nonscanning spectrometers focused for selected wavelengths of the solar spectrum between 19 and 34 Å. During the high altitude portion of the flight the instrument axis was aligned toward the sun by an attitude control system.

Four of the spectrometers used lead stearate soap film analyzers. Three were focused for the Lyman- α , - β , and - γ lines of C VI. The fourth was focused to obtain a measurement of the continuum intensity at 26.0 Å. Three spectrometers using KAP crystals were focused for the first three lines of the N VII Lyman series. The eighth spectrometer had the crystal replaced by a polished aluminum surface to test the sensitivity of the instruments to scattered ultraviolet light.

Data were obtained from all stations on the first flight. On the second flight two of the KAP spectrometers failed, probably because of broken crystals. The count rates in all stations were

essentially constant during the entire five minute period that the packages were above the atmosphere. On both flights excellent data on atmospheric absorption were obtained during the reentry portion of the flight.

From the data of the first flight, intensities of 1.8 and 0.5×10^{-3} erg/cm²-sec were determined for the N VII Lyman- α and - β lines respectively. The x-ray flux at 19.83 Å was interpreted as continuum radiation with an intensity of 5×10^{-3} erg/cm²-sec-Å.

The expected line structure for the C VI Lyman series was not observed. Because of an inconsistency in the absorption data it was suspected that the stearate stations were sensitive to x-ray wavelengths outside the expected instrumental resolution. Laboratory measurements were made of the specular reflection of long wavelength x-rays from lead stearate crystals. For those spectrometers focused on the weaker lines and the continuum, specularly reflected x-rays from the 40-120 Å region almost certainly introduced large errors. The measurement of the strong C VI Lyman- α line was less seriously affected. When a correction was made for the specular reflection the intensity of this line was found to be 2.9×10^{-2} erg/cm²-sec on August 8 and 2.2×10^{-2} erg/cm² sec on August 11. The continuum intensity at 26.0 Å was 6×10^{-3} and 4×10^{-3} erg/cm²-sec-Å on the two days.

ACKNOWLEDGMENTS

I am indebted to R. F. Taschek, Physics Division Leader, James H. Coon, Group Leader, and the administration of the Los Alamos Scientific Laboratory for the opportunity of performing this work under the Graduate Thesis Program.

I wish to thank Prof. C. P. Leavitt who supervised this research for the University of New Mexico. I am especially grateful to George A. Sawyer who directed this research program. His assistance during the course of the work and his many helpful suggestions concerning the interpretation of the data and the preparation of this dissertation are gratefully acknowledged.

To each of the following persons who contributed directly to the design and construction of the instrument packages, and without whose assistance the project could never have been completed, I wish to express my sincere appreciation: J. A. Bergey, R. J. Youngblood, T. A. Carroll, Harold V. Argo, W. R. Everett, Marilyn Freyman, Ralph Garza, R. J. Gill, R. H. Greenwood, Lynne Mutchler, Sidney Singer, and Pauline Stone.

The Sandia Corporation of Albuquerque, New Mexico, provided the rocket motors, the attitude control system, the flight telemetry system, and the launch facilities and personnel. I gratefully acknowledge the contributions of the many persons from Sandia Corporation who contributed to this program.

TABLE OF CONTENTS

	Page
ABSTRACT	iii
ACKNOWLEDGMENTS	v
LIST OF FIGURES	vii
LIST OF TABLES	x
INTRODUCTION	1
I. DESCRIPTION OF THE EXPERIMENT	13
Flight Spectrometers	
Crystals	
Geiger Counters	
Counter Gas Supply	
Data System	
Complete Package and Pointing Control	
Description of the Two Flights	
Observed Count Rates	
II. SPECTROMETER SENSITIVITIES	64
Johann Curved Crystal Geometry	
The Sun as a Source	
The Effect of Aperture Width and Pointing Errors	
Spectrometer Resolution	
X-Ray Calibration	
Flight Spectrometer Efficiencies	
III. DATA ANALYSIS	102
Solar Activity	
Uncorrected Flux Values	
Atmospheric Absorption Data	
Comparison with a Standard Atmosphere	
Test of the Data for Internal Consistency	
Final Flux Values	
IV. CONCLUSIONS	133
The Results from the KAP Stations	
The Results from the Stearate Stations	
Summary	
LIST OF REFERENCES	166

LIST OF FIGURES

Figure	Page
1 Emission lines from the hydrogen- and helium-like ions of carbon, nitrogen, and oxygen. For the one electron C VI, N VII, and O VIII the lines are the first three members of the Lyman series ($^2S_{1/2}$ - $^2P_{3/2, 1/2}$). For the two electron C V, N VI, and O VII, the lines are from the resonance series (1S_0 - 1P_1) plus the intercombination line (1S_0 - 3P_1)	7
2 The Johann curved crystal geometry	17
3 Drawing of a flight spectrometer	21
4 Photograph of two partially assembled flight spectrometers.	23
5 Photograph of two assembled flight spectrometers	25
6 Drawing of a flight Geiger counter	29
7 Photograph of a flight Geiger counter, a pressure window, and an ultraviolet filter.	35
8 Schematic drawing of the counter gas supply system . . .	39
9 Block diagram of the electronics system.	43
10 Photograph of a battery pack and a complete set of electronics.	45
11 Photograph of a completely assembled instrument package.	47
12 Photograph of four instrument packages in different stages of assembly	49
13 Nike-Tomahawk rocket trajectory for the flight of August 8, 1966	53
14 Observed counting rates for the high altitude portion of the August 8, 1966 flight	55

15	Observed counting rates for the high altitude portion of the August 11, 1966 flight	57
16	Observed counting rates for the reentry portion of the August 8, 1966 flight	59
17	Observed counting rates for the reentry portion of the August 11, 1966 flight.	61
18	The geometry of a perfectly focusing, curved crystal spectrometer.	69
19	The focusing properties of the Johann type curved crystal spectrometer in the plane of dispersion	71
20-a	The effect of beam divergence in the plane perpendicular to the plane of divergence.	73
20-b	The effect of the angular diameter of the sun	73
21-a	The effect of aperture width on the focusing and resolution of Johann curved crystal spectrometers	79
21-b	The defocusing caused by pointing errors.	79
22-a	A plan view of a curved crystal spectrometer.	85
22-b	Typical resolution curves for a lead stearate station and a KAP station	85
23	Absorption efficiency of the flight Geiger counters . . .	97
24	Observed atmospheric attenuation of the x-ray fluxes measured by the stearate stations, August 8, 1966	109
25	Observed atmospheric attenuation of the x-ray fluxes measured by the stearate stations, August 11, 1966. . . .	111
26	Observed atmospheric attenuation of the x-ray fluxes measured by the KAP stations, August 11, 1966	113
27	Calculated mass absorption coefficient of air for the wavelength region 10 to 100 Å	115
28	The apparent integrated atmospheric density as determined from the atmospheric absorption data of August 8, 1966. .	121
29	The apparent integrated atmospheric density as determined from the atmospheric absorption data of August 11, 1966 .	123

30	Specular reflection of 44.74 Å x-rays from lead stearate soap film analyzers.	149
31	Specular reflection of 67.8Å x-rays from lead stearate soap film analyzers.	151
32	Specular reflection efficiency from a lead stearate soap film analyzer as a function of x-ray wavelength. . .	153
33	Relative counter window transmission of stations 100 and 700 as a function of x-ray wavelength	155
34	Spectral response of stations 100 and 700	157

LIST OF TABLES

	Page
Table	
1 Ionization Energy (Electron Volts) of the Various Ions of Carbon, Nitrogen, Oxygen.	3
2 Spectrometer Station Numbers and Focus Wavelengths.	13
3 Design Parameters for Curved Crystal Spectrometers.	19
4 Average Count Rates Observed Above the Atmosphere	63
5 Pressure Window and Ultraviolet Filter Transmissions. . . .	99
6 Flight Spectrometer Efficiencies.	101
7 Uncorrected Flux Values	103
8 Comparison of Atmospheric Densities for August 8 Flight	127
9 Comparison of Atmospheric Densities for August 11 Flight.	128
10 Corrected Flux Values	132
11 Relative Contributions of Specular Reflection to the Observed Count Rate of Station 100 and 700 in Ten Angstrom Intervals from the Spectral Region 30-100 Å. . .	159
12 Summary of Experimental Results	164

INTRODUCTION

Studies of the solar spectrum in the extreme ultraviolet and x-ray region have been possible since sounding rockets and satellites have been available to carry instruments above the earth's atmosphere. Progress was slow at first, but techniques have improved rapidly in recent years and a considerable body of experimental data has been accumulated since the first rocket flights in the late 1940's.

The general character of this portion of the sun's spectrum has been well established and is discussed in detail in a paper by Tousey (1). Down to a wavelength of 2085 Å the spectrum is very similar to the visible region, consisting of a strong continuum with prominent Fraunhofer lines. Starting at 2085 Å and continuing to shorter wavelengths a region of continuous absorption occurs but Fraunhofer lines are still visible. Between 2000 Å and 1500 Å a gradual change in the spectrum occurs. Emission lines appear and become more and more numerous as the Fraunhofer lines become fewer. For wavelengths shorter than 1530 Å the spectrum has changed completely and consists entirely of strong emission lines above a smooth continuum. This general appearance is maintained down to wavelengths well within the x-ray region.

The emission spectrum is mainly of chromospheric origin but there are a large number of strong lines that come from the corona, especially in the shorter wavelength region. In 1942, Edlen (2) identified many of the coronal lines as produced by transitions in highly ionized atoms. The presence of such emission lines, including many produced by forbidden transitions, the absence of Fraunhofer lines in the K corona, and radio emission measurements all support the present picture of the corona as a strongly ionized, low density plasma surrounding the sun and extending to large radial distances. Although different techniques give somewhat inconsistent results, the average coronal temperature has been shown to be around one million degrees Kelvin. Temperatures as high as four million degrees have been measured for active regions of the sun (3). Electron densities are about 10^9 per cm^3 in the lower part of the corona and decrease radially to about 10^3 per cm^3 at 40 solar radii (3). The corona has no known outer boundary; it extends far beyond the earth's orbit and interacts strongly with the earth's magnetic field and upper atmosphere.

The characteristics of the corona in the vicinity of the earth can be measured directly with instrumented satellites and probe rockets. Accurate, long-time measurements of particle density, temperature, and flow velocity are currently being made. Although these properties are largely determined by the physics of the corona near the sun, only very general properties of the near-sun corona can presently be deduced from such near-earth measurements. The extension of this type of direct observation offers exciting possibilities for the future, but present

information about the corona, as with all other astrophysical plasmas, must be deduced from observations of the emitted and scattered radiation.

The measurement of emission line intensities from various elements in different stages of ionization is a particularly powerful diagnostic tool for the study of plasma properties for both laboratory and astrophysical plasmas. As mentioned above, a large number of such emission lines originating in the corona have been observed, and the measurements of these lines have already provided valuable information about coronal conditions. The emission lines from carbon, nitrogen, and oxygen are particularly interesting. These elements are relatively abundant in the solar corona and produce intense lines, an important experimental advantage. Table 1 shows the ionization potential of the various ionic species of the three elements (4). Considering only the helium-like and hydrogen-like ions, it is seen that the ionization energy varies from the 64 electron volts necessary to produce C V from C IV up to 871 electron volts to remove the single electron from O VIII.

TABLE 1

IONIZATION ENERGY (ELECTRON VOLTS) OF THE
VARIOUS IONS OF CARBON, NITROGEN, OXYGEN

Element	I	II	III	IV	V	VI	VII	VIII
Carbon	11	24	48	64	392	490		
Nitrogen	14	30	47	77	98	552	667	
Oxygen	14	35	55	77	114	138	739	871

The ionization potentials of these elements are of the proper magnitude to insure that their one and two-electron ions will be present in

reasonably large abundance at coronal temperatures. Carbon V and VI will be present even at the lowest measured temperatures, and O VIII has a sufficiently high ionization energy to remain abundant even at the extreme temperatures of excited regions. The calculation of line intensities for coronal conditions is an extremely difficult problem, and the theoretical simplicity of the hydrogen- and helium-like ions makes these spectral lines even more useful. The series limit for O VIII is at 14.23 Å and the resonance lines for C V are just above 40 Å. The resonance lines of the one and two electron ions of carbon, nitrogen, and oxygen lie between 14 and 41 Å. X-rays in this spectral region are absorbed in the atmosphere in the altitude region from about 90 km to 150 km and must have a very important influence on the formation of the E region.

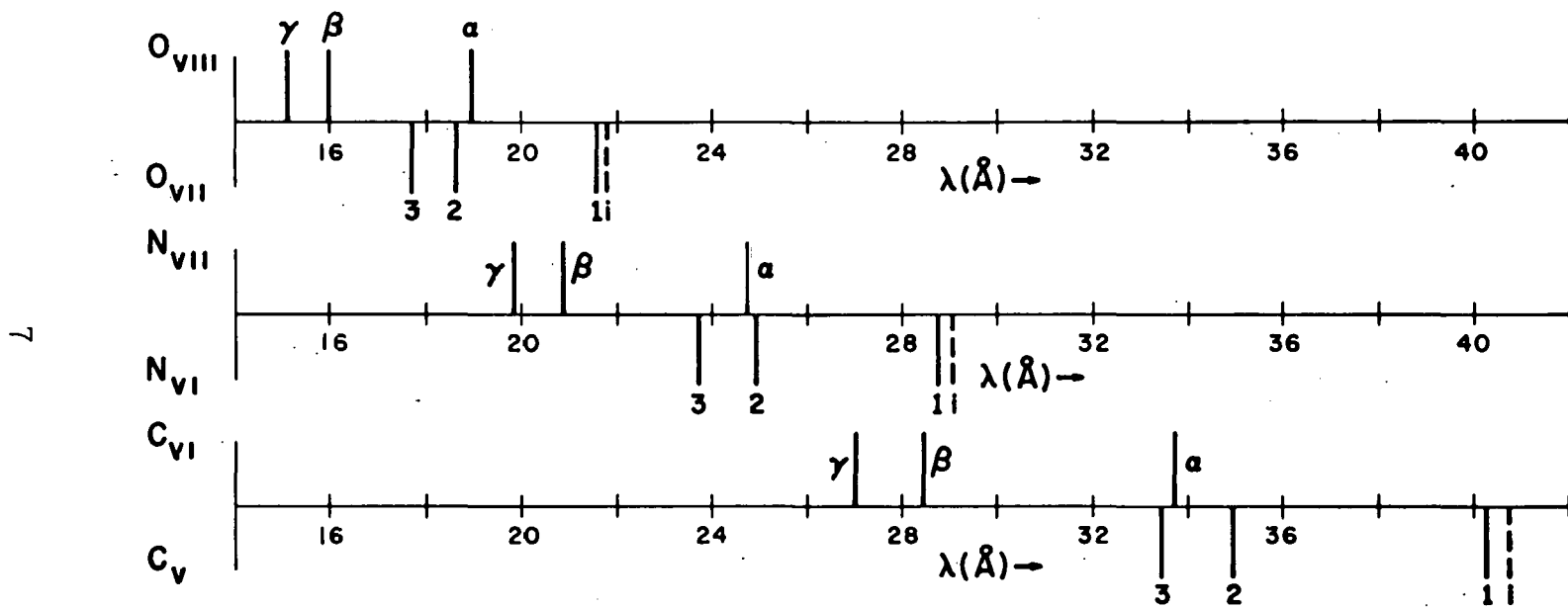
Figure 1 shows the wavelengths of some of the lines of the hydrogen- and helium-like series from carbon, nitrogen, and oxygen. All wavelengths were taken from reference (5). Fawcett, Gabriel, Jones, and Peacock (6) have used grazing incidence gratings to obtain photographs of the short wavelength spectrum emitted from a high temperature laboratory plasma. All of the lines shown in Fig. 1, with the exception of the N VII Lyman- γ line, are seen in the laboratory spectrum and the wavelengths agree with the indicated values.

The short wavelength region is interesting not only for the potential information that can be obtained about the solar corona but also because it represents the region of overlap between the extreme ranges of grating and Bragg crystal instrumentation. As mentioned above (6), gratings in grazing incidence have been used in the

laboratory to make spectral measurements down to a wavelength of 13 Å. However, the shortest wavelength reached with a grating in measurements of the solar spectrum was 30 Å, the photograph obtained by Tousey (1) in 1963. The two C V resonance lines at 40.27 and 40.74 Å, and the C VI Lyman- α line at 33.74 Å were clearly recorded in this photograph. Crystal scans can also be made in this region as long as wavelengths are shorter than the limit set by the Bragg condition, $\lambda_{\text{max}} = 2d$, where d is the appropriate crystal lattice spacing. Mica has $2d = 19.9$ Å, and beryl can be used for wavelengths up to 15.95 Å. Potassium acid phthalate (KAP) crystals can be used to extend this limit to about 25 Å. Crystal diffraction measurements above 25 Å must be made using either "soap film" crystals of the type studied by Blodgett and Langmuir (7) and recently developed extensively by Henke (8), or one of the more exotic organic crystals such as octadecyl hydrogen succinate (OHS). Blake, Chubb, Friedman, and Unzicker (9) obtained a scan of the solar spectrum from 13 to 25 Å using a KAP crystal and identified many of the lines shown in Fig. 1. Two attempts to scan with a larger 2d spacing crystal, one using a magnesium lignocerate soap film and one using an OHS crystal, were unsuccessful.

Measurements of the solar spectrum from rocket borne instruments using gratings or flat Bragg crystals require a sophisticated pointing control to maintain the required accuracy and stability of the instrument package during the time that the measurements are being made. In 1964, Argo, Bergey, Henke, and Montgomery (10) used curved Bragg crystals to make measurements that overlapped in wavelength the data of Tousey (1), obtained with a grating, and those of Blake (9),

Fig. 1.-Emission lines from the hydrogen- and helium-like ions of carbon, nitrogen, and oxygen. For the one electron C VI, N VII, and O VIII the lines are the first three members of the Lyman series ($^2S_{1/2}$ - $^2P_{3/2,1/2}$). For the two electron C V, N VI, and O VII, the lines are from the resonance series 1S_0 - 1P_1) plus the intercombination line 1S_0 - 3P_1).



CARBON, NITROGEN, OXYGEN EMISSION LINES

obtained with a flat crystal scan. A combination of mica and lead stearate soap film crystals were used in eight, nonscanning, curved crystal spectrometers to measure the intensity of selected lines in the 16-44 Å region. Included, among others, were the O VIII Lyman- α and Lyman- β lines at 18.97 and 16.01 Å observed by Blake (9), the two C V resonance lines at 40.27 and 40.74 Å, and the C VI Lyman- α line at 33.74 Å photographed by Tousey (1). The curved crystal geometry has the advantage of integrating uniformly over the entire solar disk and has a much larger angular acceptance than a grating or a flat crystal. Thus the pointing requirements are much less stringent. The resolution was comparable to that of a flat crystal spectrometer using the same crystal but measurements were made only at fixed wavelengths and a continuous scan was not obtained. The results of these earlier measurements are discussed in more detail in Part IV.

Although the intensities of several of the lines in the 16-44 Å wavelength region have been previously measured, only the first lines of the C VI and N VII Lyman series are included. The relative intensities of two or more lines from the same series is an important parameter for direct comparison with coronal models. Carbon is particularly attractive because of its high solar abundance and because the small ionization potential of C V should make the intensities of the emission lines less sensitive to local active areas on the sun. Nitrogen, being less abundant and having larger ionization potentials, would be expected to produce weaker lines that are more variable with solar activity; but a measurement of the Lyman lines of N VII was considered feasible

and important for comparison with the carbon data and the previously measured oxygen data. The purpose of this experiment was to measure the intensities of the first three lines of the Lyman series from C VI and N VII in the solar spectrum.

The solar x-ray spectrum in the 16-44 Å region is not completely established, but based on the results of the scanning crystal spectrometer, Blake (9) concluded that most of the energy was contained in the emission lines. Widing (11), in an interpretation of the grating photographs of reference (1), also assumed that the emission lines were very strong compared to the continuum. For a spectrum in which emission lines are dominant, the absolute intensities of selected lines can be measured with nonscanning spectrometers focused for the proper wavelength. In many respects this type of measurement is simpler and more accurate for absolute line intensities than either a scanning spectrometer or a grating.

Measurements of the solar spectrum with a scanning spectrometer or a grating require an alignment of the instrument axis toward the sun with an accuracy of a few minutes of angle. A fixed-focus, curved crystal spectrometer can be made to have a resolution comparable to a scanning spectrometer but with angular acceptance of a few degrees. The pointing accuracy required for the fixed-focus spectrometer is at least an order of magnitude less stringent.

Calibration is a difficult problem for any type of instrumentation in the soft x-ray region. The determination of line intensities from scanning spectrometer data is difficult because of the complicated folding together of the instrumental angular response and the spatial

distribution of sources on the solar disk. Grating photographs provide excellent resolution but uncertainties in instrumental sensitivities, particularly film sensitivities, make absolute intensity measurements difficult. Using open photomultipliers to scan the spectrum from a grating avoids the problem of film sensitivity but replaces it with the almost equally difficult task of determining the photoelectric sensitivity of the multiplier cathode. In Part II of this paper the sensitivity of the curved crystal spectrometers is discussed in detail. It is shown that this type of instrument integrates uniformly over the solar disk to give an average intensity for the x-ray wavelength to which it is sensitive. It is also shown that the curved crystal geometry simplifies considerably the crystal efficiency calibrations.

For a scanning spectrometer any particular emission line is observed only during the time that it takes the spectrometer to scan across that line. For the fixed-focus spectrometers each emission line is continuously observed during an entire rocket flight. The continuous observation significantly increases the statistical accuracy of the measurement of an emission line intensity and makes it possible to measure much weaker lines. The continuous observation of particular lines is important for measurements of the x-ray absorption in the atmosphere since it provides an accurate determination of the exact altitude where absorption occurs.

The nonscanning spectrometers provide spectral information only at pre-selected wavelengths, and the interpretation of results from this type of instrument must be based on independent information or

assumptions about possible competing lines and continuum intensities at the selected wavelengths. The N VII Lyman series lies in the spectral region covered by the scanning spectrometer of reference (9). Here the assumption that the emission lines can be isolated and measured by fixed-focus spectrometers seems to be quite good. The grating photograph of reference (1) shows the C VI Lyman- α at 33.74 Å as an isolated line that can be measured with a nonscanning instrument. The rest of the carbon Lyman series lies between 25 and 28.47 Å, a region of the solar spectrum that has never been successfully observed with either a grating or a scanning spectrometer. The presence in this spectral region of emission lines from elements other than carbon, nitrogen, or oxygen could certainly introduce ambiguities into the data from nonscanning instruments.

The advantages of less stringent pointing requirements, more accurate calibration, and continuous observation of a particular line make fixed-focus spectrometers very attractive at this time for measurements of absolute line intensities, despite the lack of spectral information.

As with all measurements of the extreme ultraviolet and x-ray region of the solar spectrum, observations must be made above the earth's absorbing atmosphere. During the past several years the Sandia Corporation of Albuquerque, New Mexico, has developed the two-stage Nike-Tomahawk sounding rocket as a small, high performance launch vehicle. The sixteen-inch diameter Nike is used as a booster for the nine-inch Tomahawk rocket. The two-stage combination can lift a nine-inch, 150-pound payload to an apogee of about 330 kilometers. This

gives a flight time above 180 kilometers of more than five minutes. Since 1964, Sandia Corporation and the Los Alamos Scientific Laboratory have cooperated in a series of solar x-ray measurements using the Nike-Tomahawk rocket as a launch vehicle. Sandia maintains and operates a complete rocket launch facility on the island of Kauai, Hawaii, and several of the launches have been made from that range.

The present experiment was a continuation of this series of rocket launches to measure solar x-ray emission. A rocket package containing eight curved crystal spectrometers, each focused for a particular wavelength, was designed to fit into the nine-inch payload compartment of the Tomahawk rocket. The package was mounted on an attitude control system, also developed by Sandia, that was designed to point the experimental package toward the sun to an accuracy of better than one degree. These were the first instrument packages to be flown with the new pointing control.

Two launches were made, on August 8 and 11, 1966, from the launch range on Kauai. On both flights the attitude control system performed well and excellent data were obtained. In Part I the instrument package is described and the raw data are presented. The spectrometer sensitivities are discussed in Part II, and x-ray flux values are determined from the raw data. For several of the stations the flux values were quite surprising. In Part III the data are examined in detail to assure their validity. In particular, the atmospheric absorption data obtained during reentry are used to show that the measured fluxes were indeed x-rays and not spurious counts. Part IV is a discussion of the possible significance of the measured flux levels.

I. DESCRIPTION OF THE EXPERIMENT

Flight Spectrometers

Two identical instrument packages were flown aboard Nike-Tomahawk sounding rockets launched from Kauai, Hawaii, on August 8 and 11, 1966. Each package contained eight curved crystal, nonscanning spectrometers. Each spectrometer was focused for a particular x-ray wavelength. Table 2 lists the wavelengths for each of the stations, the emission lines

TABLE 2
SPECTROMETER STATION NUMBERS AND FOCUS WAVELENGTHS

Station Number	Focus Wavelength (\AA)	Type of Crystal-2d (\AA)	Emission Line
100	33.74	Pb-S - 100	Lyman- α
200	28.47	Pb-S - 100	Lyman- β
300	26.99	Pb-S - 100	Lyman- γ
400	24.78	KAP - 26.59	Lyman- α
500	20.91	KAP - 26.59	Lyman- β
600	19.83	KAP - 26.59	Lyman- γ
700	26.00	Pb-S - 100	Continuum
800	(19.83)	None - Al mirror	Uv Background

expected at that wavelength, and the type of crystal that was used.

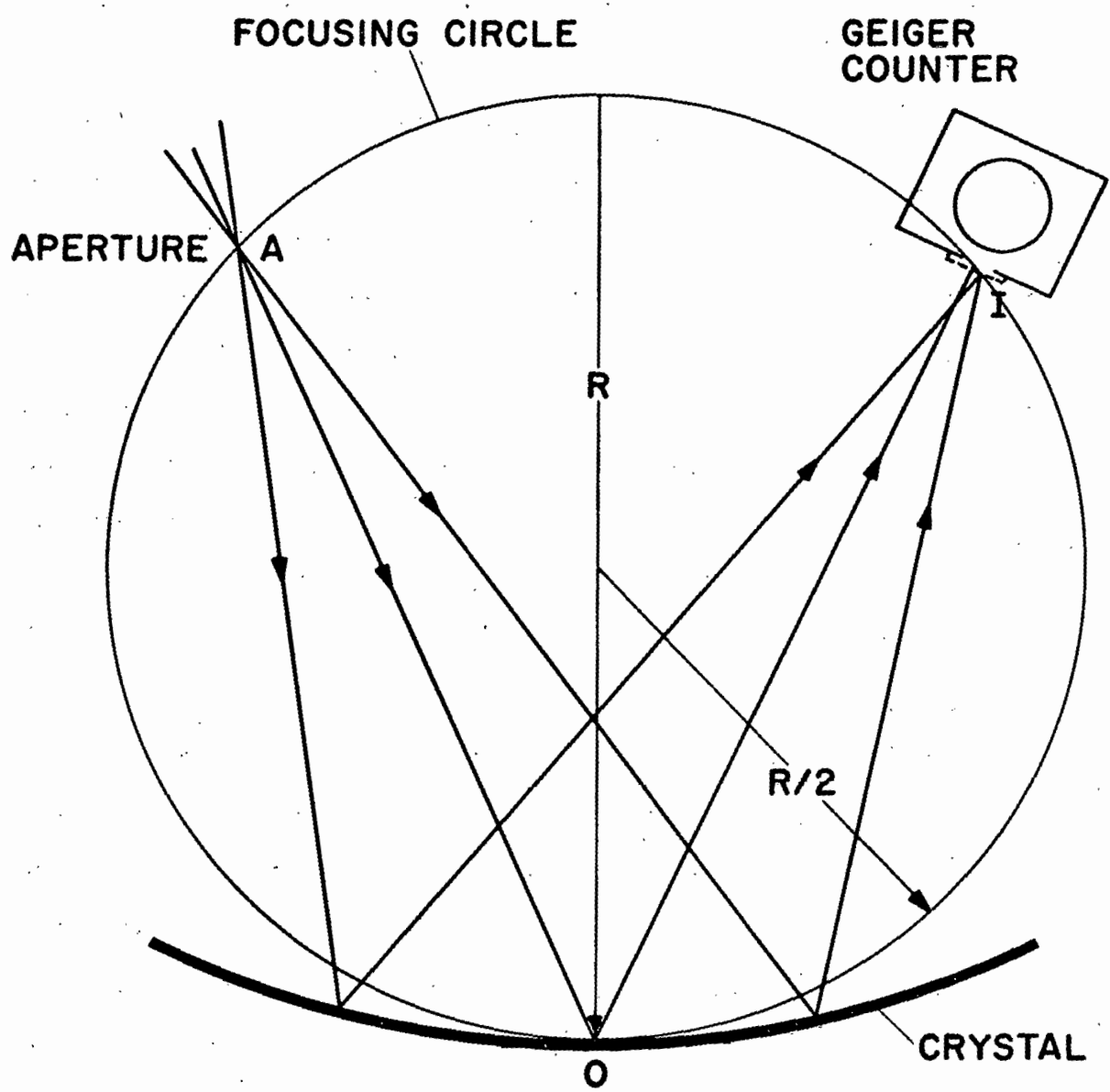
Stations 100, 200, and 300 were focused for the C VI Lyman- α , β and γ lines respectively. Lead stearate soap film crystals ($2d = 100 \text{ \AA}$) were used for these carbon stations. A fourth lead stearate station, number 700, was focused for a wavelength of 26 \AA , where no strong emission lines were expected. Since the stearate crystals have relatively poor resolution and thus integrate over a wavelength interval that is large ($\approx 1 \text{ \AA}$) compared to line widths, a weak continuum can introduce considerable background into measurements of the intensities of sharp lines. Station 700 was meant to provide a measurement of the strength of the continuum at a wavelength close to the C VI γ line that could be used for a first-order correction for this error. Stations 400, 500, and 600 were focused for the first three lines of the Lyman series from N VII and used KAP crystals with $2d = 26.6 \text{ \AA}$.

There was little choice available in the selection of the type of crystal to be used for the various lines. For observing the carbon lines the soap film crystals were the only ones available with a sufficiently large $2d$ spacing that could be made large enough for use in this type of spectrometer. The only available crystal with a large enough $2d$ spacing to be used for the N VII Lyman- α line and at the same time with good enough resolution to separate this line from the neighboring N VI, $1s^2 1S_0 - 1s3p 1P_1$, line was KAP. Since it was considered important to measure all the lines of one series with the same type of crystal to improve the accuracy of relative intensities, KAP was also used for the other two nitrogen lines.

Scattered ultraviolet photons present a very difficult problem for measurements in this wavelength region. To provide a check on how effectively the spectrometers discriminated against scattered ultraviolet light, station 800 was included in the package. This station was an exact replica of station 600, except that it was flown with the crystal replaced by a polished aluminum mirror. To the degree that station 800 was "blind" to the sun, it would provide assurance that the counter windows and ultraviolet filters were effective in eliminating counts caused by scattered photons of longer wavelength. The behavior of station 800 did not, of course, give any specific information about the behavior of any of the other seven stations, and random failures or undetected flaws in other counters were always a possibility. Station 600 was in a sense an additional check on possible ultraviolet contamination since the intensity of the N VII Lyman- γ line was expected to be close to the detection threshold. If the line or continuum intensity proved higher than expected, this would be a valuable measurement; but even if this station recorded no counts above cosmic ray background it would provide additional assurance that scattered ultraviolet was not causing a problem.

Figure 2 is a line drawing of the Johann curved crystal geometry. The crystal is bent to a radius "R" and the entrance aperture is located on the focusing circle of radius "R/2" at the appropriate Bragg angle. The detector is located on the focusing circle symmetrically opposite the entrance aperture. A drawing of a flight

Fig. 2.-The Johann curved crystal geometry.



spectrometer is shown in Fig. 3. The knife edge "stop" was placed a distance "h" above the crystal surface to limit the angular acceptance in the plane of dispersion to 2.5° . All of the design parameters are defined in this drawing and the values of these parameters for each of the eight stations are given in Table 3. Figures 4 and 5 are photographs of flight spectrometers. Figure 4 shows a station 400 and a station 700 spectrometer in "skeleton" form. Figure 5 shows two station 700 spectrometers, one with only the crystal attached and the other after assembly was complete. The crystal is in place, the Geiger counter window and ultraviolet filter are mounted, and the aluminum cover plates have been attached. All openings except the entrance aperture have been covered with Teflon tape to prevent any ultraviolet light leaks. The geometry of each station is, of course, different and this to some extent influences the focusing properties and resolution of the various spectrometers. This is discussed in detail in Part II in connection with the spectrometer sensitivities.

Crystals

The lead stearate crystals (more accurately, lead stearate-deconoate crystals since a mixture of stearic and deconoic acid was used) flown in the spectrometers were made in the laboratory according to the procedure developed by Henke (8). A mixture of 25% stearic and 75% deconoic acids was dissolved in N-hexane, using about one milligram of the acid mixture to one milliliter of N-hexane. A few drops of this mixture were placed on the surface of a dilute solution of lead chloride contained in a large Teflon tank. The acids reacted

TABLE 3
DESIGN PARAMETERS FOR CURVED CRYSTAL SPECTROMETERS *

Station	$\lambda(\text{\AA})$	2d(\AA)	θ	R(in.)	h	K(in.)	a	X_2 (b 2)	X_1 (b $^{-1}$)	c	d	f	l
100	33.74	100	19° 43'	10	142	0.80	675	18	18	675	136	90	675
200	28.47	100	16° 32'	10	118	0.80	569	13	0	569	112	80	569
300	26.99	100	15° 40'	15	166	1.20	810	18	18	810	154	90	810
400	24.78	26.6	68° 46'	6	560	0.48	895	23	33	895	225	110	895
500	20.91	26.6	51° 52'	6	291	0.48	755	12	28	755	192	90	755
600	19.83	26.6	48° 13'	6	257	0.48	716	12	24	716	177	80	716
700	26.00	100	15° 04'	15	160	1.20	780	17	17	780	148	90	780
800	Uv	none	48° 13'	6	257	0.48	716	12	24	716	177	80	716

* All linear dimensions in mills unless noted otherwise.

Fig. 3.-Drawing of a flight spectrometer.

21

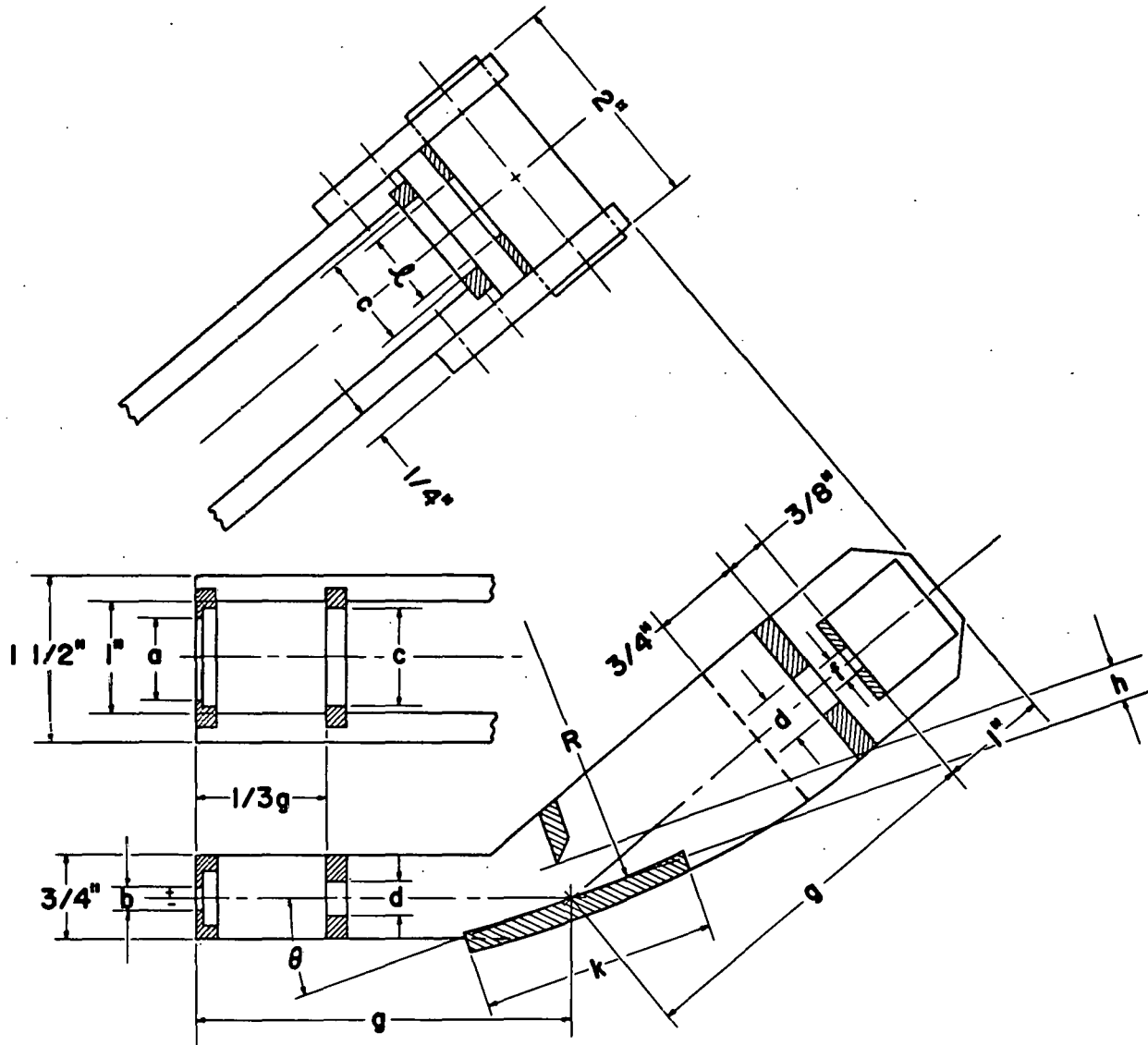


Fig. 4.-Photograph of two partially assembled flight spectrometers.

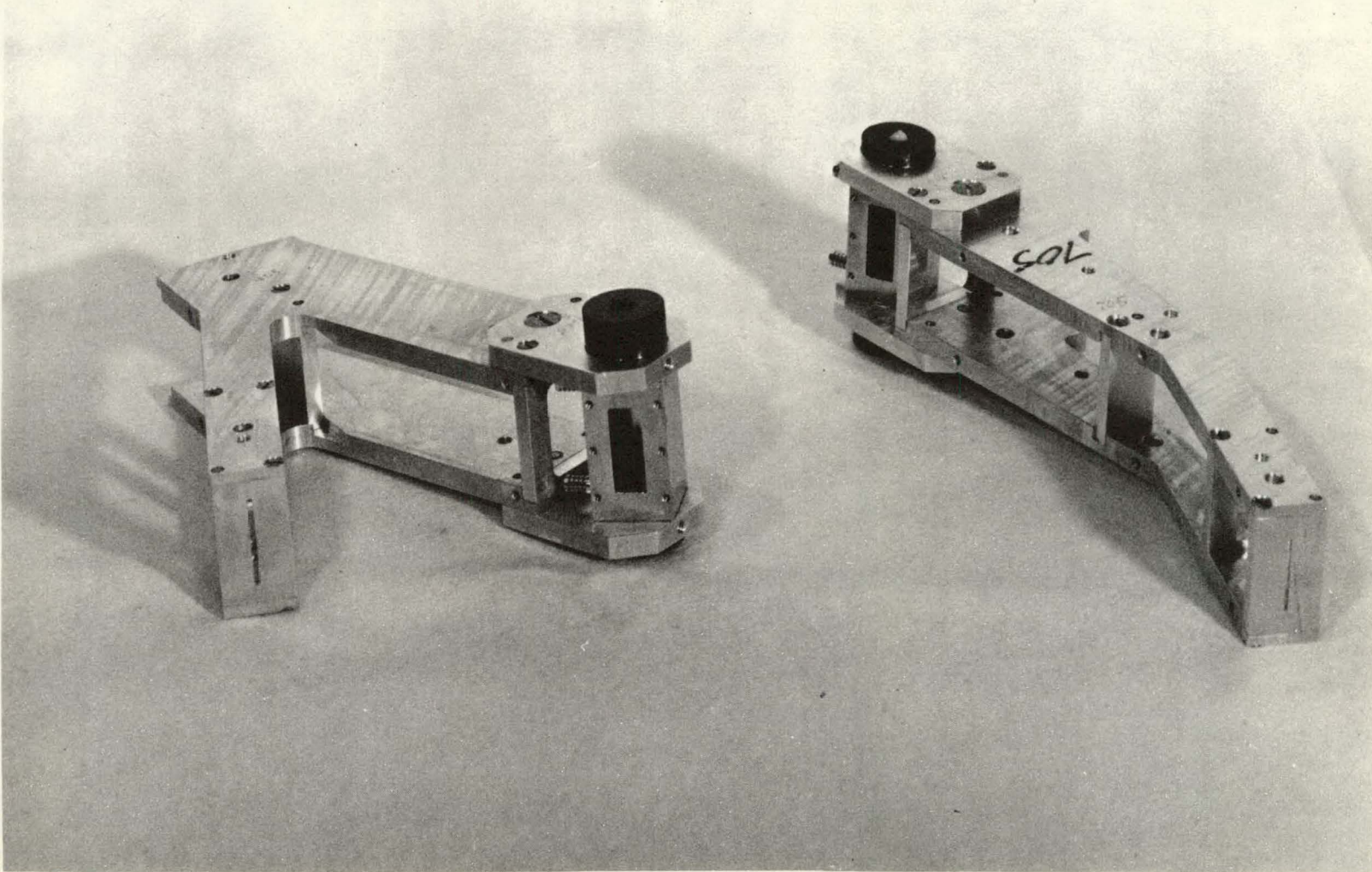
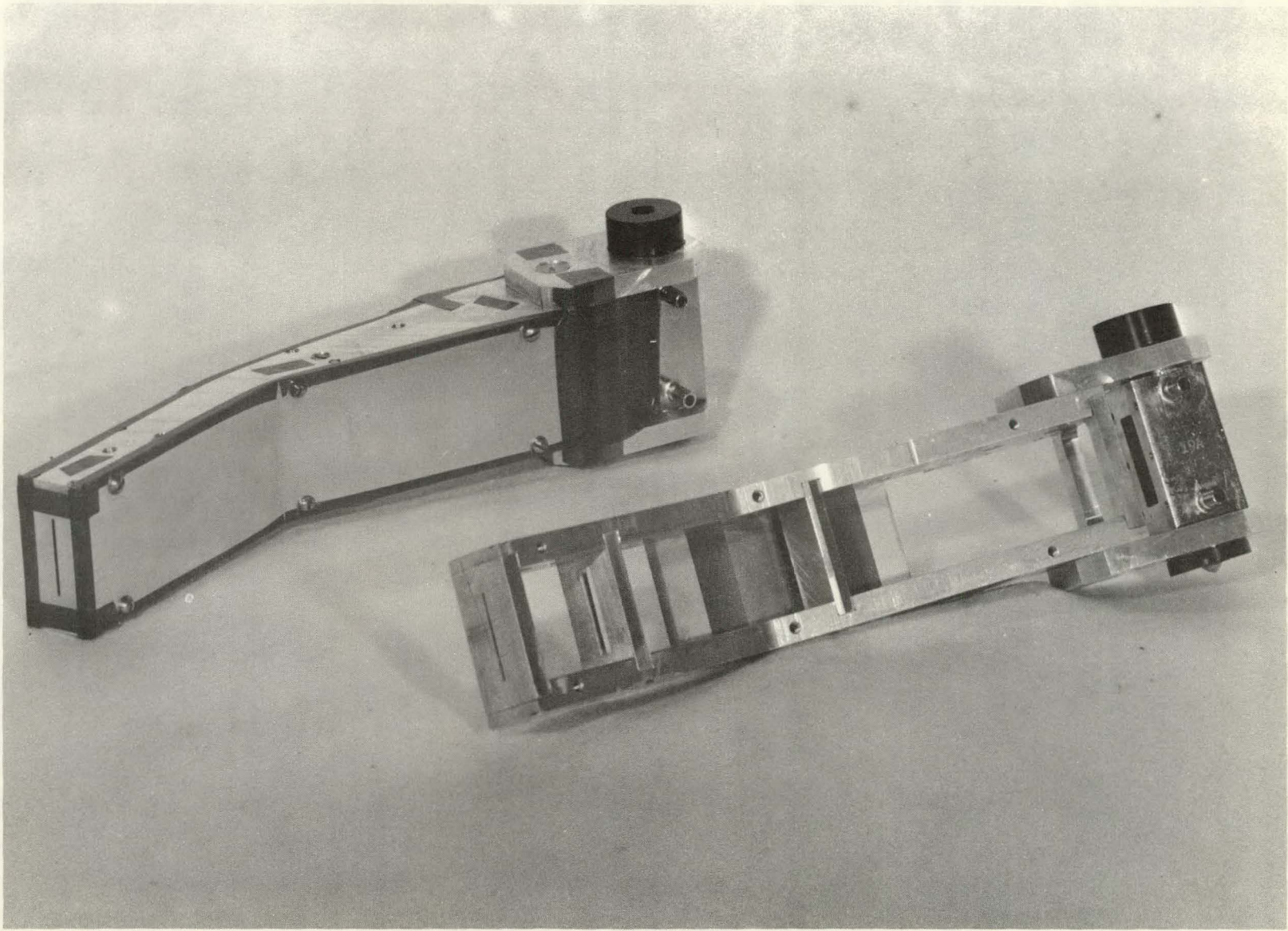


Fig. 5.-Photograph of two assembled flight spectrometers.

25



with the lead ions in the solution to form an insoluble "soap film" of lead stearate-deconoate. Successive layers of the film were deposited on carefully cleaned mica substrates by alternately dipping the substrate vertically into the solution and then slowly withdrawing it. The film was thus "folded" onto the substrate, resulting in double layers of metal ions separated by a distance equal to twice the length of the molecular chains. The film was confined to the central section of the rectangular tank by a floating barrier that was connected to two wire "arms" that passed through the centers of solenoids. By adjusting the current through the solenoids a constant force was applied to the barrier and thus to the film throughout the dipping process. The quality of the crystals produced in this way is very sensitive to such things as the optical flatness and degree of cleanliness of the mica substrates, the pH of the tank solution, the temperature of the tank solution, the speed with which the substrate was raised and lowered, and the number of dust particles inadvertently picked up with the film. The procedure was mechanized to the extent of a motor-driven dipping arm with adjustable speed and an automatic counter, and the crystals were made on a "dust-free" bench. In spite of a considerable effort the crystals were not all of uniform quality. Each crystal was checked for reflection efficiency and natural width and only the best were selected for the flight instruments.

The KAP crystals were obtained by cleaving 0.005-in. thick sheets from 2 x 1 x 1/4-in. thick single crystals purchased from Isomet Corporation.

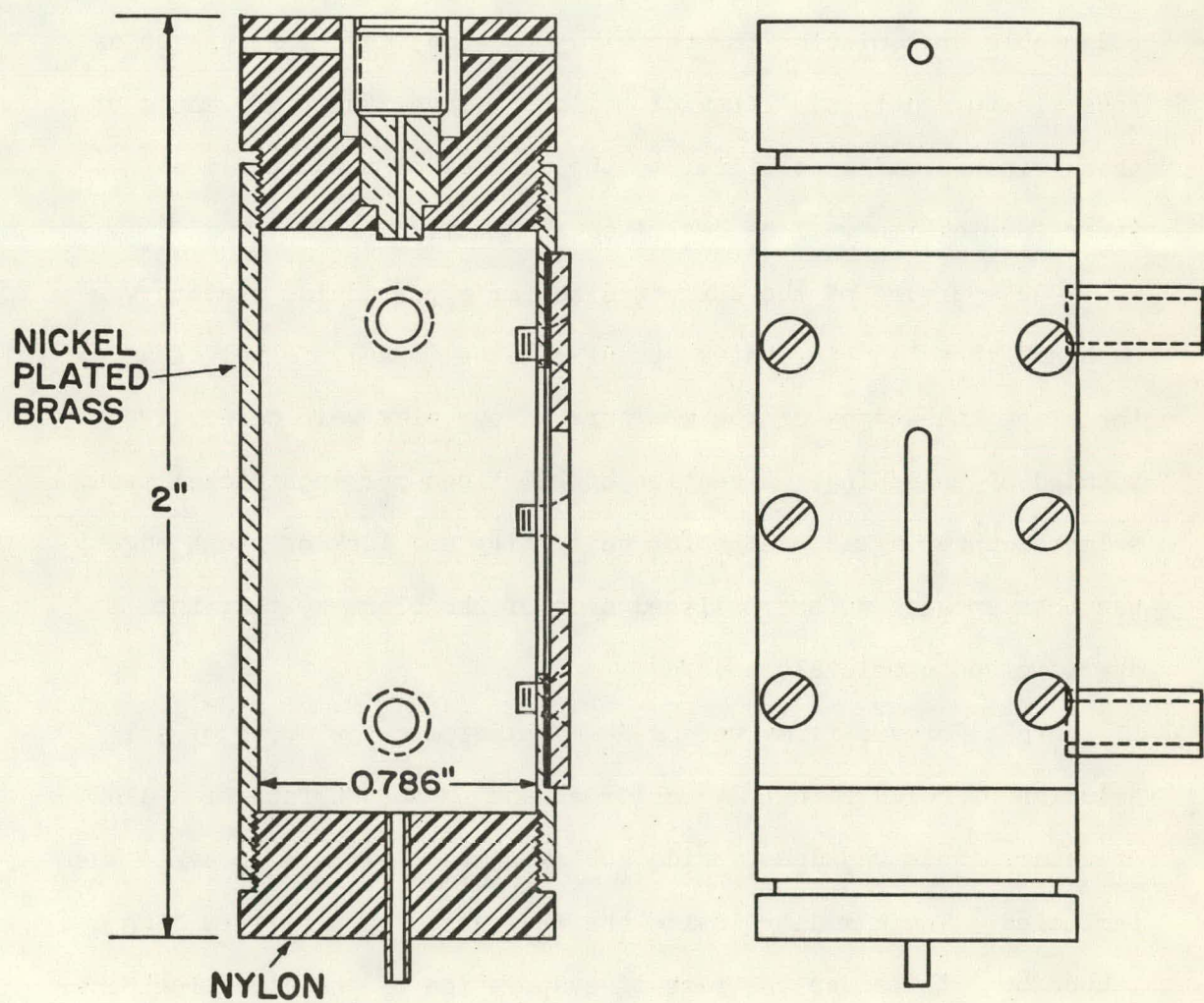
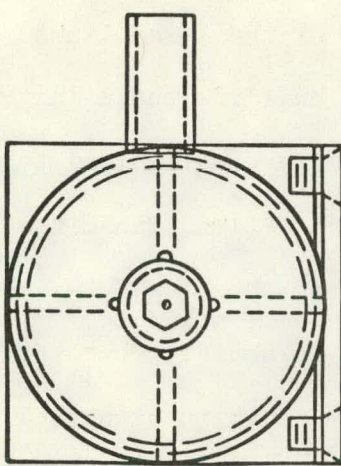
Both types of crystals were mounted to the concave surface of aluminum "mirrors" machined to the proper radius. Considerable care was taken to insure that the crystals were held firmly against the surface of the backing mirrors. The KAP crystals were held in place by an aluminum frame machined to mate to the curvature of the backing mirror. The larger stearate crystals on the mica substrates were held along their curved edges with strips of phosphor-bronze that acted as springs.

Geiger Counters

Continuous flow Geiger counters were used as photon detectors for all eight spectrometers. With the exception of entrance aperture sizes, the counters were identical for all stations. A drawing of the counter is shown in Fig. 6. The counter bodies were machined from brass and then all surfaces were plated with a thin layer of nickel. The nickel plating on the inside surfaces was found to be very effective in reducing background counting rates. The counter wire was 0.002-in. tungsten, and black nylon was used to fabricate the insulating end-caps. The small nipples on the side of the counter were the entrance and exit ports for the counter gas. The counters were operated at one atmosphere of pressure during the flights.

As mentioned in the introduction, scattered ultraviolet light is a very serious problem for any measurement made in this wavelength region. Ultraviolet photons that enter the Geiger counter volume will produce counts with a reasonably high efficiency, and the integrated intensity of all ultraviolet photons is many orders of

Fig. 6.-Drawing of a flight Geiger counter.



magnitude greater than the intensity of the x-ray lines. For this reason a major part of the effort of building these instruments was devoted to insuring that the spectrometers were blind to scattered ultraviolet light, but would at the same time transmit a reasonable fraction of the incident x-rays.

The Geiger counter windows had to satisfy four stringent requirements: they had to be strong enough to withstand the environment of a rocket launch, be able to support a pressure difference of one atmosphere during the flight, be thin enough to have a reasonable transmission for the x-ray photons, and be as opaque as possible to scattered ultraviolet light. Since the performance of these windows was so critical to the success of the experiment, their fabrication will be described in detail.

An aperture of the correct size for a particular station was machined in a 1/16-in. thick stainless steel blank. After cleaning the blank, the edges of the aperture on one side were carefully rounded by polishing. A section of 200 lines-per-inch nickel mesh, selected under a microscope for uniformity and lack of rough edges, was then epoxied to the polished side of the blank so that the aperture was completely covered.

Thin Formvar films were made by placing a few drops of a 1% solution of Formvar in 1,2-dichloroethane on the surface of a dish of water. This was done inside a Plexiglass enclosure to avoid dust particles. The humidity inside the enclosure was kept very high (about 80%) to reduce the rate of evaporation of the dichloroethane.

This was found to give a decided improvement in the uniformity of the film. The thickness of the Formvar film could be judged fairly accurately by its color. When a film of the desired thickness was obtained, it was lifted off the water by raising a thin aluminum frame up from below the surface. The film was lifted in such a way that it folded over the frame to form a double layer. This effectively eliminated most of the pinholes in the film. The Formvar double layers were then laid over the window blanks so that they covered the aperture and were supported by the nickel mesh. Two double layers were used for the long wavelength stations and three double layers were used for the shorter wavelength stations where the mass absorption coefficient of Formvar was much smaller. Each single layer of Formvar was about $15 \mu\text{g}/\text{cm}^2$ thick, so the total thickness of the pressure windows varied from approximately $60-90 \mu\text{g}/\text{cm}^2$.

After the films were dry they were tested in a vacuum-pressure test chamber for leaks. The test chamber was arranged so that the volume on one side of the counter window could be evacuated to a few microns while at the same time the volume on the other side could be pressurized to 1.2 atmospheres. For each window the final pressure attained in the vacuum chamber was recorded and compared with the pressure that could be attained when the window was replaced with a solid blank. Any window for which there was a measurable difference was discarded.

The final, and most difficult, step was to vacuum-deposit a uniform layer of aluminum $25-30 \mu\text{g}/\text{cm}^2$ thick onto one side of the

Formvar film without damaging it. The windows were placed on a rotating table, and the aluminum was evaporated from a tungsten filament located seven inches above and to the side of the table. To avoid damage to the films from the heat of the filament, the deposition was done very slowly, taking about an hour to deposit a $25 \mu\text{g}/\text{cm}^2$ layer. After the deposition was complete the films were again pressure-tested as described above and all defective windows were discarded.

The surviving windows were then tested for light leaks using an ultraviolet source and were then x-ray calibrated. They were pressure-tested a third time before being accepted for use on the flight instruments.

It was found that a single aluminized Formvar window was not sufficiently opaque to ultraviolet radiation. Even with windows having much thicker than normal aluminum layers that were almost certainly free of pinholes, the counters still had high count rates when exposed to an ultraviolet flux. The counts were apparently caused by photoelectrons that were ejected from the aluminum layer and entered the counter volume.

To avoid this problem, a second aluminized Formvar film was placed behind the pressure window. This second ultraviolet filter consisted of a very thin ($25 \mu\text{g}/\text{cm}^2$) Formvar film that covered, unsupported, a large aperture in an aluminum frame. Approximately $30 \mu\text{g}/\text{cm}^2$ of aluminum were vacuum-deposited on each side of the Formvar film. These filters were extremely fragile, but by mounting

them behind the pressure window (i.e., inside the counter) they were protected from the sudden pressure changes that occurred in the package during the early parts of the flight.

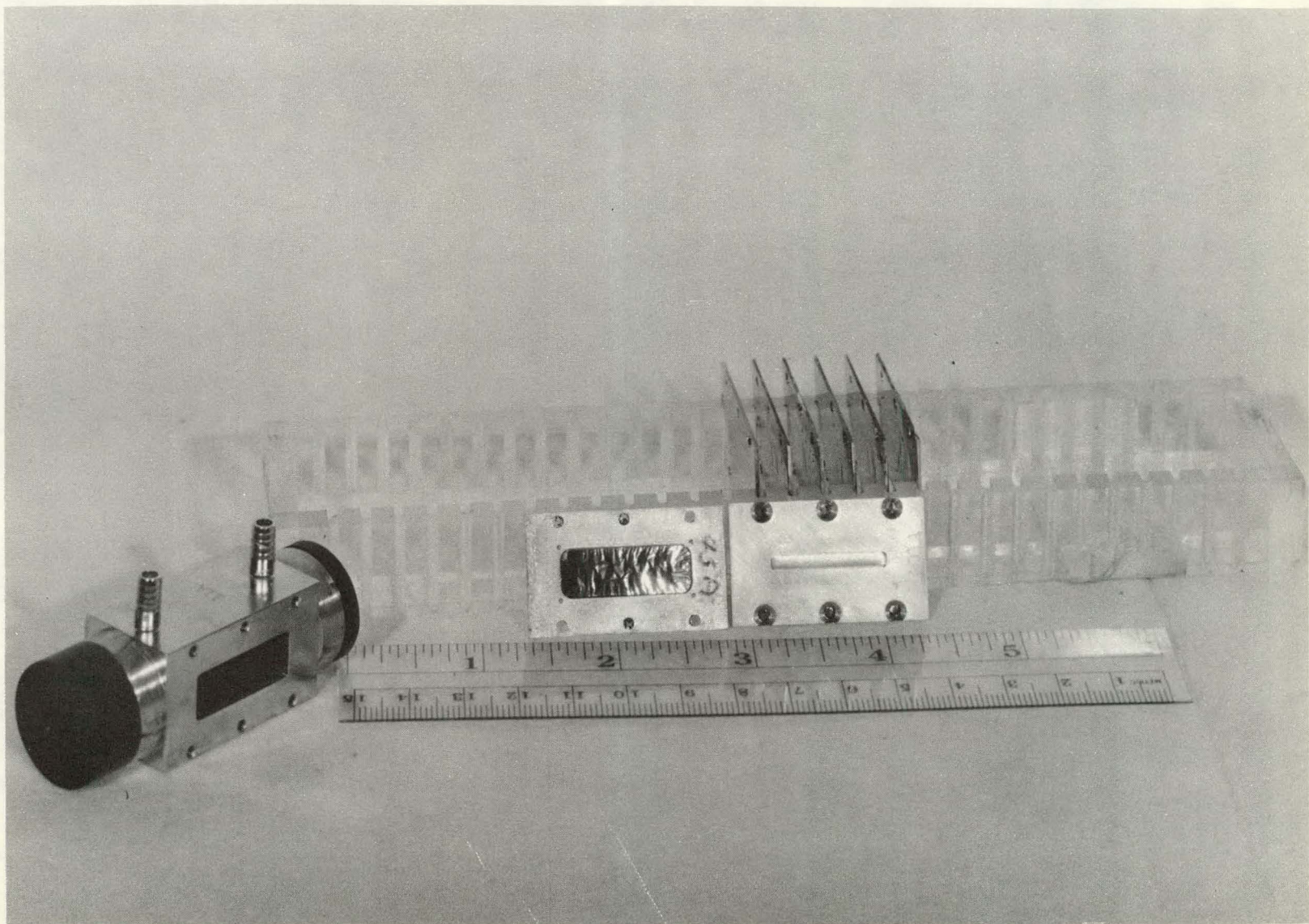
The complete window-ultraviolet filter assembly consisted of a "sandwich" containing, from the outside in, the pressure window, a thin neoprene gasket, the ultraviolet filter, and a second neoprene gasket. The soft gaskets provided a seal to prevent gas leaks from the counter and also protected the ultraviolet filter from mechanical shock. The "dead" gas space between the pressure window and the ultraviolet filter was only as thick as the compressed neoprene gasket that separated them, and the x-ray absorption in this volume was negligible compared to the absorption in the aluminum and Formvar. The two films had a total thickness of about $90 \mu\text{g}/\text{cm}^2$ of aluminum in three layers and about $90-120 \mu\text{g}/\text{cm}^2$ of Formvar. A photograph of a counter body, a pressure window, and an ultraviolet filter is shown as Fig. 7.

Counter Gas Supply

The window structure described above precluded the use of a sealed Geiger counter assembly because the windows could not be made sufficiently vacuum tight to prevent poisoning of the counter gas over long periods of time. A supply of counter gas sufficient to provide a continuous flow during the entire flight was carried as part of the package. The pressure vessel for the counter gas was a doughnut shaped container designed to provide a maximum volume in a shape that was convenient for packaging in a rocket. It was filled to a pressure of 2400 psi. Gas from the supply bottle passed through

Fig. 7.-Photograph of a flight Geiger counter, a pressure window, and an ultraviolet filter.

35



a regulator which reduced the pressure to 10/9 of an atmosphere and then into an input manifold. From the input manifold the gas was supplied in parallel to each of the eight counters, then from each counter back to an exhaust manifold. Neoprene tubing with 1/4-in. o.d. and 1/8-in. i.d. was used for the gas plumbing. For each separate counter a flow restrictor (Type A) was placed in the gas path ahead of the counter and a second flow restrictor (Type B) was placed in the exhaust path. The upstream restrictor prevented a catastrophic exhaustion of the gas supply in the event of a pressure window failure on any of the counters during the flight. The flow restrictors were made by Dell Manufacturing Company and consisted of a sintered metallic powder compressed to give the desired flow resistance. They were ordered with a resistance less than the desired value and then adjusted to the final value in the laboratory.

Figure 8 is a schematic of the gas supply system. The flow rate through any counter was

$$f = \frac{P_r - P_e}{R_A + R_B} \quad [1]$$

where

P_r = output pressure of regulator

P_e = exhaust pressure

R_A = flow resistance of Type A restrictor

R_B = flow resistance of Type B restrictor.

The total flow rate was the sum for all eight stations. The pressure in a counter was

$$P_c = P_e + R_B f = P_e + R_B \left(\frac{P_r - P_e}{R_A + R_B} \right). \quad [2]$$

Requiring that $P_c = 1$ atmosphere when $P_e = 0$ (during the flight) and that $P_c = 1.1$ atmospheres when $P_e = 1$ atmosphere (maintains a positive pressure in the counters while on the launcher) leads to the following conditions:

$$\frac{R_B}{R_A} = 9; \quad [3]$$

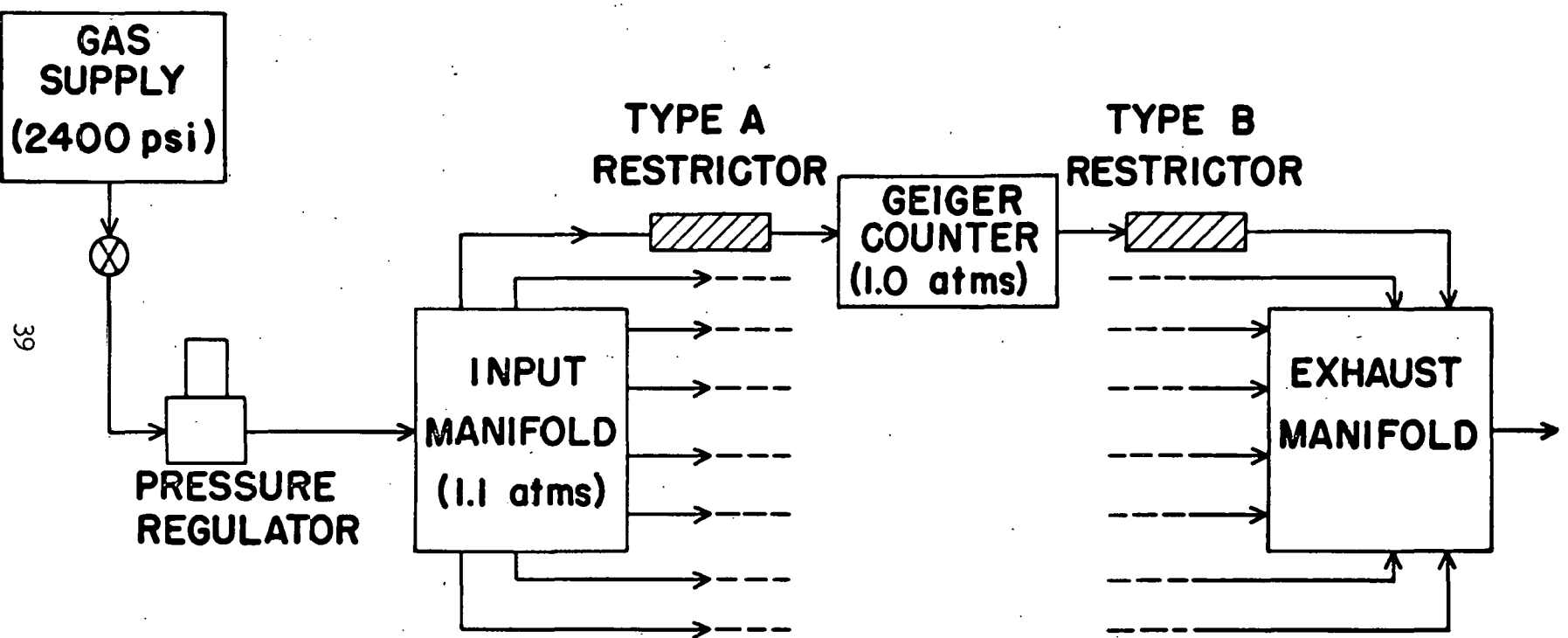
$$P_r = \frac{10}{9} \text{ atmospheres.} \quad [4]$$

The actual values of R_A and R_B are determined by the desired flow rate. Maintaining an exact flow rate was not critical, but the ratio of R_A to R_B determined the pressure in the counter and had to be adjusted accurately. For this reason the restrictors were calibrated in pairs, one Type A and one Type B, and were carefully adjusted to give one atmosphere of pressure in the counter under flight conditions. This adjustment could be made to an accuracy of one percent. The restrictors were then kept together and used as a set. The pressure regulators were adjusted for the proper output pressure while a flow rate that was approximately the same as would exist during the flight was maintained. Each regulator was tested to insure that the output pressure remained constant for variations of input pressure from 3000 psi down to less than 100 psi.

Data System

The individual counts from each detector were recorded in separate ten-bit scalers. These scalers were read serially into the telemetry

Fig. 8.-Schematic drawing of the counter gas supply system.



system, and reset to zero after each reading. A ten-bit sync word always preceded the data from station 100. The complete data frame consisted of 90 bits; the ten-bit sync word followed by eight ten-bit data words. The data were telemetered to the ground at a rate of 360 bits per second, or four complete data frames per second. For each counter, then, counts were accumulated for $1/4$ second, after which the scaler was read and erased. This provided for count rates up to 4096 counts/sec without exceeding the scaler capacity. The data were transmitted on two telemetry channels for redundancy and recorded on the ground on magnetic tape. A block diagram of the electronics is shown in Fig. 9. A completed set of electronics and a battery pack is shown in Fig. 10.

Complete Package and Pointing Control

Figure 11 is a photograph of a completely assembled package, and Fig. 12 shows four packages in various stages of assembly. The pressure vessel for the counter gas is at the bottom and above this the electronics is mounted around the outside of the battery pack. Directly above the electronics is the base plate that supports several heavy vertical plates. The individual spectrometers are attached to the vertical plates. As mentioned earlier, the curved crystal spectrometers have a very wide angular acceptance compared to either a flat crystal spectrometer or a grating. Angular misalignments of as much as $1/4$ deg change the spectrometer sensitivities by no more than a few percent. By fabricating all the structural parts of the package on tape-operated machines and carefully inspecting

each part to ensure that the specified tolerances were met, alignment accuracies better than $1/4$ deg were easily obtained.

The instrument packages were mounted on a biaxial attitude control system (ACS) developed by Sandia Corporation of Albuquerque, New Mexico. Approximately 68 seconds after the launch of the Nike-Tomahawk rocket, the nose cone covering the payload compartment was ejected. After nose cone ejection the payload was separated from the Tomahawk rocket. The rocket was spin stabilized during the flight through the atmosphere, and the payload at this time had a significant spin rate (about 8 rps). The first function of the ACS was to reduce this spin rate to zero. Two heavy weights that had been attached in recessed compartments to opposite sides of the payload were released by cutting with an explosive guillotine the cables that held them in place. The weights were attached to long, flexible cables wound in a spiral recessed groove around the outside of the payload. As the weights unwound from the payload, the payload spin rate decreased. When the cables were completely unwound they were released from the payload. This so-called "yo-yo" despin mechanism removed most of the spin angular momentum of the payload. A rate gyro was used to sense the magnitude of the residual spin rate and the signal from the rate gyro was used to activate vernier gas jets that reduced the spin rate to zero. After the spin rate was reduced to zero, the next function of the ACS was to align the payload axis to point at the sun. A solar sensor mounted to the payload and optically aligned with the experiment base plate provided angular position data on the location of the solar

Fig. 9.-Block diagram of the electronics system.

ELECTRONICS BLOCK DIAGRAM

43

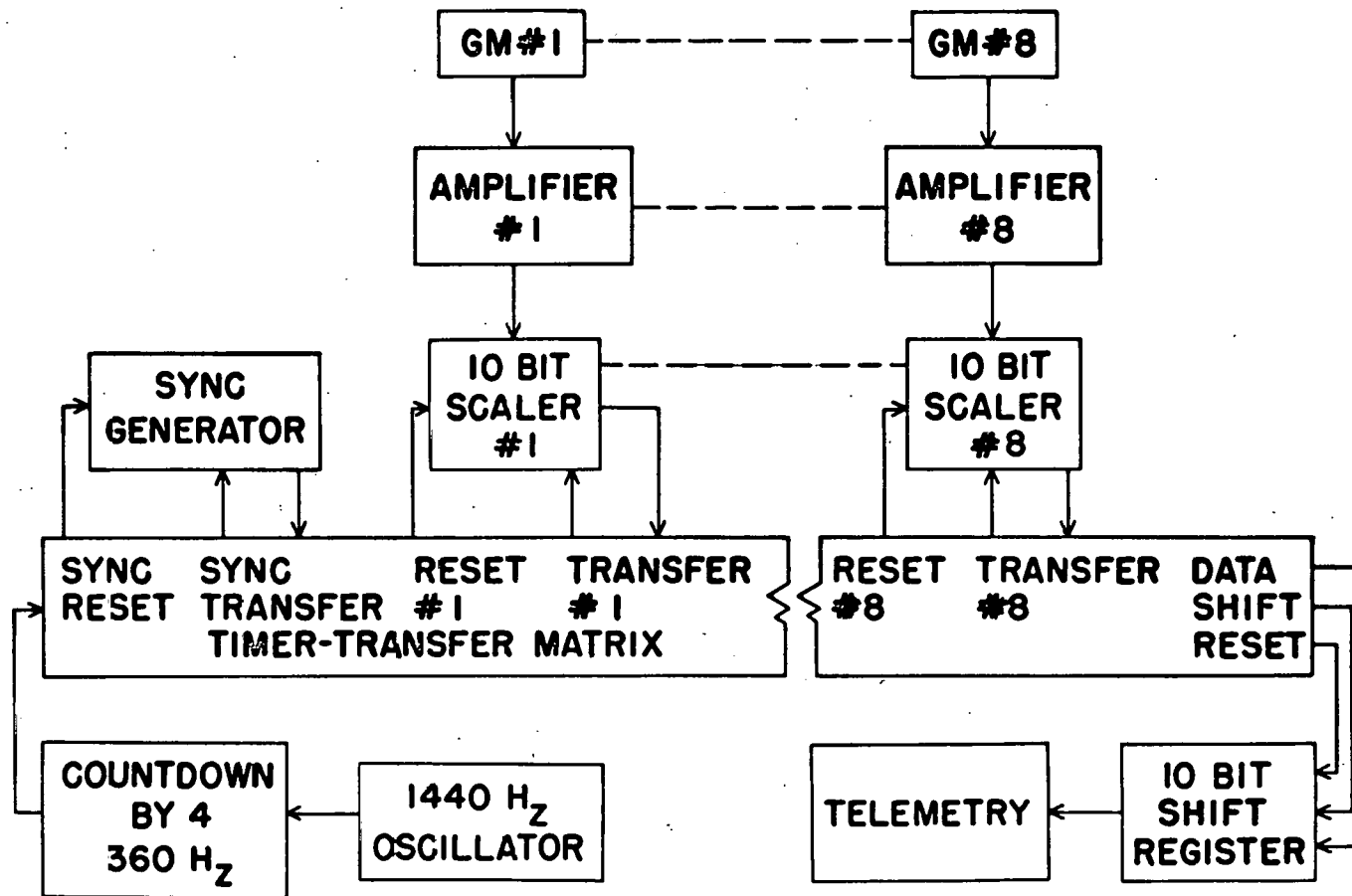


Fig. 10.-Photograph of a battery pack and a complete set of electronics.

45

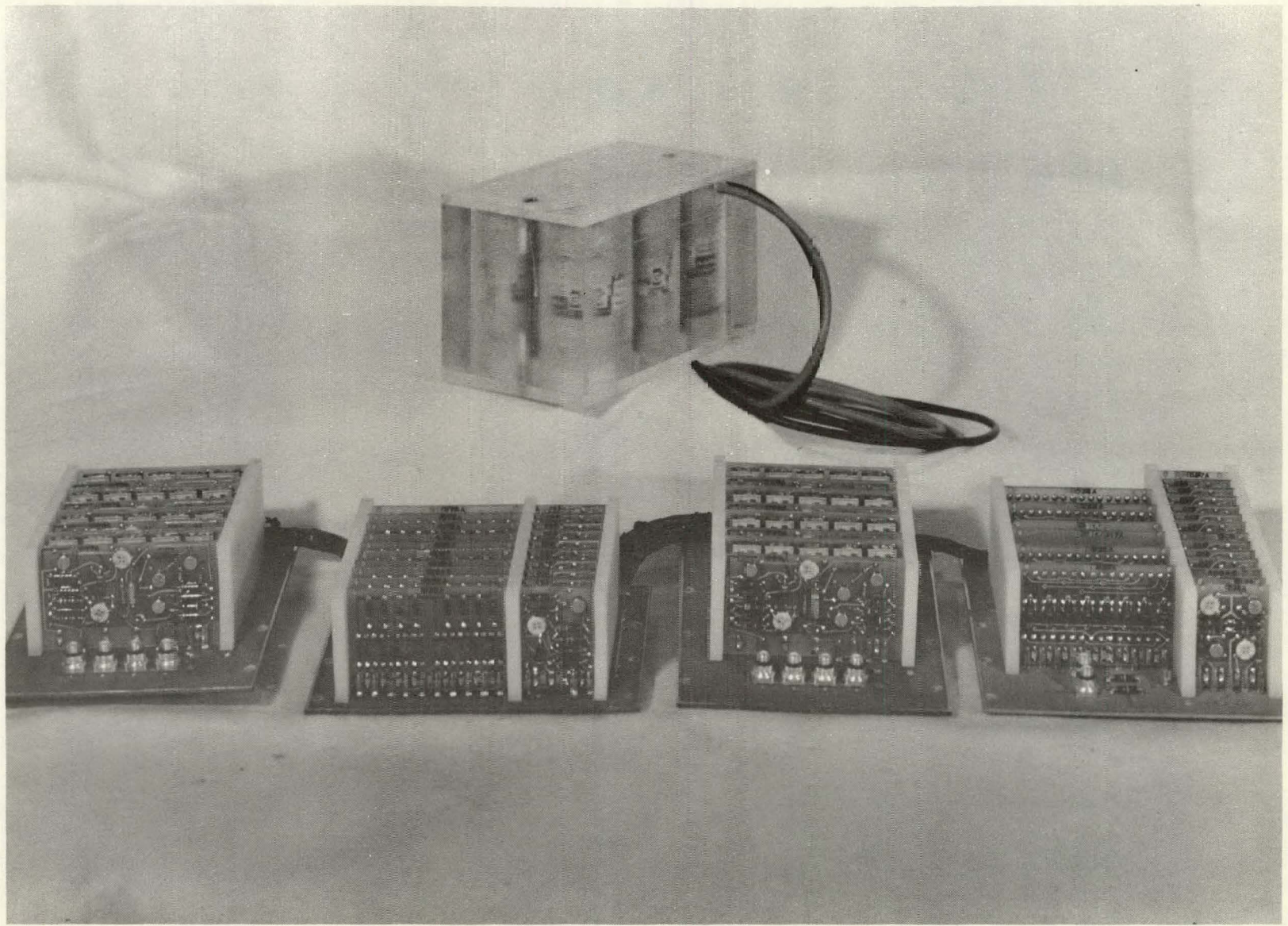


Fig. 11.-Photograph of a completely assembled instrument package.

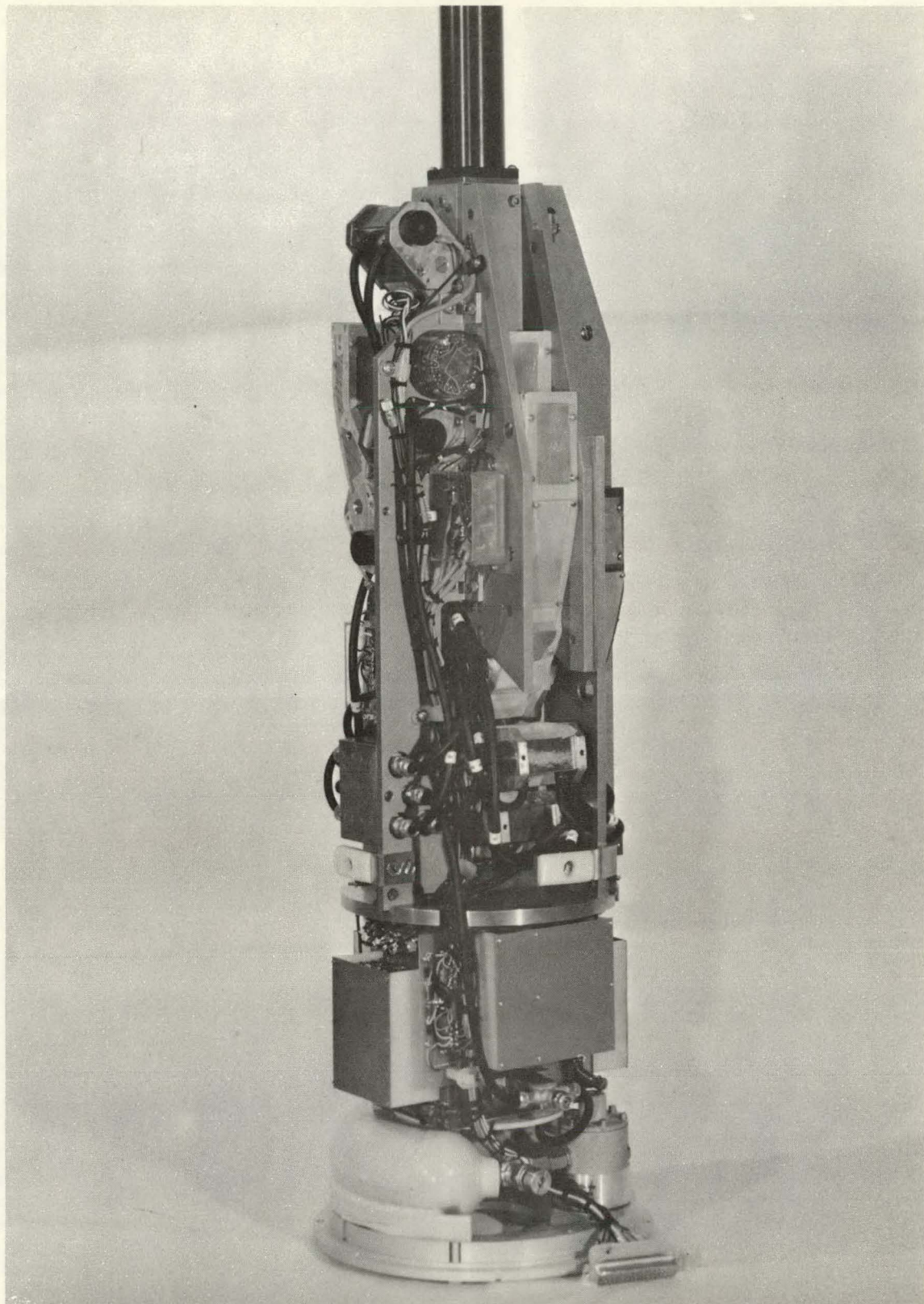
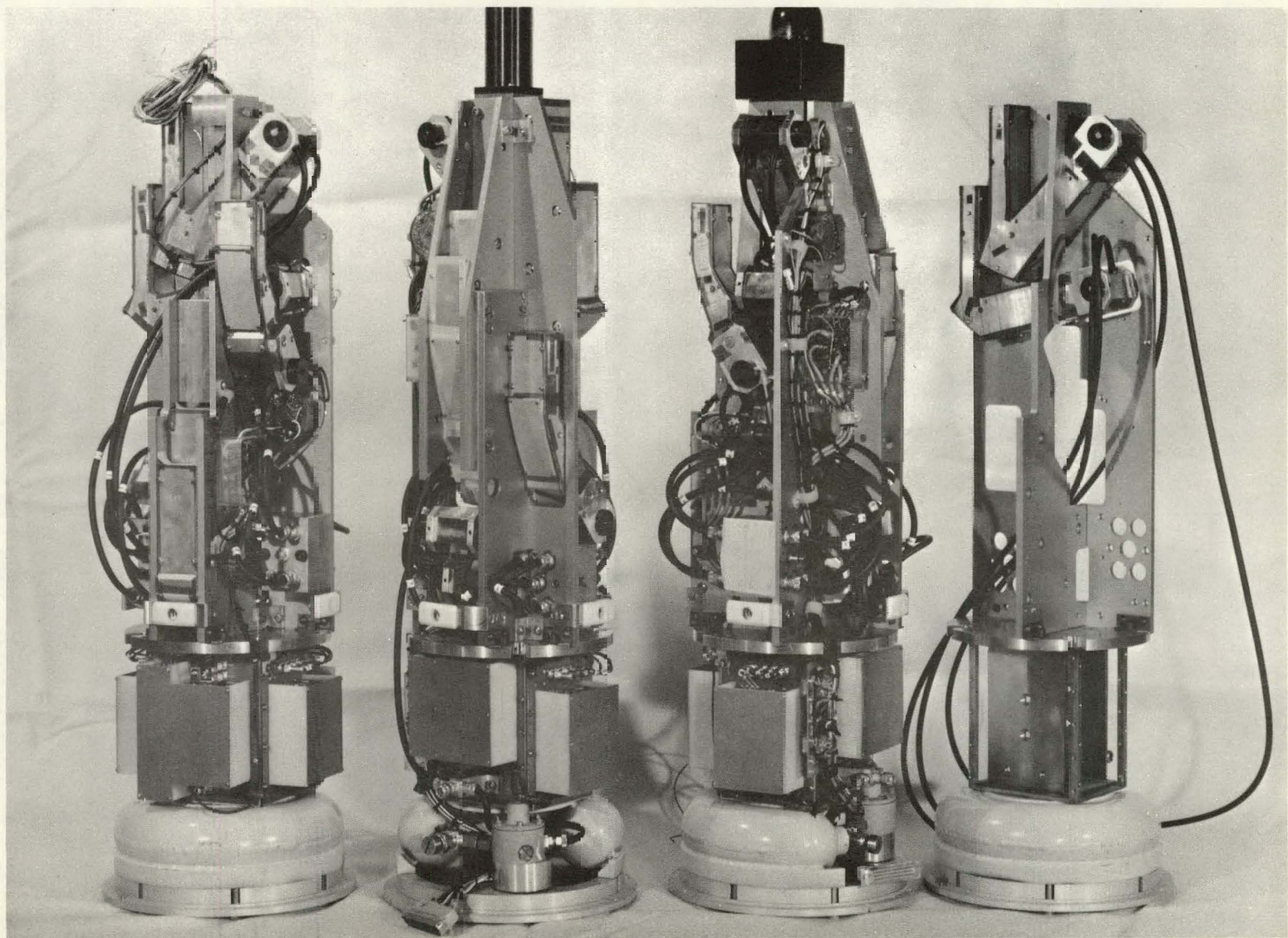


Fig. 12.-Photograph of four instrument packages in different stages of assembly.

49



disk relative to the payload axis. Analog error signals from the sun sensor were used to activate gas jets that provided the thrust to orient the payload. The ACS system was designed to provide a pointing accuracy of better than $1/4$ deg.

Description of the Two Flights

For the first flight on August 8, the ACS performed generally as expected. The payload spin rate was reduced to zero immediately after separation from the Tomahawk rocket, and at $11\frac{1}{4}$ seconds after launch the payload axis was pointed to within one eighth of a degree of the center of the solar disk. The pointing was maintained throughout the high altitude portion of the flight. The pointing system lost control of the payload during the reentry phase of the flight at an altitude of about 85 kilometers when the aerodynamic drag forces became too large. The trajectory of the first flight is shown in Fig. 13. Launch corresponds to time zero and the telemetry signal was lost at 518 seconds.

On the first flight there was a fairly serious electrical noise problem. The pitch and yaw gas nozzles fired intermittently during the entire flight, and the firing of the nozzles fed noise into the data system causing bit errors in the data word. This happened at random times, but often enough to make it very difficult to read the magnetic tapes with a computer. To recover the data it was necessary to read by hand high-speed visicorder traces made from the tapes. About one third of the data words were found to be unaffected by the noise. The payload was above any sensible atmosphere for about

360 seconds, so there was a total of about 120 seconds of good data. Since the count rates ranged from 70 counts/sec for station 600 to over 12,000 counts/sec for station 300, and were effectively constant in each station throughout the flight, it is clear that 120 seconds of good data were more than sufficient to give statistical limits that were much smaller than other uncertainties in the experiment. For the measurement of the incident flux above the atmosphere the noise problem caused no real degradation of the data. However, data were obtained continuously during the early reentry portion of the flight down to an altitude of 85 kilometers. Essentially total absorption for all the observed x-ray lines occurs above 90 kilometers, and the loss of two thirds of the data words during the very short time that it took the payload to fall through the region of the atmosphere where absorption takes place did seriously degrade the absorption-versus-altitude information for the low count rate stations 400, 500, and 600.

On the second flight the attitude control system acquired the sun at 95 seconds after launch and maintained excellent pointing from that time until reentry. As on the previous flight, data were obtained continuously down to an altitude of less than 90 kilometers. There were no electrical noise problems on this flight. However, two of the KAP stations recorded extremely low count rates, barely above the cosmic ray background level, indicating a failure in the stations. Shortly after this flight a spare package was disassembled and one of the three KAP crystals was found to be broken. Since the 0.005-in.

Fig. 13.-Nike-Tomahawk rocket trajectory for the flight of August 8, 1966.

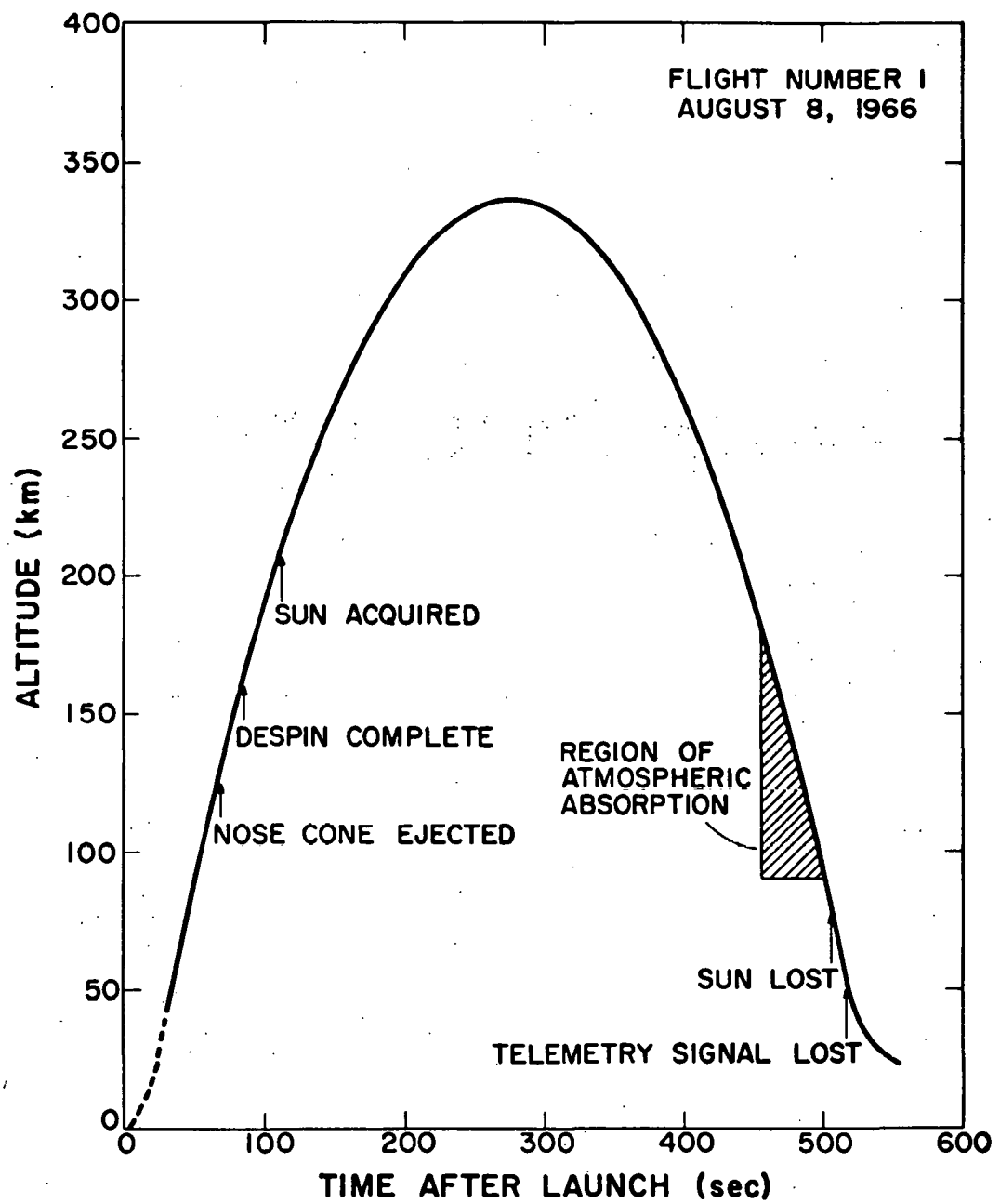


Fig. 14.-Observed counting rates for the high altitude portion of the August 8, 1966 flight.

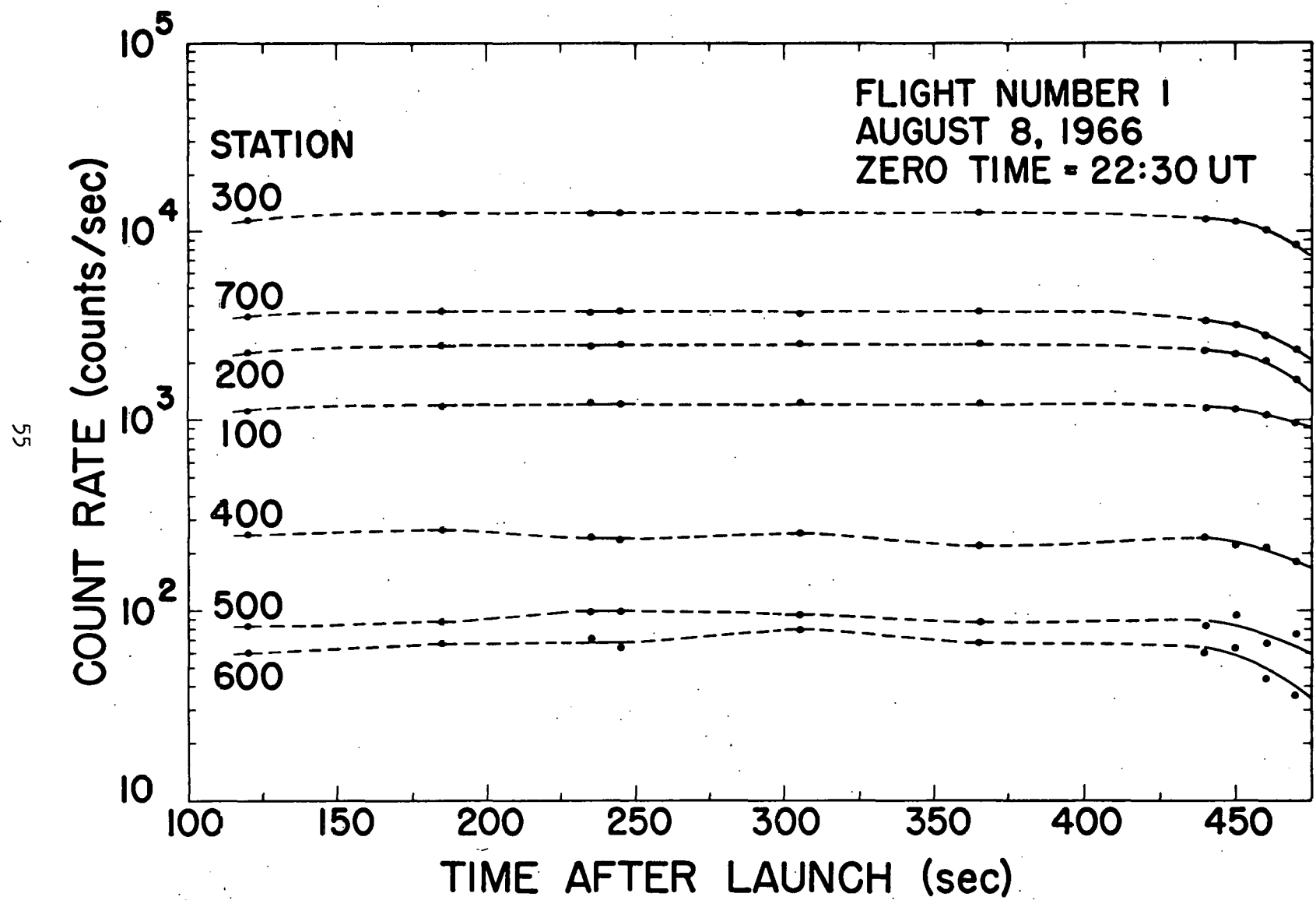


Fig. 15.-Observed counting rates for the high altitude portion of the August 11, 1966 flight.

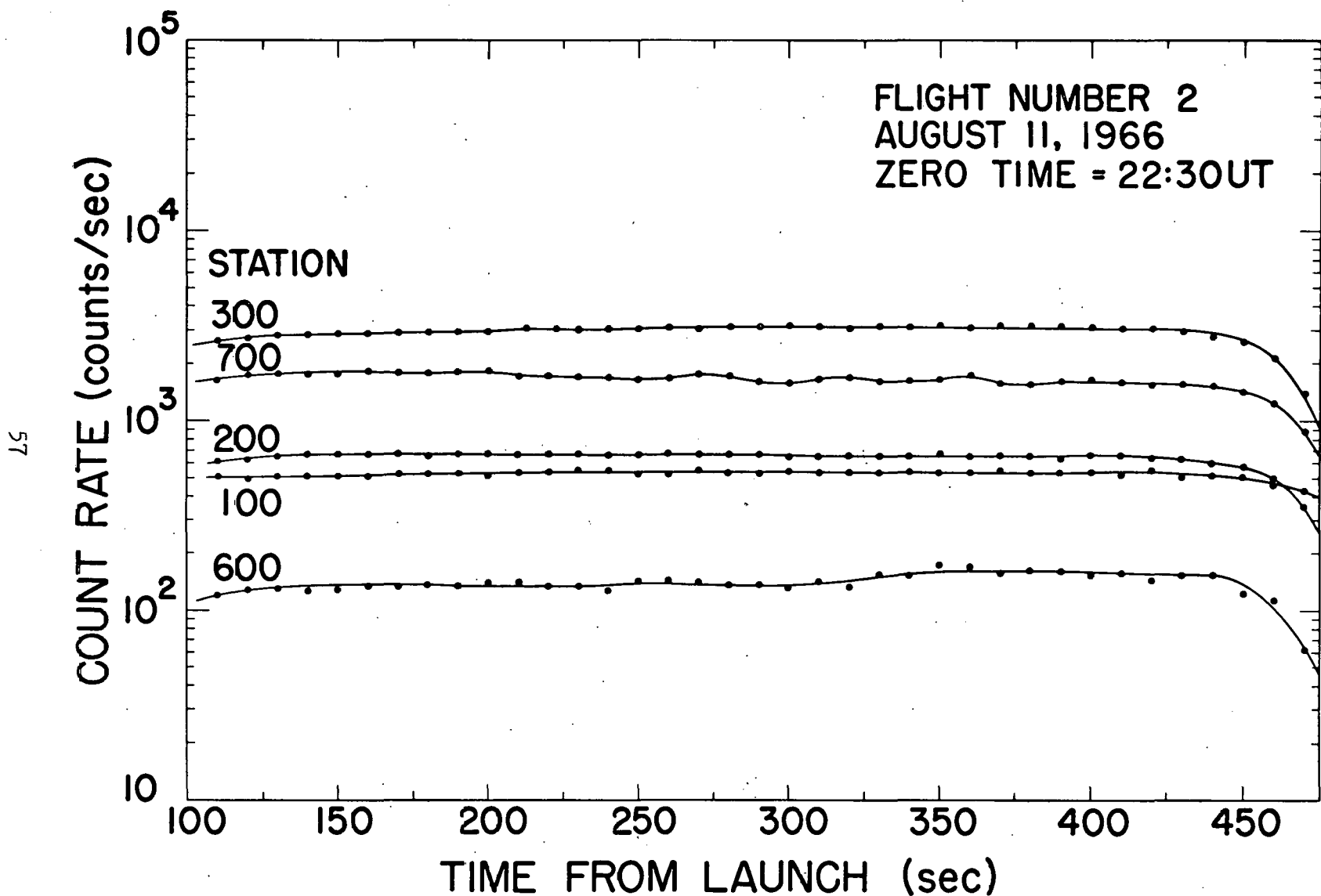


Fig. 16.-Observed counting rates for the reentry portion of the August 8, 1966 flight.

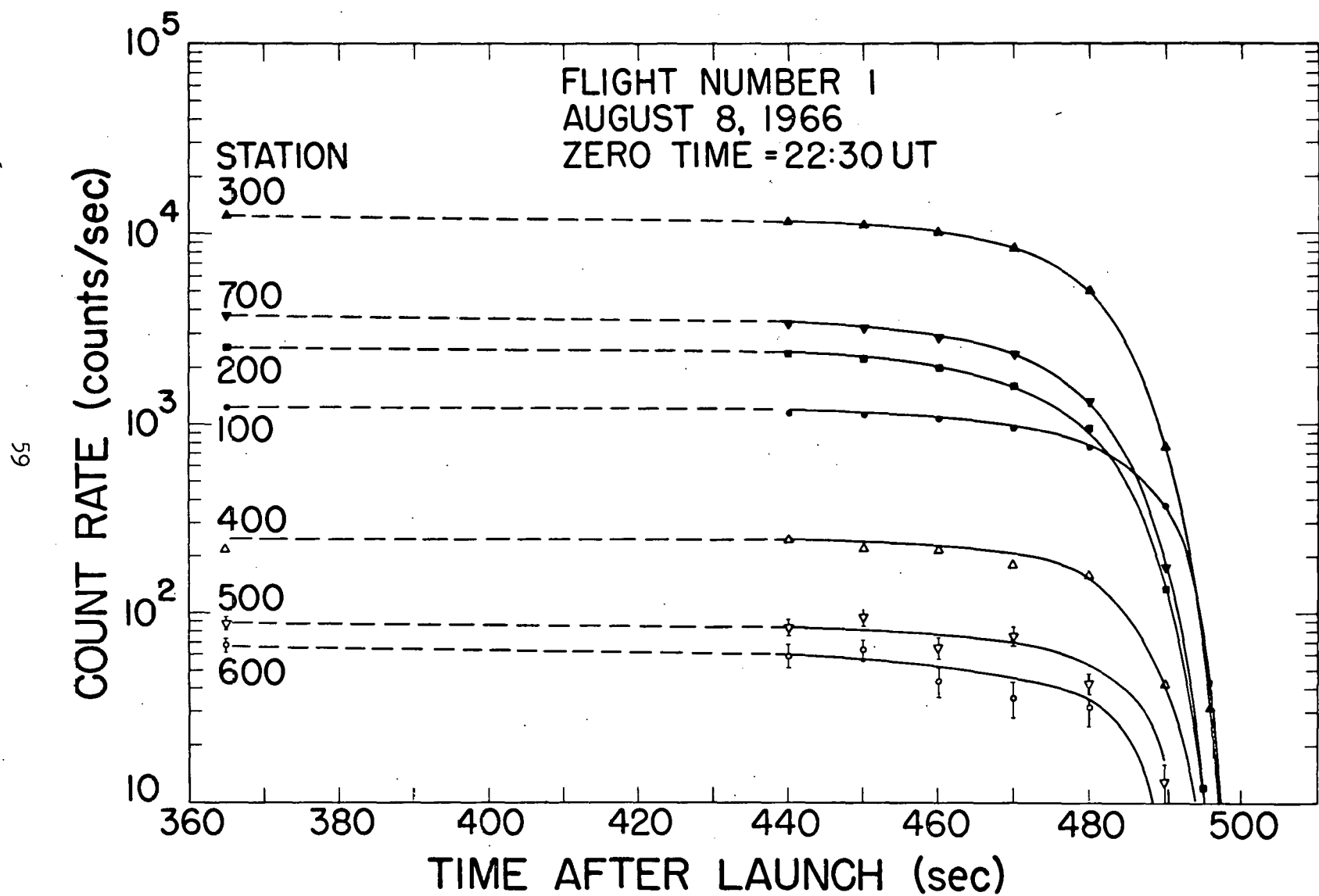
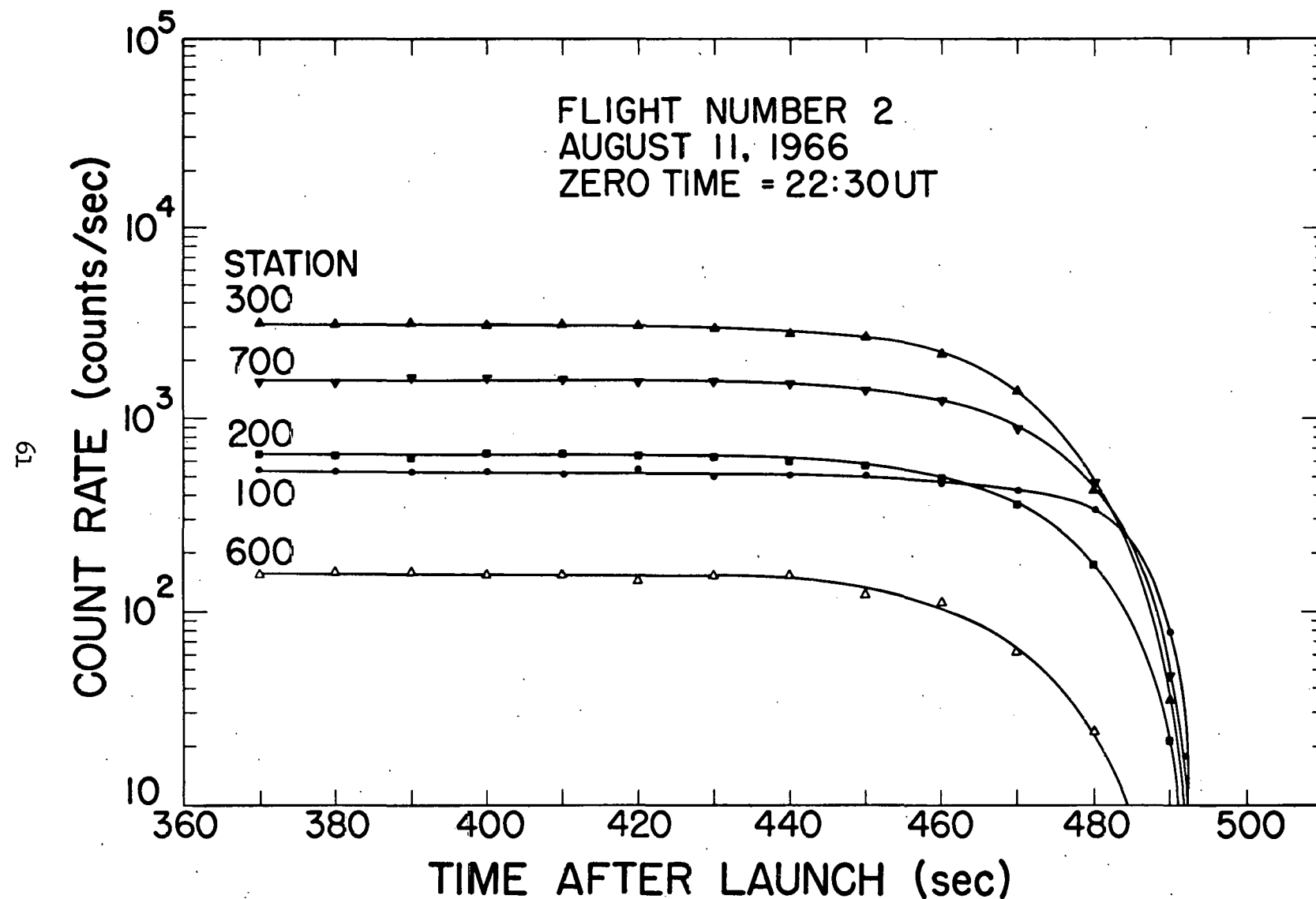


Fig. 17.-Observed counting rates for the reentry portion of the August 11, 1966 flight.



sheets of KAP used on the spectrometers were very fragile, the failure of these two stations could have been caused by broken crystals.

Observed Count Rates

The count rate data from the two flights are shown in Figs. 14 through 17. The first two figures show the portion of the flight from acquisition of the sun to the beginning of atmospheric absorption. Figures 16 and 17 show on an expanded time scale the portion of the flight during which atmospheric absorption occurred. The data from station 800, the ultraviolet background station, are not shown because the count rates were too low to plot on this scale. Each point on the curves is the average count rate over a 10-sec interval.

Because of the excessive time required to read by hand the data from the first flight and because of the essentially constant count rates while the package was above the atmosphere, averages were taken at several selected times but not for the entire flight. However, all the data for this flight were read for that portion of the flight during reentry where atmospheric absorption occurred. The background count rates for all stations prior to acquisition of the sun were very low, averaging about 4 counts/sec. In the first flight the count rate in station 800 increased to around 14 counts/sec when the pointing control acquired the sun, indicating a slight sensitivity to scattered ultraviolet photons. On the second flight there was no detectable change in the count rate of station 800 when the sun was acquired.

As can be seen from Figs. 14 and 15, the count rates were very nearly constant through the portion of the flight above the atmosphere.

Table 4 gives the average count rate for each of the stations for both flights. To convert these count rates to flux values it is necessary to know the efficiencies of each of the stations. The spectrometer efficiencies are the subject of Part II, where the focusing and resolution are considered in detail and the calibration methods are discussed.

TABLE 4
AVERAGE COUNT RATES OBSERVED ABOVE THE ATMOSPHERE

Station	Wavelength (Å)	Average Count Rate (counts/sec)	
		August 8, 1966	August 11, 1966
100	33.74	1,224	530
200	28.47	2,504	672
300	26.99	12,536	3,100
400	24.78	234	---
500	20.91	82	---
600	19.83	58	129
700	26.00	3,736	1,800
800	Uv	14	4

II. SPECTROMETER SENSITIVITIES

Johann Curved Crystal Geometry

Flux values are determined from the counting rates of the stations by the relation

$$F = E_t C \quad [5]$$

where F = incident flux (photons/cm²-sec)

C = observed count rate (counts/sec)

E_t = total spectrometer efficiency (photons/cm²-count).

Ideally the value of E_t would be determined in one experimental step by exposing a completely assembled spectrometer to a known flux of x-rays of the appropriate wavelength and measuring the resulting count rate. In practice this is not possible. Once the crystals have been bent to the proper radius and attached to the spectrometers, the instrument is sensitive only to x-rays of the wavelength for which the spectrometer is designed. The emission lines of the one electron ions of carbon and nitrogen cannot be generated using conventional x-ray sources and none of the x-ray lines available in the laboratory has the correct wavelength. The emission lines from these one electron ions can be obtained in the laboratory from high temperature plasmas but their usefulness as calibration sources is limited because of the extreme difficulty of obtaining reproducible, calibrated intensities.

Since a direct calibration of the complete spectrometer was not possible, the spectrometer sensitivities were determined by deriving as accurately as possible the functional relationship between the various parameters of the spectrometer system and then measuring experimentally the values of each of these individual parameters. This procedure is clearly less desirable than a one-step type of calibration and introduces some uncertainty into the final flux values. It should be pointed out, however, that this type of calibration difficulty is shared to about the same degree by all experiments done in this wavelength region.

To arrive at an analytical expression for the spectrometer sensitivities it is necessary to consider in more detail the geometry of the curved crystal spectrometer. An instrument of this type was first built by Johann (12). Ditsman (13) discusses in detail the reflection properties of a bent crystal in the case of a micro-source. The expressions derived below are in part a restatement of the results of Ditsman from a somewhat different viewpoint and an extension of this work to apply to the case where the sun is the source.

Referring again to Fig. 2, the Johann spectrometer uses a thin section of a crystal, bent so that it becomes part of a cylindrical surface of radius R. The entrance aperture, or source, is located on the focusing circle of radius $1/2 R$ so that the ray from the aperture to point O on the crystal makes an angle θ_0 with the tangent to the crystal surface. The detector is also located on the focusing circle, opposite the aperture.

Dumond and Kirkpatrick (14) have shown that if a crystal is bent so that the atomic planes lie in concentric circles of radius R and then a surface of radius $1/2 R$ is formed by grinding the crystal, perfect focusing can be obtained. This is illustrated in Fig. 18.

X-rays of wavelength λ_0 incident along the spectrometer axis AO make an angle θ_0 with the crystal surface at O and are diffracted along the path OI . Consider the ray AO' which makes an angle β with the spectrometer axis and the ray $O'I$. To be a perfectly focusing instrument in the plane of dispersion it is necessary that the angle θ be equal to θ_0 so that x-rays of the same wavelength λ_0 will be diffracted from O' . It is also necessary that φ be equal to θ_0 so that the diffracted ray from O' will converge at I with the diffracted ray from O . That this is true can be seen as follows. Angle A is equal to angle B since both are inscribed angles of a circle subtended by the same chord AC . Since

$$B + \theta = A + \theta_0 \quad [6]$$

and

$$A = B,$$

then

$$\theta = \theta_0.$$

Also, since the chord CI equals the chord CA , angle B equals angle B' . Therefore, $\varphi = \theta_0$.

The Johann geometry includes only the crystal bent to radius R without the subsequent grinding of a surface $1/2 R$ and is therefore not a perfectly focusing arrangement. The amount of "defocusing" in the plane of dispersion can be expressed analytically as a function of the angle β .

Referring to Fig. 19, consider x-rays of wavelength λ_0 incident through an aperture at A with an angular spread in the plane of dispersion. The ray AO is the central axis of the spectrometer and x-rays following this path are incident on the crystal an an angle θ_0 , where $\lambda_0 = 2d \sin \theta_0$. The path of the diffracted ray is along OI. In the previous example, x-rays incident along the path AO'', at an angle β to the central ray, would reach the crystal surface at O' and be diffracted along O'I. For the Johann arrangement these same x-rays continue along this path until they reach the crystal surface at O'' and are then diffracted along the path O''I'. The angle of incidence for this path is not equal to θ_0 , but is larger by an amount $\delta\theta$.

To a very good approximation

$$\delta\theta = \frac{S}{R} \quad [7]$$

and

$$S = d \cotan \theta_0, \quad [8]$$

where

$$d = R(1 - \cos \beta). \quad [9]$$

Therefore

$$\delta\theta(\beta) = (1 - \cos \beta) \cotan \theta_0. \quad [10]$$

For small angles this reduces to

$$\delta\theta(\beta) \approx 1/2 \beta^2 \cotan \theta_0. \quad [11]$$

The x-rays are incident onto the crystal surface at an angle $\theta_0 + \delta\theta(\beta)$, and the diffracted ray reaches the focusing circle at a point I', slightly displaced from I. Since $\delta\theta(\beta)$ depends on the square of β it is positive ($\theta > \theta_0$) for β positive or negative.

Figure 20-a illustrates the situation for a beam that has an angular spread perpendicular to the plane of dispersion. The points A, O, and D define the dispersion plane of the instrument and the

Fig. 18.-The geometry of a perfectly focusing, curved crystal spectrometer.

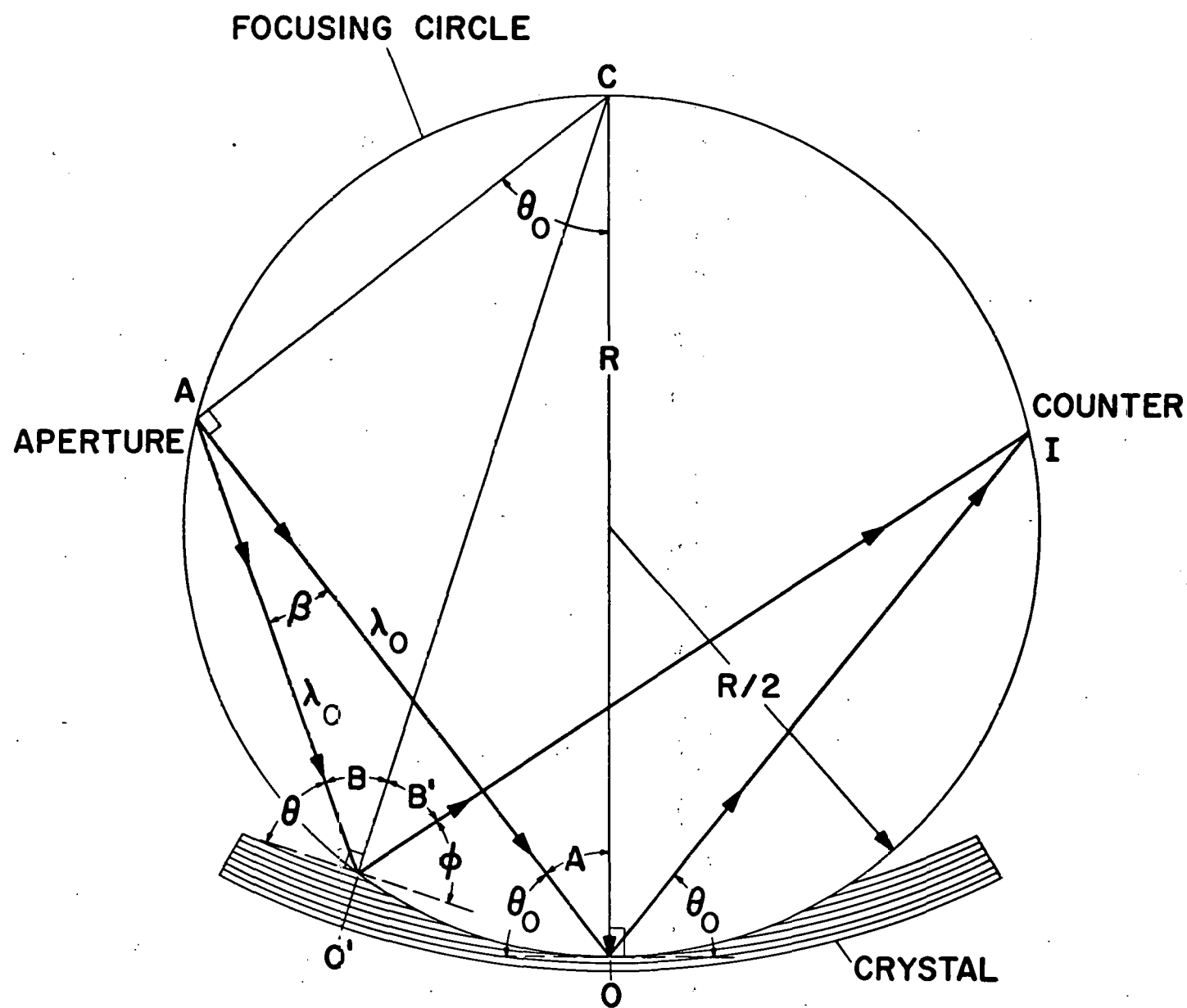


Fig. 19.-The focusing properties of the Johann type curved crystal spectrometer in the plane of dispersion.

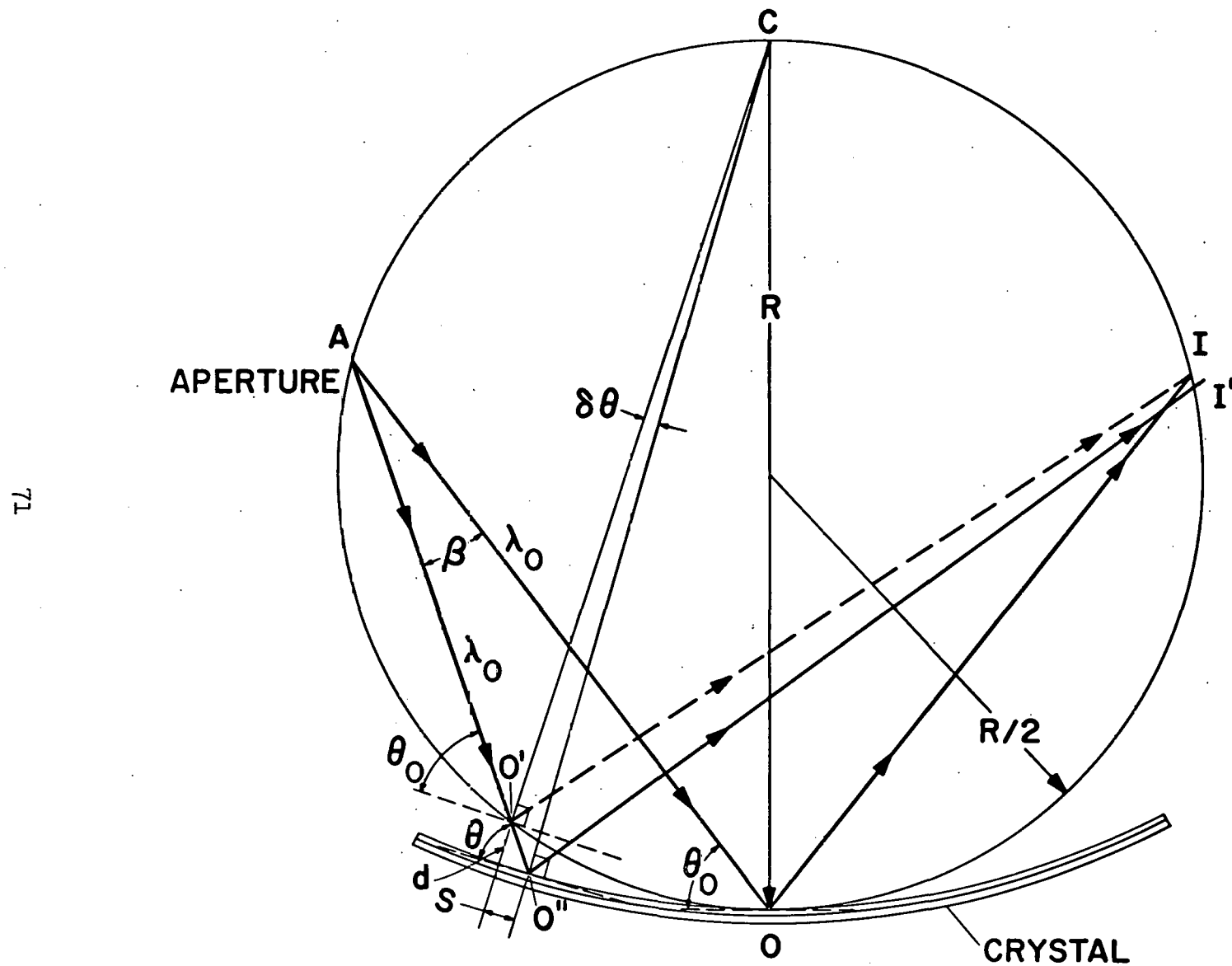
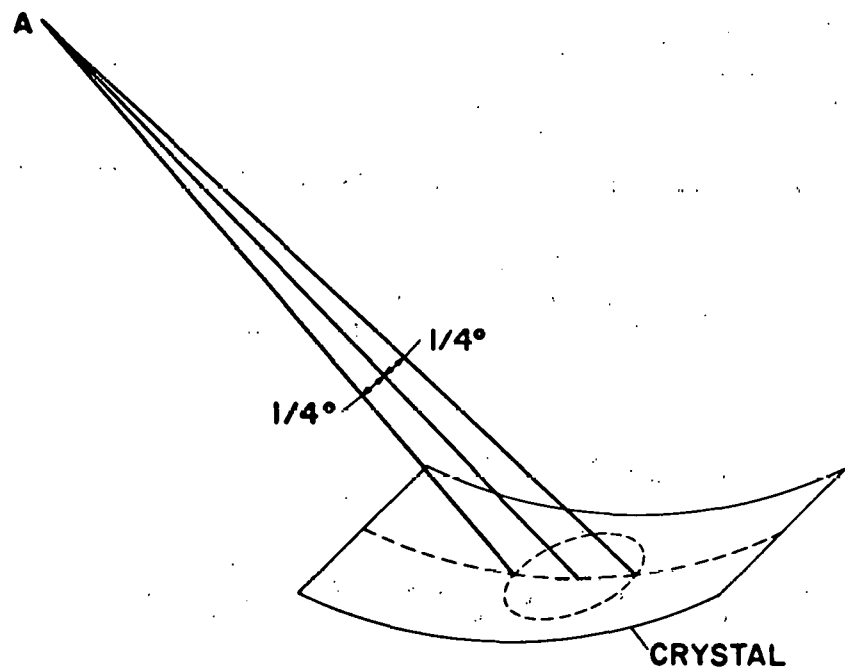
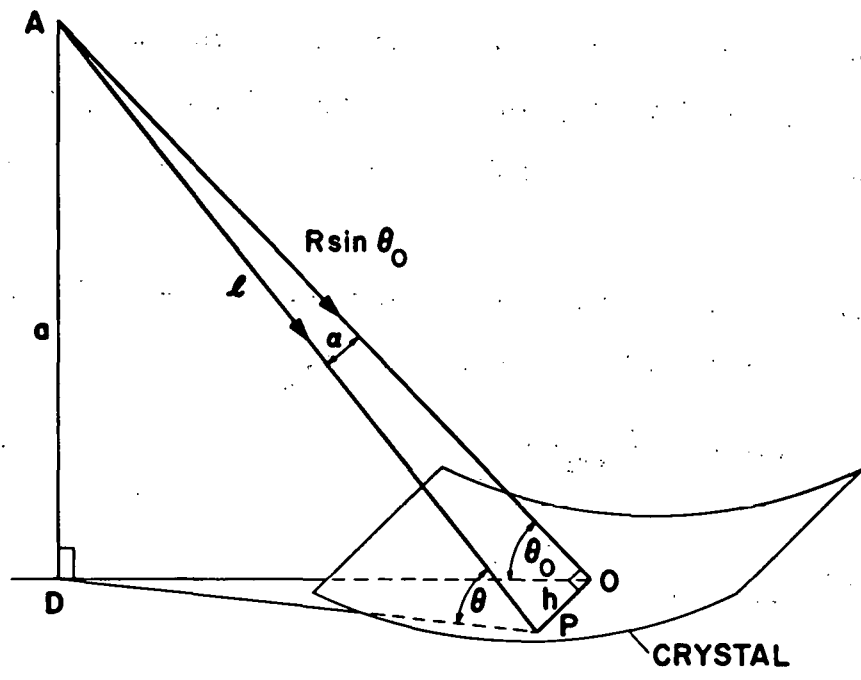


Fig. 20-a.-The effect of beam divergence in the plane perpendicular to the plane of divergence.

Fig. 20-b.-The effect of the angular diameter of the sun.



chord AO is the central axis as before. The ray AP represents a path of x-rays that are incident at point P, located a distance h , from point O. The distance h is measured perpendicular to the plane of dispersion.

The angle OAP is denoted by α , and the angle between AP and the tangent to the crystal surface at P is θ . Since

$$\sin \theta = \frac{a \cos \alpha}{R \sin \theta_0} \quad [12]$$

and

$$\cos \alpha = \left(1 - \frac{h^2}{l^2}\right)^{1/2}, \quad [13]$$

then

$$\begin{aligned} \sin \theta &= \frac{a}{R \sin \theta_0} \left(1 - \frac{h^2}{l^2}\right)^{1/2} \\ &= \frac{a}{R \sin \theta_0} \left(1 - \frac{\frac{h^2 \cos^2 \alpha}{R^2 \sin^2 \theta_0}}{1 - \frac{h^2 \cos^2 \alpha}{R^2 \sin^2 \theta_0}}\right)^{1/2}. \end{aligned} \quad [14]$$

But

$$\frac{\frac{h^2 \cos^2 \alpha}{R^2 \sin^2 \theta_0}}{1 - \frac{h^2 \cos^2 \alpha}{R^2 \sin^2 \theta_0}} \ll 1. \quad [15]$$

Expanding the expression in parentheses and keeping the first two terms gives

$$\sin \theta \approx \sin \theta_0 \left(1 - \frac{1}{2} \frac{\frac{h^2 \cos^2 \alpha}{R^2 \sin^2 \theta_0}}{1 - \frac{h^2 \cos^2 \alpha}{R^2 \sin^2 \theta_0}}\right). \quad [16]$$

If

$$\theta - \theta_0 = \delta \theta(\alpha), \quad [17]$$

then

$$\sin \theta = \sin(\theta_0 + \delta \theta) = \sin \theta_0 \cos \delta \theta + \cos \theta_0 \sin \delta \theta. \quad [18]$$

Using the small angle approximations

$$\sin \delta\theta \approx \delta\theta$$

$$\cos \delta\theta \approx 1$$

gives

$$\sin \theta = \sin \theta_0 + \cos \theta_0 (\delta\theta). \quad [19]$$

Equating the two expressions for $\sin \theta$ gives

$$\delta\theta(\alpha) \approx -\frac{1}{2} \alpha^2 \tan \theta_0. \quad [20]$$

To first order, the effects of α and β are independent and

$$\begin{aligned} \delta\theta(\alpha, \beta) &= \delta\theta(\beta) + \delta\theta(\alpha) \\ &= \frac{1}{2} \beta^2 \cotan \theta_0 - \frac{1}{2} \alpha^2 \tan \theta_0. \end{aligned} \quad [21]$$

The Sun as a Source

The magnitude of the defocusing effect when the sun is the source and the spectrometer axis is aligned with the instrument-sun line is illustrated in Fig. 20-b. For a pinhole aperture (or an element of area $dxdy$ of a finite aperture) located on the spectrometer axis, an image of the sun is formed on the surface of the crystal. The angle of incidence of the incoming x-rays varies over the illuminated area according to relation [21] above. Since the sun has an angular diameter of about $1/2$ deg, the maximum absolute value of α and β is $1/4$ deg. The maximum value of $\delta\theta(\alpha, \beta)$ is therefore very small (< 0.1 min of arc for the KAP stations and < 0.13 min of arc for the stearate stations) for the divergence of the sun, and for all the stations of this experiment the deviation from the proper Bragg angle caused by the sun's finite angular extent can be neglected compared to the width of the crystal rocking curves. The effect of the bent crystal is to

compensate for the angular divergence of the sun so that x-rays from all parts of the solar disk are incident at very nearly the same angle and are reflected with equal efficiency.

For the case where the instrument is not pointed accurately at the center of the sun, or for a small aperture that is displaced from the instrument axis, the image of the sun is formed away from the center of the crystal. Large values of $\delta\theta(\alpha, \beta)$ can result in these instances, but the value of $\delta\theta$ is essentially constant over the entire image of the sun. The x-rays from all parts of the solar disk are still reflected with the same, but a lower, efficiency. The fact that x-rays from all parts of the solar disk are reflected with the same efficiency is an important consideration since it means that the measured flux is the integrated flux from the entire solar disk.

The uniform integration over the entire disk is an advantage of the curved crystal geometry over a flat crystal spectrometer when it is desired to measure the total flux in a particular wavelength region. A flat crystal scanning spectrometer used without collimation has a resolution limited by the angular width of the sun. Sharp lines that are emitted from the entire solar disk are observed as broad lines, with their widths determined by a combination of the divergence of the source and the natural width of the crystal. Emission from discrete areas on the sun can result in a single emission line producing several distinct lines in the observed spectrum. The observed shape of any line results from the complicated folding together of the instrumental angular sensitivity and the spatial distribution of the source over the solar disk. The separation of these two effects to deduce the

total flux in a particular line in general requires precise knowledge of the crystal rocking curve and a priori information about the source distribution. This complication is avoided in the curved crystal instruments at the loss, of course, of continuous scan information. It should be remembered, also, that the line ratios measured with the curved crystal spectrometers are ratios of averages taken over the entire solar disk.

The Effect of Aperture Width and Pointing Errors

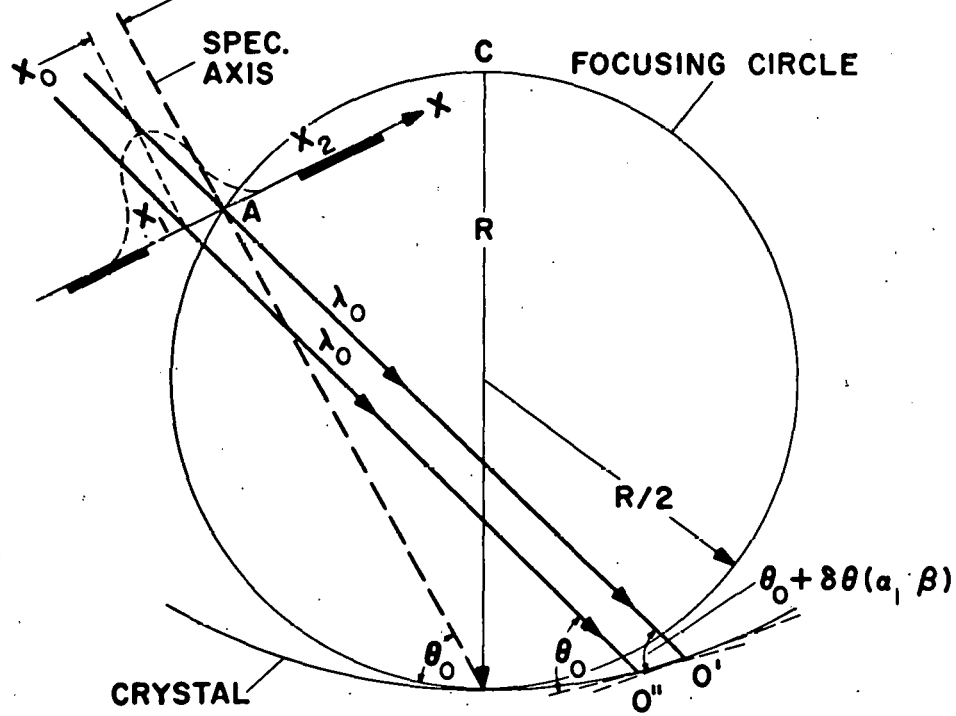
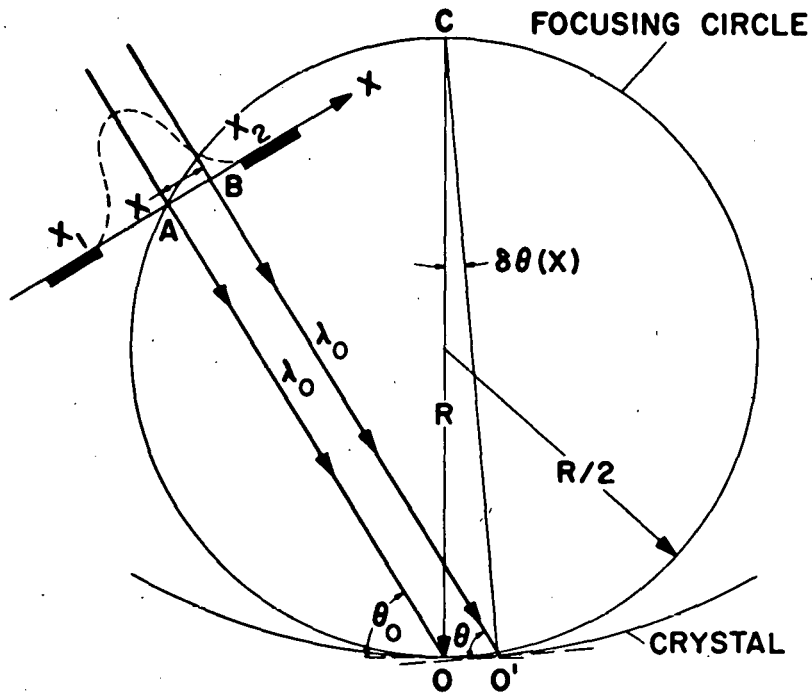
The variation of the angle of incidence with pointing errors and the effects of a finite entrance aperture must still be considered, but they can be examined for the case of a perfectly collimated beam where the x-rays from all parts of the sun are assumed to be incident parallel to the ray from the center of the sun. The situation for a wide entrance aperture is shown in Fig. 21-a for the case of perfect pointing. AO is again the instrument axis and the aperture width is measured from this line, extending to x_1 in one direction and x_2 in the other. (The slit width is exaggerated for clarity.) The path AO makes an angle θ_0 with the crystal surface at O. Because of the curvature of the crystal the ray BO', parallel to AO but displaced from it a distance x, does not make an angle θ_0 with the crystal surface at O'. X-rays that travel along this path have an angle of incidence θ , where

$$\delta\theta(x) = \theta - \theta_0 = \frac{S}{R} = \frac{x}{R \sin \theta_0}. \quad [22]$$

This means that only the x-rays entering the aperture at $x = 0$ are

Fig. 21-a.-The effect of aperture width on the focusing
and resolution of Johann curved crystal spectrometers.

Fig. 21-b.-The defocusing caused by pointing errors.



diffracted with the maximum efficiency. X-rays entering the aperture at any point for which $x \neq 0$ will be diffracted with less efficiency, depending on the shape of the crystal rocking curve. The entrance aperture also has a finite length perpendicular to the plane of dispersion, but the above effect is independent of the position along the length of the slit.

The crystal rocking curve is the function that gives the reflection efficiency of the crystal as a function of the angle of incidence for a perfectly collimated, monochromatic incident beam. An excellent approximation to this ideal function can be measured experimentally using double-crystal spectrometers. The exact shape of the curve depends on the type of crystal and the wavelength of the x-rays for which the measurement is made. In general it can be said that the curve has a peak at the angle $\theta = \theta_0$ where θ_0 satisfies the Bragg condition, and is roughly symmetrical about θ_0 . When expressed as a function of $\delta\theta = \theta - \theta_0$, it is maximum at $\delta\theta = 0$ and is symmetrical about this origin. Whatever its exact shape, the result for the curved crystal spectrometer is that the reflection efficiency of the crystal for the incident x-rays is a function of the variable x . This is shown schematically by the dashed curve in the figure.

For the case of perfect pointing, illustrated in Fig. 21-a, and a monochromatic beam of wavelength λ_0 , the expression for the efficiency of the spectrometer can be derived as follows. Consider a small element of area $dxdy$ of the entrance aperture located at $x = x_0$ and $y = y_0$. If F is the incident flux in photons/cm²-sec, then $F dxdy$ photons/sec are incident on the crystal surface through this area. The angle of

incidence of these x-rays is given by

$$\theta = \theta_0 + \delta\theta(x_0)$$

If $I(x)$ defines the reflection efficiency as a function of x , then these x-rays are reflected with an efficiency $I(x_0)$, and $I(x_0) F dx dy$ photons/sec will reach the Geiger counter. The overall efficiency of the counter is given by the product $T_w T_{uv} E_{gc}$, where

T_w = transmission of the counter window,

T_{uv} = transmission of the ultraviolet filter,

and E_{gc} = counting efficiency of the Geiger counter for photons that enter the sensitive volume.

The incremental count rate will be

$$dC = F T_w T_{uv} E_{gc} I(x) dy dx$$

and

$$C = F T_w T_{uv} E_{gc} \int_y^x \int I(x) dy dx . \quad [23]$$

The above relation applies to the special case of monochromatic radiation incident parallel to the spectrometer axis. To extend this to the more general case where the flux is not parallel to the axis and has a wavelength different from λ_0 it is useful to express equation [23] in a somewhat different form. The integral in [23] is over the geometrical area of the entrance aperture and $I(x)$ expresses the crystal reflection efficiency as a function of x . The limits of integration are the edges of the slit. Using equation [22] to change the integration variable from x to $\delta\theta$ gives

$$C = F T_w T_{uv} E_{gc} R \sin \theta_0 \int_y^{\delta\theta_2} \int_{\delta\theta_1} I(\delta\theta) d(\delta\theta) dy \quad [24]$$

where $I(\delta\theta)$ is the rocking curve of the crystal. The limits on the integral over $\delta\theta$ are given by

$$\delta\theta_1 = \frac{x_1}{R \sin \theta_0}$$

$$\delta\theta_2 = \frac{x_2}{R \sin \theta_0}$$

where x_1 and x_2 define the edges of the slit.

The situation for an incident beam that is not parallel to the spectrometer axis is shown in Fig. 21-b. Let AO' be the path of the incident photons from the center of the entrance aperture to any general point O' on the crystal surface, not necessarily in the plane of dispersion. The angles α and β define the direction of AO' relative to the instrument axis AO , with β being the angle (measured in the plane of dispersion) between AO and the projection of AO' into the dispersion plane, and α the angle (measured perpendicular to the plane of dispersion) between AO' and the projection of AO' into the plane of dispersion. Referring to equation [21], the angle of incidence of AO' is given by

$$\theta = \theta_0 + \delta\theta(\alpha, \beta) = \theta_0 + \left(\frac{1}{2} \beta^2 \cotan \theta_0 - \frac{1}{2} \alpha^2 \tan \theta_0 \right), \quad [25]$$

and the ray from the center of the aperture is not reflected with the peak efficiency. However, the shape of the efficiency curve across the entrance aperture is exactly the same as for the previous case

when α and β were zero. The only difference is that the curve has been shifted relative to the center of the aperture. The peak reflection efficiency still occurs for the ray which has an angle of incidence equal to θ_0 . Since the total change in the angle of incidence for a ray entering the aperture at x with a direction defined by α and β is given by

$$\delta\theta(\alpha, \beta, x) = \frac{1}{2} \beta^2 \cotan \theta_0 - \frac{1}{2} \alpha^2 \tan \theta_0 + \frac{x}{R \sin \theta_0} \quad [26]$$

the ray for which $\delta\theta = 0$ enters the aperture at

$$x' = R \sin \theta \left(\frac{1}{2} \alpha^2 \tan \theta_0 - \frac{1}{2} \beta^2 \cotan \theta_0 \right). \quad [27]$$

Expression [24] can then be applied directly to this more general case. The function $I(\delta\theta)$ is still exactly the same rocking curve as before so the only difference is the limits of integration. For α and β not zero, these limits are

$$\delta\theta_1 = \frac{1}{2} \beta^2 \cotan \theta_0 - \frac{1}{2} \alpha^2 \tan \theta_0 + \frac{x_1}{R \sin \theta_0}$$

$$\delta\theta_2 = \frac{1}{2} \beta^2 \cotan \theta_0 - \frac{1}{2} \alpha^2 \tan \theta_0 + \frac{x_2}{R \sin \theta_0}$$

and

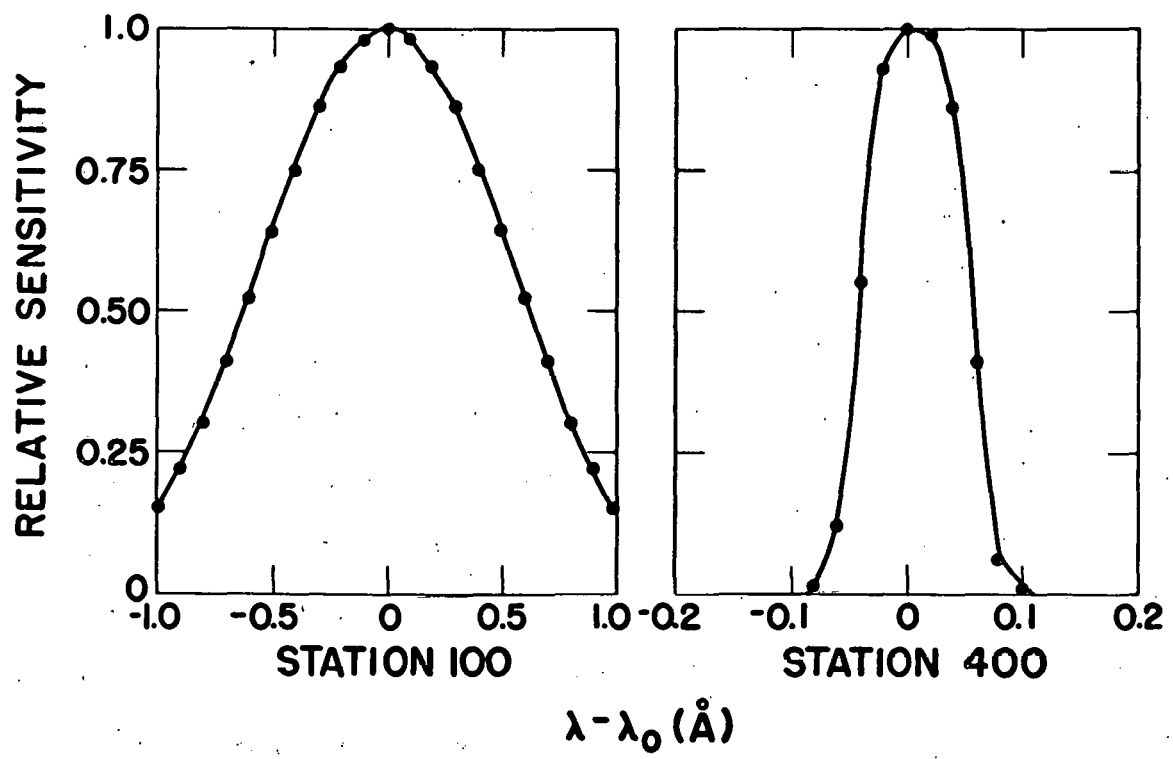
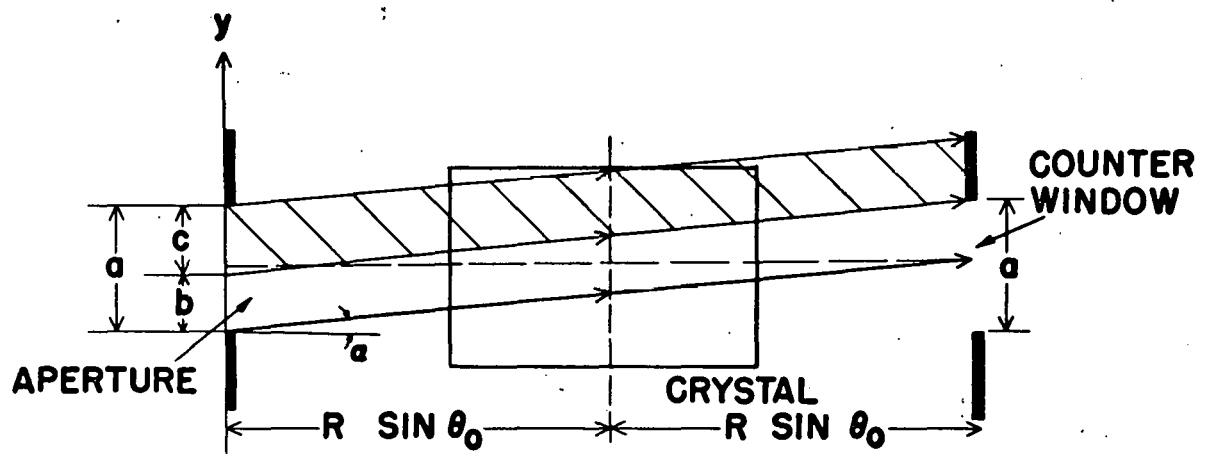
$$\delta\theta_2(\alpha, \beta, x_2)$$

$$C(\alpha, \beta) = F T_w T_{uv} E_{gc} R \sin \theta_0 \int_y \int_{\delta\theta_1(\alpha, \beta, x_1)}^{\delta\theta_2(\alpha, \beta, x_2)} I(\delta\theta) d(\delta\theta) dy. \quad [28]$$

The integration over y is straightforward, involving only the geometrical conditions of the spectrometer. This is illustrated in Fig. 22-a which shows a plan view of a spectrometer. The aperture has a total length a , exactly equal to the length of the counter window. For

Fig. 22-a.-A plan view of a curved crystal spectrometer.

Fig. 22-b.-Typical resolution curves for a lead stearate station and a KAP station.



$\alpha = 0$ all of the flux entering the aperture and reflected from the crystal reaches the counter window. The figure shows the situation for $\alpha \neq 0$. Photons entering the aperture through the region "c" do not enter the counter window and are lost. Only those photons entering through the region "b" can reach the counter window. The integral over y can be performed immediately as

$$\int_a^b dy = \int_a^b (1)dy + \int_b^c (0)dy = b(\alpha), \quad [29]$$

where

$$\left\{ \begin{array}{ll} b(\alpha) = a - 2 R \sin \theta_0 \tan \alpha & \text{for } \alpha < \alpha_{\max} \\ = 0 & \text{for } \alpha > \alpha_{\max} \end{array} \right.$$

and

$$\alpha_{\max} = \frac{a}{2 R \sin \theta_0}.$$

This gives

$$C(\alpha, \beta) = F T_w T_{uv} E_{gc} R \sin \theta_0 b(\alpha) \int_{\delta\theta_1}^{\delta\theta_2} I(\delta\theta) d(\delta\theta). \quad [30]$$

The integral over $\delta\theta$ requires in principle an exact knowledge of the shape of the rocking curve $I(\delta\theta)$. There is a situation, however, for which no knowledge of the shape of $I(\delta\theta)$ is required. If the entrance aperture is wide in the x direction in the sense that it subtends an angle on the crystal that is large compared to the width of the rocking curve, then the value of the function $I(\delta\theta)$ at the limits of integration is effectively zero. In this case the limits can be replaced by $+\infty$ and $-\infty$ and [30] becomes

$$C(\alpha, \beta) = F T_w T_{uv} E_{gc} R \sin \theta_0 b(\alpha) \int_{-\infty}^{+\infty} I(\delta\theta) d(\delta\theta) \quad [31]$$

where the integral in [31] is the total area under the rocking curve and is exactly equal to the quantity called the "coefficient of reflection" by Compton and Allison (15). In this case [31] becomes

$$C(\alpha, \beta) = F T_w T_{uv} E_{gc} R \sin \theta_0 b(\alpha) R_0 \quad [32]$$

where

$$R_0 = \int_{-\infty}^{+\infty} I(\delta\theta) d(\delta\theta) \quad [33]$$

The value of R_0 can be measured in the laboratory without the complication of a double-crystal spectrometer. It is the most direct and easily measured parameter of a crystal that relates to its reflection properties.

For the KAP stations the condition of a "wide" aperture is completely satisfied since the aperture has an effective angular width several times as large as the width of the KAP rocking curves. For the stearate stations the effective angular width of the apertures is greater than the natural width (full width at half maximum) of the stearate crystals, but less than twice the natural width. For these stations it is not possible to replace the integral in [31] by R_0 without introducing an error. It is convenient to write [32] as

$$C(\alpha, \beta) = F T_w T_{uv} E_{gc} R \sin \theta_0 b(\alpha) R_0 K(\alpha, \beta, x_1, x_2) \quad [34]$$

where

$$K(\alpha, \beta, x_1, x_2) = \frac{1}{R_0} \int_{\alpha_1}^{\alpha_2} I(\delta\theta) d(\delta\theta), \quad [35]$$

with

$$\alpha_1 = \delta\theta_1(\alpha, \beta, x_1)$$

and

$$\alpha_2 = \delta\theta_2(\alpha, \beta, x_2).$$

K is then the ratio of the actual area of the rocking curve subtended by the aperture to the total area of the rocking curve.

Spectrometer Resolution

One further property of the spectrometers should be discussed. As mentioned earlier, the measured fluxes will be the sum of the line intensity plus the integrated continuum. The contribution of the continuum depends on its intensity and the resolution of the instrument. The shape of the resolution curve can be obtained by calculating the value of K for wavelengths close to but different than λ_0 . Assuming a wavelength slightly different than λ_0 simply causes an additional slight shift of the crystal rocking curve relative to the edges of the aperture, resulting in a change in the limits of the integral in equation [35]. The limits become functions of λ as well as α , β , and x .

To calculate the value of K (for values other than K = 1) it is necessary to specify the function I($\delta\theta$). Since the exact shape of I($\delta\theta$) was not known for the stearate crystals and could not be measured accurately at these wavelengths, it is important to consider the sensitivity of the various calculations to the shape of this curve.

As discussed in Part I, pointing errors were extremely small throughout both flights. This simplifies very much the necessary calculations since α and β can be considered zero. The function b(α)

in equation [34] reduces to a, the length of the aperture, and equation [35] becomes

$$K(x_1, x_2, \lambda) = \frac{1}{R_0} \int_{\ell_1}^{\ell_2} I(\delta\theta) d(\delta\theta) \quad [36]$$

where for this case

$$\ell_1 = \delta\theta_1(x_1, \lambda)$$

and

$$\ell_2 = \delta\theta_2(x_2, \lambda).$$

Consider first the calculation of K for $\lambda = \lambda_0$, the wavelength for which the spectrometer is focused. For the KAP stations $K(x_1, x_2, \lambda_0) = 1$ with essentially no error. For the stearate stations the limits on the integral are symmetrical about $\delta\theta = 0$ and are larger than the full width at half maximum of $I(\delta\theta)$. Although the exact details of the rocking curve could not be measured for the stearates, the general shape could. Because the natural widths of the soap film crystals are quite large, a good approximation of the rocking curve can be obtained by simply making a Bragg scan of a well filtered emission line collimated so that the instrumental width is small compared to the natural width of the crystal. Such a measurement was made for each stearate crystal that was flown. There were differences in natural widths between the crystals but the shape of the curves were all the same and had the general appearance of a gaussian. Since the integral in [36] includes all of $I(\delta\theta)$ except the wings of the curve, the assumption that $I(\delta\theta)$ was a gaussian with the measured half-width was considered to be a good one. The error in this assumption amounts to the difference

in area under the wings of a gaussian and the area under the wings of the true rocking curve.

The calculation of the resolution curve for the spectrometers requires the evaluation of [36] as a function of λ for values of λ near λ_0 . The qualitative way in which $K(x_1, x_2, \lambda)$ varies with λ can be visualized by referring to Fig. 21-a. When $\lambda = \lambda_0$ the rocking curve is centered with respect to the limits set by the edges of the aperture. For a slightly different value of λ , the rocking curve is shifted to one side. As λ differs more and more from λ_0 , the rocking curve moves farther from the center of the aperture until, for sufficiently large values of λ , the rocking curve is entirely outside the limits of the aperture. The relative efficiency for any λ is just the ratio of the area of the rocking curve subtended by the slit to the area subtended at $\lambda = \lambda_0$. If the rocking curve were a delta function, then the resolution curve would clearly be rectangular with the limits determined by the width of the aperture. This is very nearly the case for the KAP stations. As the width of the rocking curve increases the resolution curve becomes rounded at the edges. As long as the rocking curve is narrow compared to the aperture angular width, then the wavelength for which the relative efficiency is equal to 1/2 the value at λ_0 is always the same. It is clear that if the natural width of the rocking curve is known, then the shape of the resolution curve is not very sensitive to small departures of the rocking curve from a gaussian shape. The resolution of each of the spectrometers was calculated and Fig. 22-b shows the resulting curve for a KAP station

and a stearate station. The equivalent width of the stearate stations is about 1 \AA compared to about 0.1 \AA for the KAP stations. This means that the KAP crystals have ten times better line-to-continuum discrimination than the stearates.

It should be emphasized that the details of the calculations of $K(x_1, x_2, \lambda)$ described above, both to determine the spectrometer sensitivities for $\lambda = \lambda_0$ and to determine the shape of the resolution curve, cannot affect the finally determined sensitivities in any important way. For all the KAP stations, $K(x_1, x_2, \lambda_0)$ is equal to unity. For the stearate stations the apertures were designed to subtend at least one full crystal width of the rocking curve. The value of $K(x_1, x_2, \lambda_0)$ is therefore greater than 0.76 and less than unity if the rocking curve is a gaussian. Even if $K(x_1, x_2, \lambda_0)$ is set equal to one for all the stations, the worst error that can be introduced is less than 25%. The evaluation of $K(x_1, x_2, \lambda_0)$ is a first order correction, and the uncertainties caused by assuming a gaussian for $I(\delta\theta)$ are errors in the correction term. Similarly for the calculation of the resolution curve the actual contribution of the continuum to the measured flux is determined by an integral over the resolution curve and, for a continuum that is uniform over this interval, depends only on the area under the curve. A simple calculation shows that if R_0 and the width of $I(\delta\theta)$ are known, the area under the resolution curve is almost independent of the shape of $I(\delta\theta)$.

X-Ray Calibration

Rewriting equation [34] for α and $\beta = 0$ gives

$$C(\lambda_0) = F(T_w T_{uv} E_{gc} R_0) a R \sin \theta_0 K(\lambda_0) . \quad [37]$$

In addition to the crystal half-widths measured for use in the calculation of $K(\lambda_0)$, the four quantities grouped in parentheses had to be determined by x-ray calibration. The measurement of R_0 , the coefficient of reflection, is in principle straightforward and is described by Compton and Allison (15). The crystal was mounted in a single crystal Bragg spectrometer with a proportional counter detector. With the crystal moved aside, the intensity of the incident beam of wavelength λ_0 was determined. The crystal was then put into the beam and, starting at an angle of incidence sufficiently far removed from θ_0 , was scanned at a constant angular velocity through an angle large enough to encompass the total diffracted beam. The integrated intensity of the diffracted beam was measured by counting continuously during the scan. The coefficient of reflection was then determined from

$$R_0 = \frac{E \omega}{P_0} \quad [38]$$

where

E = integrated intensity of diffracted beam

ω = angular velocity of the scan

P_0 = intensity of incident beam.

That expression [38] is in fact equivalent to the previous definition of R_0 given in equation [33] can be seen as follows. The intensity of the diffracted beam when the crystal is at an angle θ is given by $P_0 I(\delta\theta)$, where $\delta\theta = \theta - \theta_0$. In a time dt , a number of counts given by

$$dE = P_0 I(\delta\theta) dt$$

will be observed in the diffracted beam. But

$$dt = \frac{d(\delta\theta)}{\omega}$$

and

$$dE = \frac{P_0 I(\delta\theta) d(\delta\theta)}{\omega}$$

Therefore:

$$E = \frac{P_0}{\omega} \int_{-\infty}^{+\infty} I(\delta\theta) d(\delta\theta), \quad [39]$$

where the limits of $+\infty$ and $-\infty$ assume that the scan is over a large enough angle to include the wings of $I(\delta\theta)$. The integral in [39] is exactly the previous definition of R_0 . The measured value of R_0 is independent of the angular divergence of the beam as long as the beam divergence is large compared to the crystal natural width and small compared to the total angle covered by the scan. A nonmonochromatic beam can produce large errors in R_0 since all wavelengths are included in the measurement of the incident beam, but wavelengths very different from λ_0 are absent in the diffracted beam. To reduce this effect as much as possible the incident beam was obtained by illuminating a fluorescent target with x-rays from a low voltage x-ray tube and using the fluorescent x-rays for the calibration. Characteristic lines produced in fluorescence are quite monochromatic and pulse height discrimination of the pulses from the proportional counter reduced the effect of scattered primary x-rays. The major difficulty in this calibration was the lack of intensity in the primary beam.

A general curve of R_0 vs λ for lead stearate crystals has been obtained by Henke (8) from measurements made on a number of crystals

at several different wavelengths. The relative shape of this curve was found to be the same for all lead stearate crystals, and measured values of R_0 at two particular wavelengths for each of the flight crystals were used to normalize this general curve. The appropriate value of R_0 at the wavelength for which the crystal was used was then taken from this normalized curve. Measurements of R_0 were reproducible to better than 10%, but the accuracy of the absolute values of R_0 are believed to be no better than 20%.

The Geiger counter absorption efficiency is shown in Fig. 23. This curve was calculated from the known dimensions of the counter and the appropriate absorption coefficients for the gas mixture of 1.4% butane, 4.8% argon, and 93.8% helium. Since the absorption was nearly total for all stations, errors in this calculation are negligible. Considerable care was taken to insure that double pulsing did not occur in the counters and it was assumed that one count was recorded for each photon absorbed.

The first step in the calibration of the Geiger counter pressure windows was to determine the transmission of the nickel mesh used to support the Formvar films. In the wavelength region from 19-34 Å the wires of the mesh are opaque to x-rays, so the transmission just depends on the amount of open area of the mesh. This was measured optically for each of the windows before the Formvar film was applied. To confirm that the optically measured transmissions were the same as the x-ray transmission, several of the windows were also calibrated with x-rays and the results compared with those obtained optically. In all cases the agreement was within a few percent. The average transmission

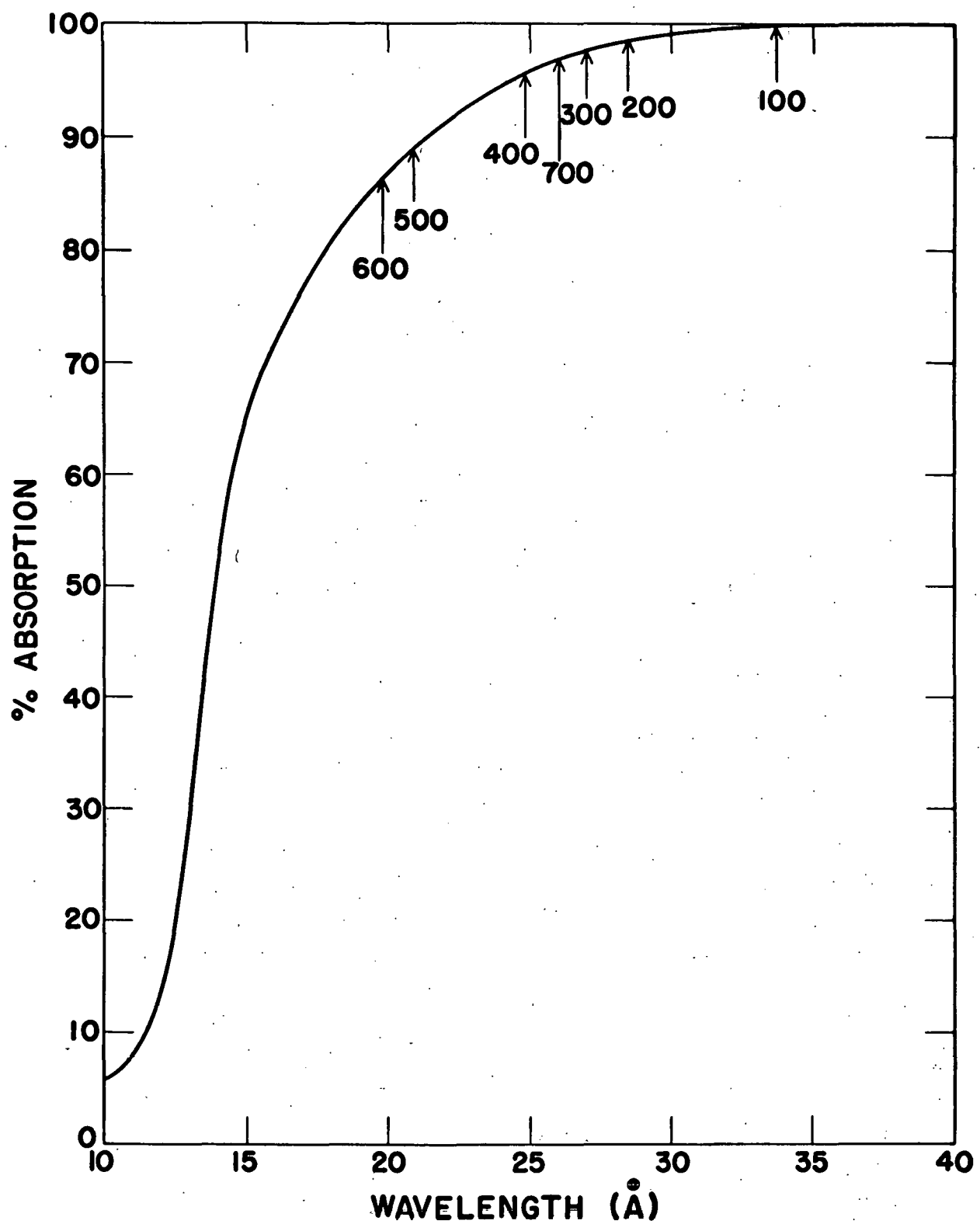
of the mesh was about 65%.

It was necessary next to determine the transmission of the aluminized Formvar films used as pressure windows and ultraviolet filters. Since the transmission of the films depends strongly on the x-ray wavelength, the transmission of each film had to be determined for the wavelength appropriate to the spectrometer on which it was used. Measurements could not be made at the exact wavelengths for which the spectrometers were focused, so it was necessary to make transmission measurements as close as possible to desired wavelengths and to extrapolate from these measurements. The complete procedure was as follows.

Using characteristic fluorescence lines obtained by illuminating targets of the appropriate elements with the primary beam from a high intensity, low voltage x-ray tube, the transmission of each of the films was measured at three x-ray wavelengths: $\lambda_1 = 18.3 \text{ \AA (F}_K\text{)}$, $\lambda_2 = 23.6 \text{ \AA (O}_K\text{)}$, and $\lambda_3 = 44.6 \text{ \AA (C}_K\text{)}$. Before being used to calibrate the films the fluorescence emission from each of the targets was scanned with a Bragg spectrometer to insure that it was essentially monochromatic. As a further precaution a proportional counter was used to measure the beam intensity and a narrow pulse height window was set to accept only those pulses corresponding to the proper x-ray energy.

The transmission of a two-element film such as these at a wavelength λ can be expressed as

Fig. 23.-Absorption efficiency of the flight Geiger counters.



$$(T)_\lambda = \left(\frac{I}{I_0} \right)_\lambda = \exp \left[-\mu_{a\lambda} t_a \right] \exp \left[-\mu_{f\lambda} t_f \right]$$

where

$\mu_{a\lambda}$ = mass absorption coefficient of aluminum at λ

$\mu_{f\lambda}$ = mass absorption coefficient of Formvar at λ

t_a = thickness of aluminum

t_f = thickness of Formvar.

If the absolute values of the absorption coefficients are known the measurement of the transmission at two wavelengths is sufficient to determine the thicknesses of aluminum and Formvar. However, if the transmission is measured at two wavelengths, λ_1 and λ_2 , then the transmission at any other wavelength, λ_3 , can be calculated by knowing only the relative values of the absorption coefficients at the three wavelengths. The absolute absorption coefficients in this energy region are somewhat uncertain, but the relative absorption coefficients at different wavelengths depend only on the shape of the absorption curve. On the small wavelength interval involved in these calculations the shape of this curve can be predicted with very little uncertainty.

The measured values of the transmission at the three wavelengths described above were first checked for internal consistency. The transmissions at λ_1 and λ_2 were used to calculate the expected transmission at λ_3 , and the calculation was compared with the measured transmission at this wavelength. If the measured and calculated values agreed, the data were assumed to be reliable. The transmission at the appropriate wavelength for each pressure window and ultraviolet filter was then calculated, using the measured transmissions at λ_1

and λ_2 . Table 5 gives the transmission of the windows and ultraviolet filters used on the flight spectrometers.

TABLE 5
PRESSURE WINDOW AND ULTRAVIOLET FILTER TRANSMISSIONS

Station	August 8		August 11	
	T_w	T_{uv}	T_w	T_{uv}
100	0.17	0.12	0.17	0.21
200	0.27	0.41	0.26	0.31
300	0.35	0.45	0.26	0.36
400	0.40	0.38	0.33	0.47
500	0.33	0.40	0.31	0.38
600	0.42	0.47	0.36	0.54
700	0.34	0.34	0.32	0.28

The precision of the measurements of the transmission of the pressure windows and ultraviolet filters was very good. The x-ray beams used for calibration were sufficiently intense to make the statistical uncertainties in the measurements negligible. The measured transmissions were reproducible to an accuracy of a few percent. Any serious errors in the transmission measurements were eliminated by the internal consistency check described above. However, it is very difficult to determine confidence limits on the absolute accuracy of the transmissions given in Table 5. For each of the stations in Table 5 the transmission was calculated for the appropriate wavelength (e.g., 33.74 Å for station 100) using the measured values of the transmission at two other wavelengths, λ_1 and λ_2 . The transmission at 33.74 Å is a complicated

function of the measured transmissions at λ_1 and λ_2 and the ratios of the absorption coefficients of aluminum and Formvar at the wavelengths λ_1 , λ_2 , and 33.74 Å. While the uncertainties in the measured transmissions at λ_1 and λ_2 can be estimated and are no more than $\pm 5\%$, only a qualitative estimate of the uncertainties in the various ratios of the absorption coefficients can be made. However, since the ratios depend only on the shape of the absorption coefficient curve and not on the absolute values of the coefficients, the uncertainties are not large. An absolute accuracy of $\pm 15\%$ for the values given in Table 5 is believed to be conservative.

Flight Spectrometer Efficiencies

Using the appropriate values of crystal half-widths, crystal efficiencies, pressure window and ultraviolet filter transmissions, and Geiger counter absorption efficiencies, the quantity

$$1/E_t = (T_w T_{uv} E_{gc} R_0) a R \sin \theta_0 K \quad [40]$$

was calculated for each station for both flights. The results are given in Table 6.

The experimental accuracy of the spectrometer sensitivities can be estimated by considering the possible errors in each of the terms of the product in equation [40]. The errors in the geometrical quantities a , R , and $\sin \theta_0$ are so small that they can be neglected. The quantity K is equal to one for the KAP stations and has a value between 0.76 and 1 for the stearate stations, with an uncertainty of about 5%. The Geiger counter efficiency, E_{gc} , is greater than 0.86 for all stations and cannot be in error by more than a few percent.

TABLE 6
FLIGHT SPECTROMETER EFFICIENCIES

Station	$1/E_t$	
	August 8	August 11
100	1.5×10^{-5}	$0.9 \times 10^{-5}^*$
200	3.6×10^{-5}	2.9×10^{-5}
300	28.0×10^{-5}	$5.6 \times 10^{-5}^*$
400	8.3×10^{-5}	8.3×10^{-5}
500	7.1×10^{-5}	6.2×10^{-5}
600	11.0×10^{-5}	10.0×10^{-5}
700	14.0×10^{-5}	12.0×10^{-5}

* The apertures of stations 100 and 300 were masked to 1/3 their original size to reduce the count rates.

As stated above, the uncertainty in the window and ultraviolet filter transmissions is no more than $\pm 15\%$ and the measured value of R_0 is believed to be accurate to $\pm 20\%$. Using these estimates the overall accuracy of the quantity E_t would be expected to be about $\pm 35\%$.

III. DATA ANALYSIS

Solar Activity

It is known that the x-ray emission from the sun is quite variable. Although there was no particularly strong solar activity on either August 8 or 11 it was certainly possible that the x-ray emission was different on the two days. As an independent check on the level of solar activity, the x-ray data obtained from detectors on two Vela satellites (16) were examined for the times of interest. These x-ray detectors are broadband instruments that integrate over two spectral bands, one from 0.5-5 Å and the other from 0.5-15 Å. No spectral data are obtained from these instruments, but they provide an excellent measure of the general level of solar activity over long periods of time. These data showed that the x-ray emission from the sun was almost a factor of two more intense on August 8 than on August 11 in the wavelength regions covered by these detectors. It is impossible to deduce in any quantitative way the effect of this difference on the flux values measured by any of the particular spectrometers, but it might be expected that the August 8 values would be somewhat higher than those measured on August 11.

Uncorrected Flux Values

The count rates for all stations are shown in Figs. 14-17, as a function of time during the flights. During the portion of the flights above the atmosphere the count rates were very nearly constant for all stations. Using the average count rates for each station over the five-minute period above the atmosphere (Table 4) and the spectrometer sensitivities (Table 6), the average values of the incident fluxes were calculated. The results are shown in Table 7.

TABLE 7
UNCORRECTED FLUX VALUES

Station	Wave-Length	Emission Line	Crystal	Uncorrected Flux (Photons/cm ² -sec)	
				August 8, 1966	August 11, 1966
100	33.74	C VI	Lyman- α	Pb-S	82 $\times 10^6$
200	28.47		Lyman- β	Pb-S	70 $\times 10^6$
300	26.99		Lyman- γ	Pb-S	45 $\times 10^6$
700	26.00	Continuum	Pb-S	26 $\times 10^6$	15 $\times 10^6$
400	24.78	N VII	Lyman- α	KAP	2.8×10^6
500	20.91		Lyman- β	KAP	1.1×10^6
600	19.83		Lyman- γ	KAP	0.5×10^6
					1.3×10^6

Without going into the details of the expected line intensity ratios or line-continuum ratios, which are discussed in Part IV, some general observations can be made about the flux values given in Table 7. Looking first at the nitrogen stations, the August 8

measurements show at least qualitatively the necessary decrease in intensity for the successively higher lines of the Lyman series. However, comparison of the results for station 600 from the two flights shows a difference that is far outside the expected accuracy of the measurements. Since the sun was more active on August 8, the higher value measured on August 11 is almost certainly not due to a difference in the incident flux levels.

The results for the lead stearate stations present a puzzling situation. The flux levels for stations 100, 300, and 700 on the two flights agree within the expected accuracy, but there is a large difference between the two flights for station 200. Even allowing for the more active sun on August 8, the difference is still larger than can be reasonably explained by experimental uncertainties. Also, the intensities of the various lines do not correspond in any apparent way to the expected pattern for lines in the same Lyman series. The values for station 700 are surprisingly high for the flux due to the continuum in this wavelength region. Even though this station integrates the higher lines of the carbon Lyman series, the measured levels would still have to be largely due to continuum.

Although the results from the number 800 stations show the spectrometers to be very insensitive to ultraviolet photons, the data from the stearate stations are very suggestive of a strong contamination by scattered ultraviolet light. The apparently high flux values, the inconsistencies between the same station for the two flights, and the apparent lack of any line structure would all be

expected if the observed count rates were due primarily to long wavelength ultraviolet photons that were scattered into the detectors. The question of whether or not the fluxes measured by the stearate stations were completely dominated by scattered ultraviolet light is of course a crucial one. The relative values for the measured fluxes given in Table 7 for the carbon lines are completely different from what would be expected for lines in a Lyman series. If the stations were sensitive to ultraviolet, the explanation is simply that the data are meaningless. If, on the other hand, it can be shown that the measured fluxes represent x-rays, it would be a satisfying confirmation of the experimental method, but the unexpected flux levels would be unexplained.

The continuous monitoring of the count rate in each station as the payloads reentered the atmosphere provided an excellent measurement of the atmospheric absorption as a function of altitude for most of the stations. In the following three sections these absorption data are analyzed in detail to determine, as definitely as possible, if the fluxes were contaminated by scattered ultraviolet light.

Atmospheric Absorption Data

To arrive at the curves of the observed transmission as a function of altitude, the count rate data shown in Figs. 16 and 17 were first normalized to give the ratio of I/I_0 as a function of time. Using the trajectory obtained from the radar tracking, a curve of transmission vs altitude for each of the stearate stations

was plotted. These curves are shown in Figs. 24 and 25. The same curves for the KAP stations on the August 8 flight are shown in Fig. 26. The curves for the KAP stations were included to illustrate the general, qualitative agreement between these stations and the stearate stations in spite of the scatter in the points introduced by the much lower count rates in the KAP stations. Shown in Fig. 27 is the absorption cross section of air for the wavelength region 10-100 Å. This curve was calculated for a standard dry atmosphere of nitrogen, oxygen, and argon as defined in reference (17) using the recently measured mass absorption coefficients of Henke (8). The wavelengths of the different spectrometers of this experiment are shown by arrows.

The first question was whether or not the measured fluxes were completely dominated by scattered ultraviolet. This question can be answered by simply comparing the transmission curves with the absorption coefficient data shown in Fig. 27.

Since the absorption coefficients for stations 200, 300, and 700 are not very different, their transmission curves should be similar. The curves for these three stations on both flights are very nearly the same. Referring again to Fig. 27, there is a very large drop in the absorption coefficient of air at 31 Å because of the K edge of nitrogen. Station 100 lies above the edge, and station 200 lies below the edge. If the fluxes measured by these two stations were in fact x-rays of the two expected wavelengths, there should be a considerable difference in the altitude at which they were

absorbed. If, on the other hand, these stations were measuring mostly scattered ultraviolet photons this difference in absorption coefficients would be completely masked. The data in Figs. 24 and 25 show that for both flights the flux measured by station 100 penetrated to lower altitudes than that of station 200. On both flights the altitude of unit optical depth ($I \cong 0.37 I_0$) is 20 kilometers lower for station 100 than for station 200.

The absorption coefficients for the wavelengths corresponding to stations 400, 500, and 600 are intermediate between those for stations 100 and 200. The absorption curves for these stations are shown in Fig. 26, and even though the statistical uncertainties are large for these stations the data are good enough to show that these curves lie between the curves for station 100 and those for station 200.

Thus the absorption data show the general features that would be predicted from the shape of the absorption coefficient curve. If the x-ray flux in the different stations had been completely masked by scattered ultraviolet photons even these general features of the absorption data would have been obscured. It is clear that x-rays of the proper wavelength comprised at least a sizable fraction of the measured fluxes.

Comparison with a Standard Atmosphere

In an attempt to provide a quantitative check of the data, the measured transmission curves were compared with transmission curves

Fig. 24.-Observed atmospheric attenuation of the x-ray fluxes measured by the stearate stations, August 8, 1966.

FLIGHT NUMBER I AUGUST 8, 1966

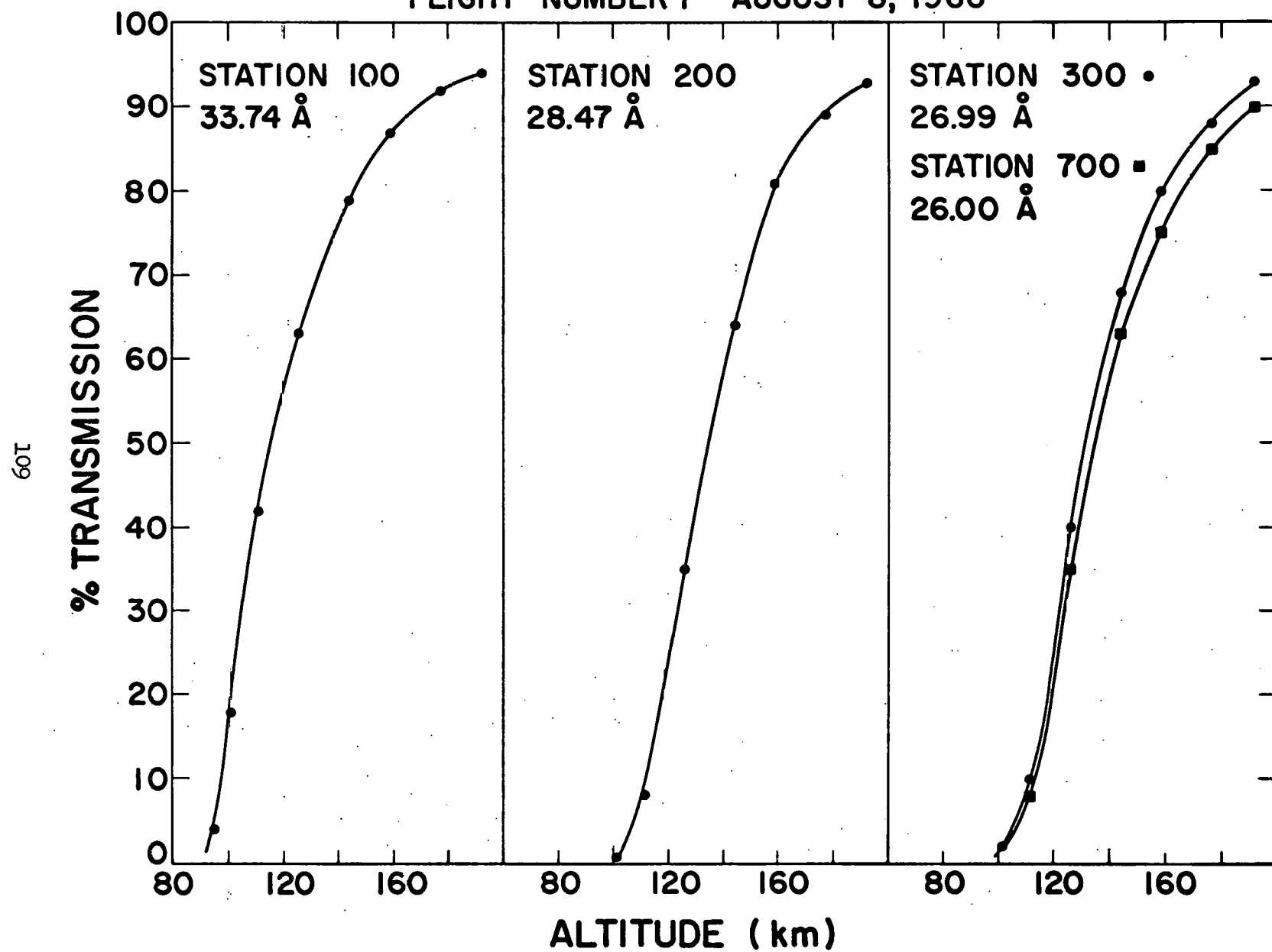


Fig. 25.-Observed atmospheric attenuation of the x-ray fluxes measured by the stearate stations, August 11, 1966.

FLIGHT NUMBER 2 AUGUST 11, 1966

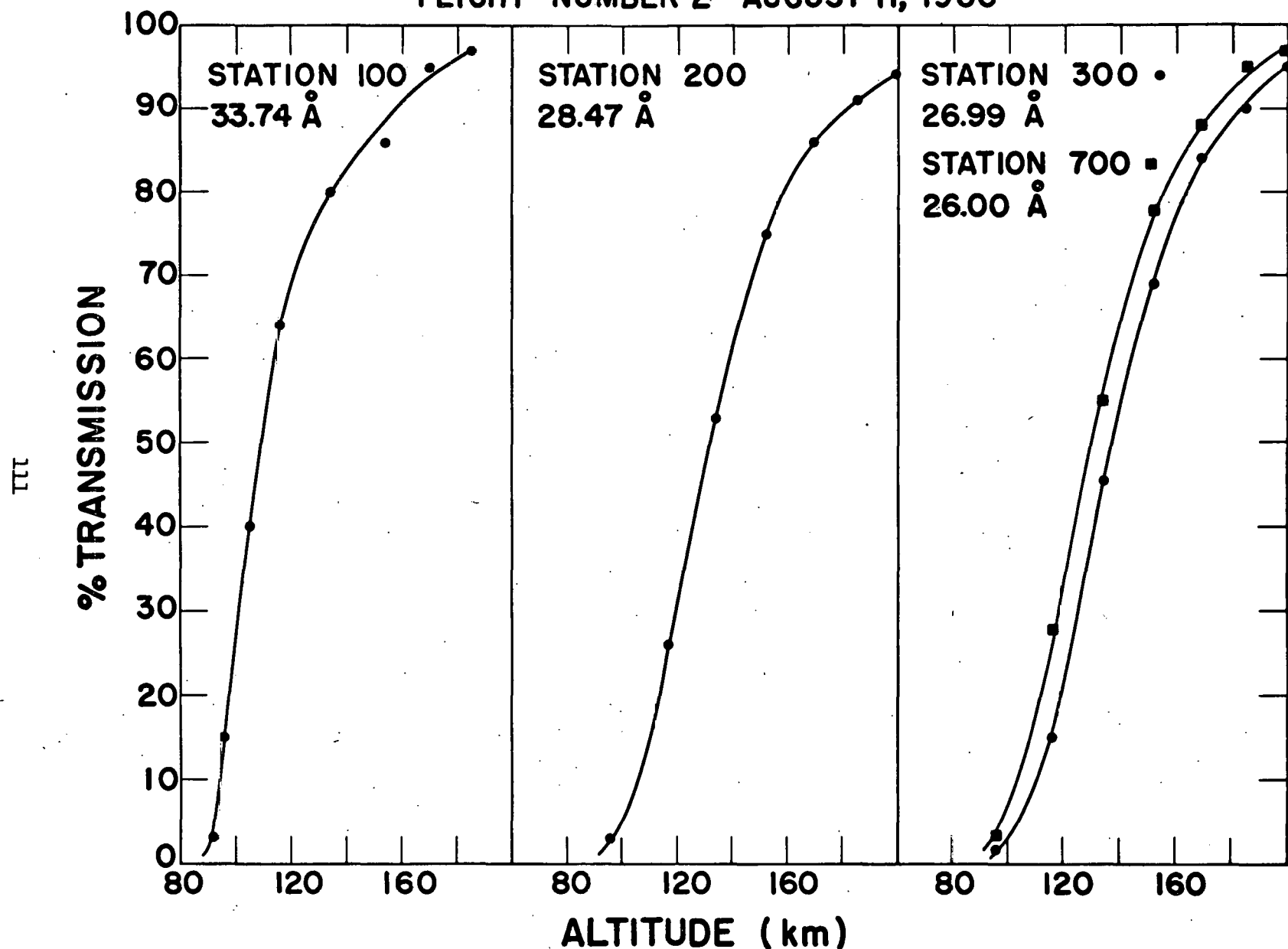
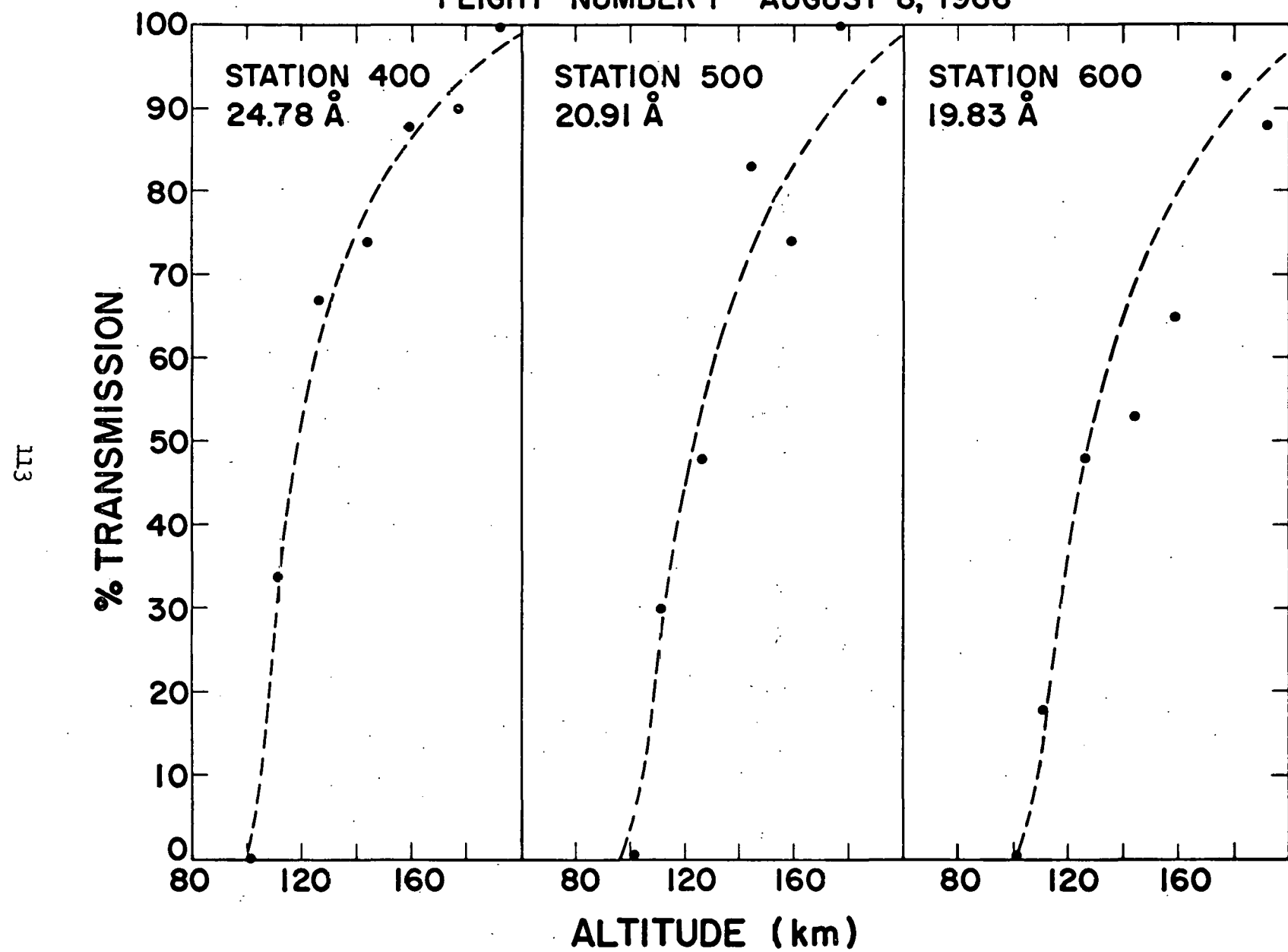
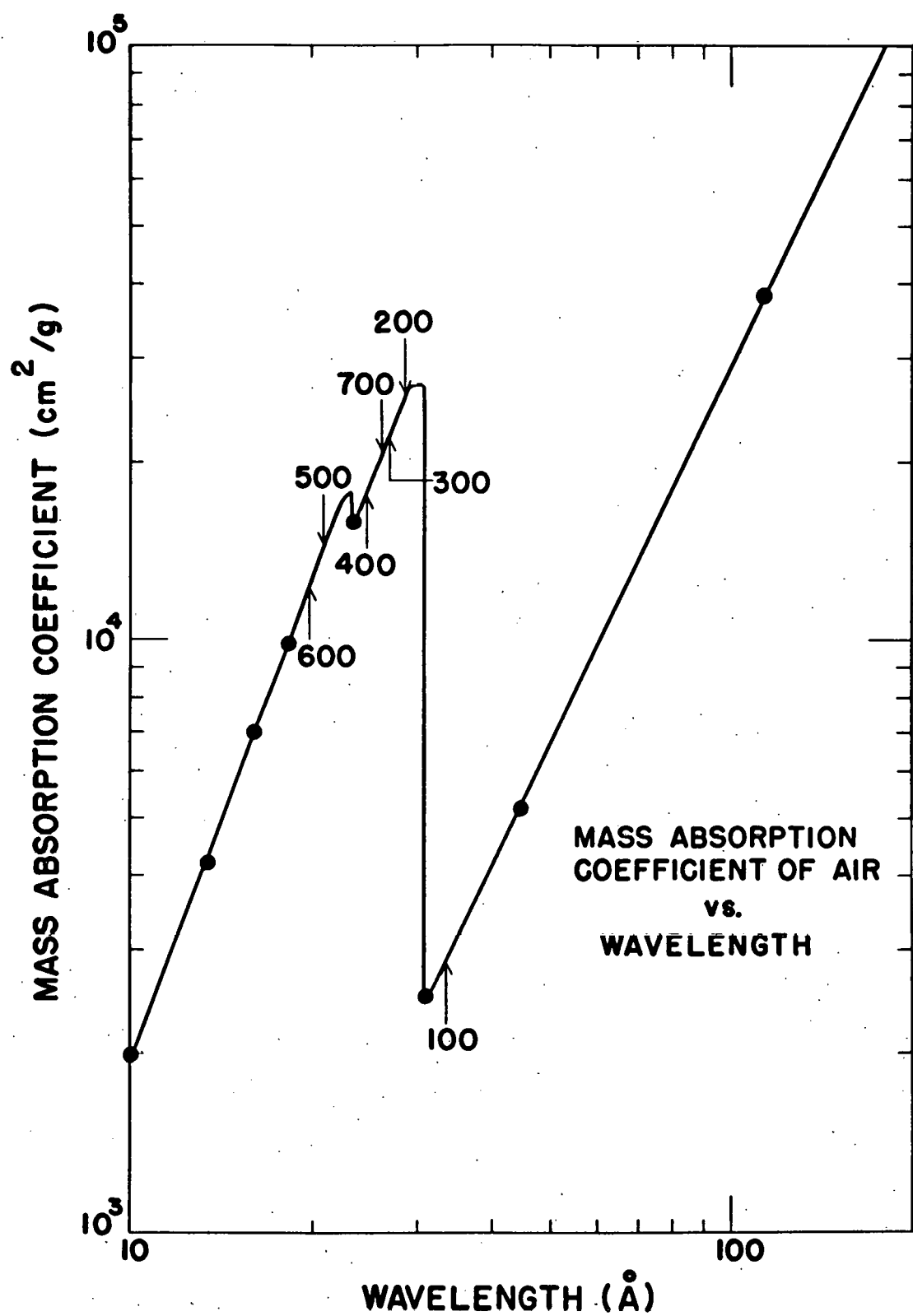


Fig. 26.-Observed atmospheric attenuation of the x-ray fluxes measured by the KAP stations, August 11, 1966.

FLIGHT NUMBER I AUGUST 8, 1966



**Fig. 27.-Calculated mass absorption coefficient of air
for the wavelength region 10 to 100 Å.**



calculated for a "standard" atmosphere, assuming that the absorption coefficients given in Fig. 27 were correct. The transmission at any altitude h is given by

$$T(h, \lambda) = \exp[-\mu(\lambda) m(h)], \quad [41]$$

where $\mu(\lambda)$ = mass absorption coefficient of air at a wavelength λ ,

and

$$m(h) = \int_h^{\infty} \rho(h') dh' = \text{integrated density (gm/cm}^2\text{) above an altitude } h \text{ along the line of sight.}$$

Since no measurement of atmospheric density was made in this experiment, it was necessary to assume a model atmosphere (ρ vs h) to calculate the transmission curves. Unfortunately the atmospheric density in the altitude region from 90 to 150 kilometers is quite variable. It depends on the latitude, the time of year, the time of day, and the general level of solar activity. Even after considerable effort to establish the best model atmosphere for the days of these measurements it was clear that the uncertainties in assumed densities were so large that no very precise conclusions about the experimental data could be drawn. The comparisons were not sufficiently accurate to exclude the possibility that for any one of the stations some fraction of the flux, perhaps as much as one fourth, was ultraviolet photons. The effects of a contamination of this amount could not be separated from possible variations in atmospheric densities. An approximate absorption coefficient was determined for each station, but the accuracy was no better than a

factor of two. It was also clear that there was a large difference in the absorption coefficients of stations 100 and 200, but whether the difference was a factor of 10 as shown in Fig. 27 or only a factor of 3 or 4 could not be determined.

However, the comparison of the experimental absorption curves with the calculated results did provide additional assurance that the spectrometers were measuring x-rays with approximately the correct absorption coefficients. The calculated curves showed the same very strong absorption over a narrow altitude region as the experimental curves, and the altitudes at which maximum absorption occurred for the different stations agreed reasonably well with what would be expected, with one exception: it was clear that the flux measured in station 600 on the second flight was absorbed at much too high an altitude. Even with the poor statistics for this station there was no doubt that a large fraction of the counts was due to photons having an absorption coefficient considerably higher than that for 19.83 Å x-rays. The data from all the other stations seemed to be qualitatively consistent and the observed absorption curves corresponded to an actual atmosphere that was not unreasonable when compared to a "standard" atmosphere and its expected variations.

Test of the Data for
Internal Consistency

Since it is clear that the data were not strongly influenced by scattered ultraviolet light, the above conclusions are encouraging,

but not completely satisfactory. It was not possible to obtain any better data on the actual density of the atmosphere on the days of the shot, but it was possible to make a much more sensitive test of the internal consistency of the absorption data. If the x-rays in each station were of the appropriate wavelength, and the absorption coefficients of Fig. 27 are correct, then the apparent atmosphere defined by the absorption curves for each station should be exactly the same. Equation [41] can be rewritten as

$$m(h) = \frac{1}{\mu(\lambda)} \ln \left[\frac{1}{T(h, \lambda)} \right].$$

Using the experimental transmission curves and assuming that the absorption coefficients of Fig. 27 were correct, the function $m(h)$ was calculated for each individual station. At any altitude h , the quantity $m(h)$ is the mass/unit area of air that would produce the observed value of $T(h, \lambda)$ for x-rays having an absorption coefficient $\mu(\lambda)$. The function $m(h)$ calculated for a particular station corresponds to the apparent atmosphere as seen by that station. Using the data for each of the four stearate stations for both flights, a total of eight curves of $m(h)$ were calculated. A comparison of these different curves provides a very accurate indication of the internal consistency of the data. If the fluxes in each station were entirely x-rays of the appropriate wavelength and the assumed absorption coefficients are correct, then all the curves of $m(h)$ vs h would be exactly the same. If any station was contaminated with ultraviolet photons having an absorption coefficient significantly

different from the assumed value, the shape of the curve for that station would be altered by an amount depending on the degree of contamination and the wavelength of the contaminant. The calculated curves are shown in Figs. 28 and 29.

Two things are immediately obvious from these figures. First, the curves for stations 200, 300, and 700 for both flights are in excellent agreement. The curves for station 700 on the August 8 flight and station 300 for the August 11 flight lie slightly above the others but the difference is small. [Similar curves for the KAP stations (400, 500, and 600) were calculated for the August 8 flight. The statistics are poorer for these KAP stations, but the results are in qualitative agreement with stations 200, 300, and 700.] The second very obvious feature of the curves is that on both flights the curves for station 100 are different from those for the other stations, and the amount of difference is almost exactly the same for both flights. This difference is clearly shown by this type of comparison although it was not readily apparent when the absorption curves were compared to curves calculated for a standard atmosphere.

Consider first the data for stations 200, 300, and 700. It might be argued that these stations could still have been contaminated with ultraviolet light and that the agreement between the curves was the result of each station having the same fraction of contaminant with the same average absorption coefficient. It is extremely unlikely that this was true. The count rates in these six stations

Fig. 28.-The apparent integrated atmospheric density as determined from the atmospheric absorption data of August 8, 1966.

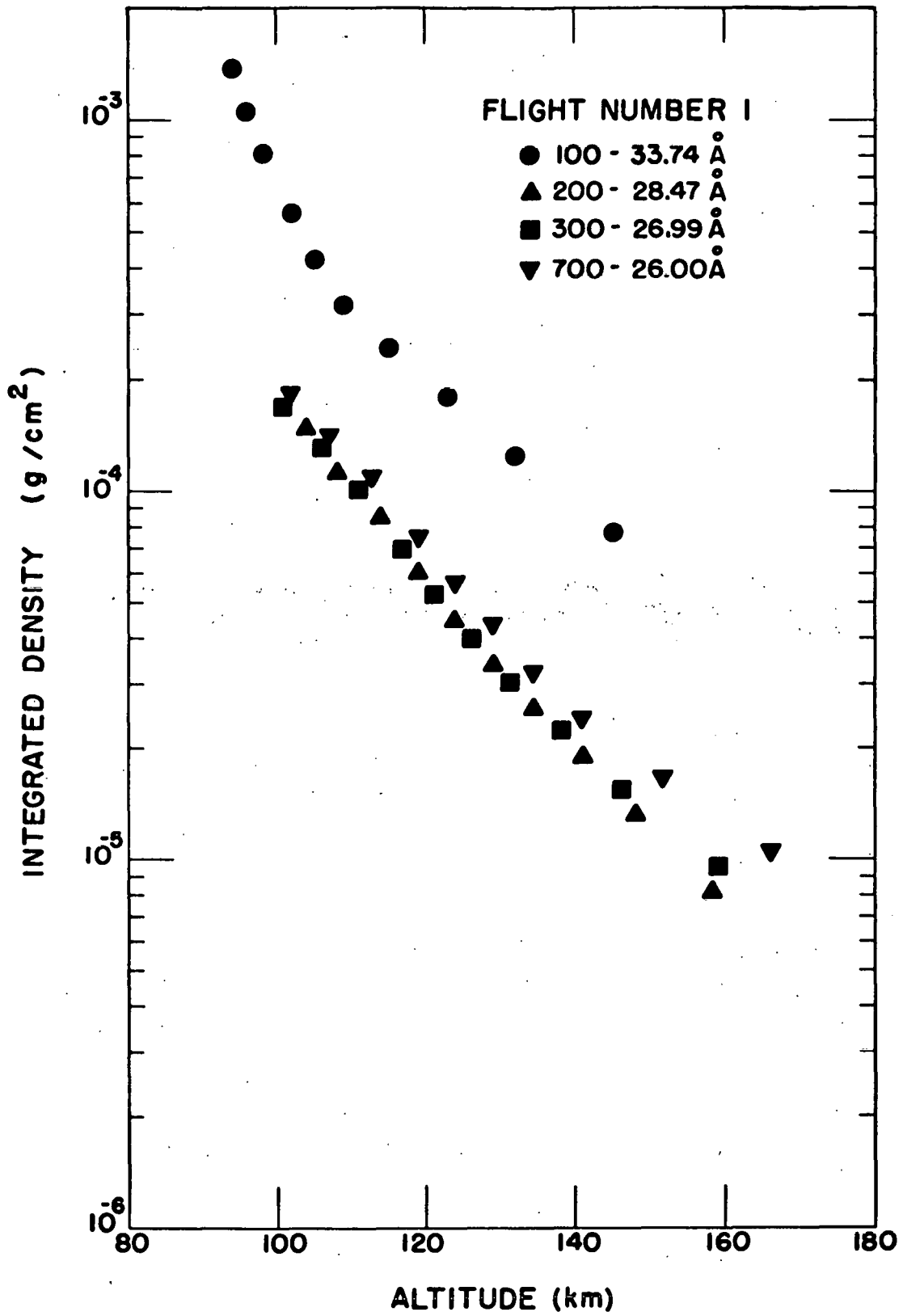
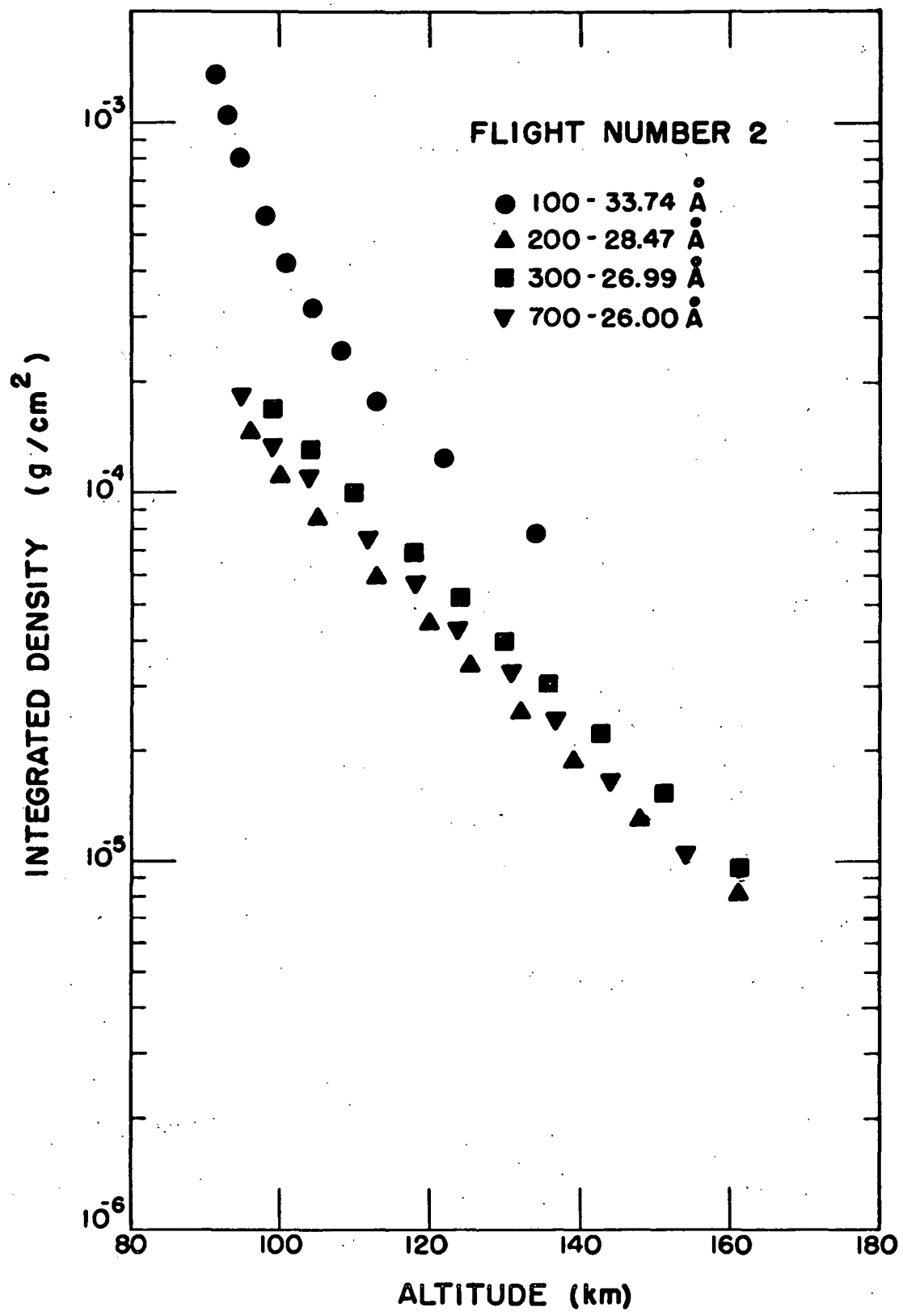


**Fig. 29.-The apparent integrated atmospheric density
as determined from the atmospheric absorption data of
August 11, 1966.**



ranged from a low of 530 counts/sec to a high of over 12,000 counts/sec. The relative sensitivity of the various stations to scattered light would almost certainly be different, and the chances would be very small of every one of the six stations having the same fraction of its total count rate caused by scattered ultraviolet light.

It is useful for the moment to assume that the data from stations 200, 300, and 700 are correct. It is then possible to compare the shapes of these curves with the curve for station 100. The values $m(h)$ calculated for station 100 depend on only two quantities: the measured values of the transmission at a particular altitude and the assumed value of the absorption coefficient of air. Experimental uncertainties in the measured transmission cannot possibly account for the large difference. The inconsistency must in some way be associated with the assumed absorption coefficient. The data for station 100 correspond to an apparent atmosphere that is more dense than was indicated by the other three stations. If the other stations are correct, then the true absorption coefficient for the flux measured by station 100 is significantly higher than the value given in Fig. 27 for 33.74 \AA x-rays.

Two possible explanations for the higher absorption were considered. First it was assumed that incident flux as measured by station 100 consisted of a mixture of 33.74 \AA x-rays and some fraction of ultraviolet photons having a much higher absorption coefficient. In the second case it was assumed that the measured

flux was entirely 33.74 Å x-rays and the discrepancy was caused by an error in the cross-section data given in Fig. 27. Since the transmission through an absorbing medium is distinctly different for a monochromatic flux and for a flux made up of a mixture of components with widely varying absorption coefficients, the shape of the $m(h)$ curve for station 100 depends upon which of the above explanations is correct.

If the station 100 flux was a mixture of x-rays of about 33 Å wavelength and some unknown amount of photons having a considerably higher absorption coefficient, then the net absorption coefficient would be the weighted average taken over the actual spectral distribution of the composite beam. This average absorption coefficient would be higher than the coefficient for 33 Å x-rays alone, and would lead to an apparently denser atmosphere. However, as such a flux traverses an absorbing medium the spectral distribution changes, since the softer components are absorbed out faster than the more penetrating components. When passing through the atmosphere the average absorption coefficient of the flux reaching a particular altitude is continuously decreasing with altitude. The simple example of a two-component beam illustrates clearly this effect.

Suppose that the incident flux of intensity I_0 consisted of a fraction K_1 of 33.74 Å x-rays with an absorption coefficient in air of μ_1 , and a fraction K_2 of photons having an absorption coefficient μ_2 , where μ_2 is much larger than μ_1 . Let $M(h)$ be the true integrated atmospheric density and $m_1(h)$ be the apparent

atmospheric density as first calculated for station 100 and shown in Figs. 28 and 29. Then at any altitude the intensity is given by

$$I = K_1 I_0 \exp[-\mu_1 M(h)] + K_2 I_0 \exp[-\mu_2 M(h)]. \quad [42]$$

As $M(h)$ gets larger (at lower altitudes) the first term becomes large compared to the second. In the limit of very large $M(h)$ the second term can be neglected and the transmission is

$$T(h) = K_1 \exp[-\mu_1 M(h)]. \quad [43]$$

Therefore $M(h) = \frac{1}{\mu_1} \ln \frac{K_1}{T(h)}$

$$= \frac{1}{\mu_1} \ln K_1 + m_1(h),$$

since $m_1(h) = \frac{1}{\mu_1} \ln \frac{1}{T(h)}$.

Therefore

$$m_1(h) - M(h) = \frac{1}{\mu_1} \ln \frac{1}{K_1} = \text{constant}. \quad [44]$$

As the depth of penetration into the atmosphere increases, the numerical difference between the apparent integrated atmospheric density and the true integrated density approaches a constant.

Consider now the second possibility: that the measured flux was essentially monochromatic but the value chosen for the absorption coefficient was in error. If μ_t is the correct absorption coefficient

then $M(h) = \frac{1}{\mu_t} \ln \frac{1}{T(h)} \quad [45]$

and $m_1(h) = \frac{1}{\mu_1} \ln \frac{1}{T(h)} .$ [46]

Therefore $\frac{m_1(h)}{M(h)} = \frac{\mu_t}{\mu_1} = \text{constant.}$ [47]

In this case the ratio of the apparent density to the true density is a constant.

Given in Tables 8 and 9 are the quantities [$m_1(h) - M(h)$] and [$m_1(h)/M(h)$] for various altitudes for the two flights. In each case the true integrated density $M(h)$ is taken as the best fit to the data for stations 200, 300, and 700.

TABLE 8

COMPARISON OF ATMOSPHERIC DENSITIES FOR AUGUST 8 FLIGHT

Altitude (km)	$m_1(h) - M(h)$ (g/cm ²)	$m_1(h)/M(h)$	$\frac{1}{3}m_1(h) - M(h)$ (g/cm ²)
150	5.8×10^{-5}	6.0	$1.1 \pm 0.1 \times 10^{-5}$
140	7.0×10^{-5}	4.5	$1.1 \pm 0.2 \times 10^{-5}$
130	9.6×10^{-5}	3.4	$0.9 \pm 0.3 \times 10^{-5}$
120	14×10^{-5}	3.3	$0.9 \pm 0.5 \times 10^{-5}$
110	20×10^{-5}	3.0	$0.0 \pm 1.0 \times 10^{-5}$
100	43×10^{-5}	3.0	$0.3 \pm 2.0 \times 10^{-5}$

The results in Table 8 indicate that for the first flight both of the possible explanations are partly true. At lower altitudes it is clearly the ratio that approaches a constant value, not the numerical difference between the curves. At higher altitudes

TABLE 9

COMPARISON OF ATMOSPHERIC DENSITIES FOR AUGUST 11 FLIGHT

Altitude (km)	$m_1(h) - M(h)$ (g/cm ²)	$m_1(h)/M(h)$	$\frac{1}{3}m_1(h) - M(h)$ (g/cm ²)
140	4.4×10^{-5}	3.4	$0.3 \pm 0.2 \times 10^{-5}$
130	6.2×10^{-5}	3.2	$0.2 \pm 0.3 \times 10^{-5}$
120	9.0×10^{-5}	3.0	$0.0 \pm 0.4 \times 10^{-5}$
110	14×10^{-5}	3.1	$0.2 \pm 0.7 \times 10^{-5}$
100	32×10^{-5}	3.1	$0.7 \pm 1.5 \times 10^{-5}$

this ratio is larger, indicating that there was certainly a small part of the flux that had been absorbed very high in the atmosphere. Below 110 kilometers the remaining flux was essentially monochromatic but with an absorption coefficient that was a factor of three larger than that given for station 100 in Fig. 27. For the second flight the flux was almost completely monochromatic and again had an absorption coefficient three times larger than was expected.

Assuming an absorption coefficient three times as large as was initially used lowers the curve of $m_1(h)$ by a constant factor of three. The last column in the above tables gives the difference $\frac{1}{3}m_1(h) - M(h)$. For the lower altitudes this is a small difference between large numbers and is therefore unreliable. For the higher altitudes on the first flight this is a fairly accurate number and appears to be a constant equal to about 1×10^{-5} . Referring to equation [44] this gives

$$\frac{1}{\mu_1} \ln \frac{1}{K_1} = 1 \times 10^{-5}.$$

For

$$\mu_1 = 3 \times 10^3$$

$$K_1 = \exp[-0.03] \approx 0.96.$$

Since K_1 is the fraction of the flux that was x-rays, even for this flight the contamination was a very small effect.

Based on the above analysis (that assumes a monochromatic flux for stations 200, 300, and 700) the flux measured by station 100 on both flights was essentially monochromatic. The disagreement between the data for station 100 and stations 200, 300, and 700 is apparently due to an error in the assumed absorption coefficients. Although in the above discussion it was assumed that the absorption coefficients used for stations 200, 300, and 700 were correct, and any error was in the coefficient assumed for station 100, the analysis actually indicates only that the difference in absorption coefficients between 100 and the other stations was considerably less than is shown in Fig. 27. By itself, the comparison between the data for the different stations gives no information about the absolute accuracy of any of the absorption coefficients. It merely indicates that the relative values of the assumed coefficients are not consistent with the data.

It is useful at this time to summarize briefly the main points of the above discussion of the atmospheric absorption data. The data from the KAP stations on the first flight appear to be reliable and to show a reasonable pattern of flux levels. The data from the stearate stations are very difficult to interpret in terms of line

intensities. The possibility that these data were unreliable because of strong contamination by scattered ultraviolet light had to be considered. An examination of the depth of penetration into the atmosphere of the flux for each station showed clearly the qualitative pattern that would be expected from the shape of the absorption coefficient curve of air. This alone was a strong indication that contamination of the measured flux by scattered ultraviolet light was not an overriding effect. Comparison of the transmission curves with curves calculated for a "standard" atmosphere supported this general conclusion. With the exception of station 600 on the second flight, all of the stations showed maximum absorption at approximately the correct altitude. However, the uncertainties in the assumed atmospheric densities were too great to give any precise answer to the question of exactly what wavelength x-rays were being measured.

To make a more sensitive check on the internal consistency of the data, the transmission curves were used to calculate, for each of the eight stearate stations and the three KAP stations of the first flight, the apparent atmospheric density as a function of altitude. The agreement between stations 200, 300, and 700 and, within the accuracy of the data, stations 400, 500, and 600 were excellent. The results suggested that there might have been a small ultraviolet contamination of station 300 on one flight and station 700 on the other. The data for station 100 were clearly inconsistent with the other stearate stations, and the nature and amount of the disagreement was almost exactly the same for both

flights. Assuming that the data for the other stearate stations were correct, the cause of this disagreement was shown to correspond most closely to an error in the assumed absorption coefficient of air for the x-rays measured by station 100.

Final Flux Values

In the opinion of the author these results from the atmospheric absorption are sufficiently conclusive to eliminate the possibility that scattered ultraviolet photons contributed more than a few percent error to the measured flux values for any station except number 600 on the second flight.

As was mentioned earlier, the elimination of scattered ultraviolet light as the explanation for the apparently anomalous results from the stearate stations leaves open the question of what significance the measured flux values have. And added to this question is now the discrepancy in absorption coefficients between station 100 and the other stations. This discrepancy was present and essentially identical in the data from both flights. In the next section the results of this experiment are compared with earlier measurements, and other effects that could explain the observed results are discussed.

As a conclusion to this section, the following table gives the final flux values after the small corrections indicated by the absorption data were made for stations 100 and 700 on the first flight and station 300 on the second flight. Stations 200 and 300 are still designated in the table as the Lyman- β and - γ lines of C VI, since it was for these wavelengths that the spectrometers were focused. The flux values given in the table for these two

TABLE 10
CORRECTED FLUX VALUES

Station	Emission	Incident Flux Above the Earth's Atmosphere (photons/cm ² -sec)	
		August 8, 1966	August 11, 1966
100	C VI	Lyman- α	80×10^6
200		Lyman- β	70×10^6
300		Lyman- γ	45×10^6
700	Continuum	23×10^6	15×10^6
400	N VII	Lyman- α	2.8×10^6
500		Lyman- β	1.1×10^6
600		Lyman- γ	0.5×10^6

stations are not believed to correspond to the actual intensities of the two lines. The data for station 600 on the second flight are omitted because they were shown to be contaminated by scattered ultraviolet light.

IV. CONCLUSIONS

The Results from the KAP Stations

The flux values given in Table 10 for stations 400, 500, and 600, which used KAP crystals, are believed to be reliable measurements of the intensity of the solar x-ray emission at the wavelengths for which spectrometers were focused. As was discussed in the introduction, the intensity of the Lyman- γ line (station 600) was expected to be very low. The observed intensity for this station was only a factor of two smaller than the intensity measured for the Lyman- β line. This suggests very strongly that most of the flux measured by this station was in fact due to continuum radiation. Assuming this to be true gives a value for the continuum intensity at 19.83 Å of 5×10^{-3} erg/cm²-sec-Å. The effective width of the spectrometer window was taken as 0.1 Å. When this value of the continuum is subtracted from the intensities of stations 500 and 600, the resulting numbers are 22×10^5 and 6×10^5 photons/cm²-sec for the N VII Lyman- α and - β lines respectively.

In the KAP scan of the solar spectrum by Blake, et al. (9), the N VII Lyman- α line was seen clearly and the intensity was given

as 5×10^5 photons/cm²-sec. Since the measurement of reference (9) was made in 1963 at a time of extremely low solar activity, the factor of four difference between it and the present measurement is certainly consistent with possible variations in solar activity. Unfortunately, there was a fairly high background counting rate present in the data of reference (9). At 24.78 Å the background was approximately one third as large as the signal from the N VII Lyman- α line. A Lyman- β line with the same relative intensity as was measured in the present experiment would have had a signal-to-noise ratio of less than one. In fact, the data of (9) indicated the possible presence of a weak line at the Lyman- β wavelength. Thus the results of the present experiment seem to be in relatively good agreement with the results of (9). It is also interesting that the results of the present experiment suggest that approximately one half of the background present in the data of (9) was probably x-ray continuum.

To deduce information about the solar corona from the measured ratio of the N VII Lyman- α and - β lines it is necessary to assume a model to describe the corona. The subject of coronal models has been considered for many years. Interest in the emission spectra from high temperature plasmas has been further stimulated in recent years by the greatly expanded research effort directed toward producing and maintaining such plasmas in the laboratory. The literature in this field is extensive and it is impossible to discuss here, in any but the most cursory manner, the details of

this very complex problem.

It is sufficient for the present purpose to describe very briefly some of the general features that are included in calculations of coronal models. The temperature of the corona is of the order of one million degrees (3). At this temperature the coronal gas is a highly ionized plasma, and the heavy ions present in the corona interact with a high temperature distribution of free electrons. Calculations of the emission spectrum must include free-free and free-bound electron transitions as well as the transitions between bound states that produce line emission. The relative intensities of emission lines from a particular ionic species depend upon the population densities of the excited states of the ion. Under conditions of true thermodynamic equilibrium the relative population densities can be calculated using the Saha-Boltzman equation (18).

However, the conditions for thermodynamic equilibrium are not satisfied for the temperatures and densities of the corona (19). To arrive at the relative population densities, it is necessary to consider all the physical processes that can fill or empty a particular excited level and to solve the resulting set of coupled rate equations, one for each excited level. The problem cannot be treated in complete generality since the set of equations to be solved is infinite when all excited levels are considered. It is usually sufficient to assume that above some particular excited level the population densities agree with the Saha-Boltzman values (20).

Only those excited states with energies less than this "cut-off" energy must be considered individually. The additional assumption is usually made that the distribution of ions among the different states of ionization and excited levels is constant in time. The problem then is to calculate the steady state distribution. The free electrons are always considered to be in equilibrium among themselves and to have a Boltzman velocity distribution characterized by a specific temperature.

Even with these assumptions, the problem is tremendously difficult. Depending on the density and temperature, certain other simplifying assumptions are justified (21). If the plasma is transparent, the electrons and ions can be treated as independent of the radiation field. In this case all excitations of ions are caused by inelastic collisions, almost entirely with electrons. In the temperature and density regime where collision times are long compared to radiative transition times, collisional de-excitation can be ignored (19). The equilibrium conditions are determined by the balancing of collisional excitations by radiative de-excitations. In the limit of very low densities, when time between collisions is very long, all ionic species can be considered to be in their ground state (22). A collisional excitation is followed immediately by a radiative return to the ground state. The last condition is frequently assumed for the corona.

The population densities of the first and second excited states of N VII are related to the measured intensities of the

Lyman- α and - β lines by

$$n(2) \approx I_{\alpha}/(h\nu_{\alpha} A_2)$$

and

$$n(3) \approx I_{\beta}/(h\nu_{\beta} A_3),$$

where A_p is the appropriate transition probability of hydrogen scaled up by Z^4 . The ratio of the population densities is then

$$\frac{n(2)}{n(3)} = \frac{I_{\alpha} h\nu_{\beta} A_3}{I_{\beta} h\nu_{\alpha} A_2} = R(2,3).$$

Taking $I_{\alpha}/I_{\beta} = 4$ gives $R(2,3) = 0.43$ for this experiment. There are no other measurements of this particular ratio for the solar spectrum with which to compare the above result. The corresponding ratio for O VIII was calculated from the measurements of Blake, et al. (9), and was found to be 0.75. The results from measurements of the intensity of the O VIII Lyman- α and - β emission from a laboratory plasma (23) gave a value of $R(2,3) = 0.38$.

When these numbers are compared to theoretical calculations, they indicate a large underpopulation of the first excited state of the hydrogen-like atoms. McWhirter and Hearn (20) have made extensive calculations of the equilibrium population densities for hydrogenic atoms in high temperature plasmas. These calculations assume a Saha distribution for all excited states above the 20th level, a Boltzman electron distribution, and a transparent plasma. According to this model, the value of $R(2,3)$ for N VII should be 1.6 at a temperature of 1.6×10^6 °K. The result of the present

experiment is much too small to agree with this model. The value of 0.38 determined from the O VIII Lyman- α and - β emission from a laboratory plasma (23) was interpreted as evidence of a departure from an equilibrium condition.

In a recent paper Elwert (24) included the effects of dielectronic recombination (25) and new estimates of elemental abundances in a calculation of the line intensities in the solar spectrum. The intensity of the N VII Lyman- α line was computed to be 4×10^{-3} erg/cm 2 -sec, compared to 1.8×10^{-3} erg/cm 2 -sec measured in this experiment. This difference again corresponds to a smaller population density of the first excited state than calculations predict.

The Results from the Stearate Stations

Unlike the nitrogen data, the results obtained with the stearate stations do not give reasonable line intensities of the Lyman series from C VI. However, when these results are compared to other measurements made in the same wavelength region a very curious pattern becomes clear.

Earlier reference has been made to the two rocket flights made in 1963 that carried scanning crystal spectrometers (9). On each of the two flights there was one spectrometer that scanned the wavelength region from about 26 Å toward longer wavelengths. In one case an OHS crystal was used and in the other instrument a soap film crystal was used. On the first flight the counting rate was high enough in the long wavelength spectrometer to saturate

the counting circuits. Scattered ultraviolet light was blamed for the high counting rate. On the second flight the counting rate for the long wavelength spectrometer was below the saturation level but still quite high, and no apparent line structure could be distinguished. Again it was assumed that scattered ultraviolet light was responsible for the high count rates and lack of line structure. In May, 1966, a scanning spectrometer using an OHM crystal was flown aboard an Aerobee rocket from White Sands, New Mexico, by Dr. Werner Neupert of Goddard Space Flight Center. The complete results of this experiment have not been published, but Dr. Neupert has kindly allowed the author to examine the preliminary results and refer to them in this paper. These results are also quite puzzling. In the wavelength region from 25-43 Å the spectrum appears almost completely flat, with a single small "bump" near 28 Å. Above 43.6 Å (the carbon absorption edge) numerous lines were distinguishable and several of these lines have been identified by Dr. Neupert. In November, 1966, the Naval Research Laboratory flew a rocket package containing three scanning spectrometers, one of which scanned the wavelength region above 25 Å with a lead stearate soap film crystal. The results of this experiment are also unpublished, but the general nature of the results were described to the author by A. E. Unzicker, J. Meekins, and G. Fritz of the Naval Research Laboratory. It is with their generous permission that the very preliminary results of this experiment are described. The most significant result was the

absence of any clear indication of line structure in the wavelength region covered by this crystal scan. The count rate was appreciable at about 25 Å and increased as the crystal was scanned toward longer wavelengths.

The four experiments described above are the only attempts, known to the author, to measure the solar spectrum at wavelengths longer than 25 Å with scanning crystal spectrometers. In each case the results failed to show any clear evidence of line structure between 25 and 43 Å, and in three of the four cases the count rates were significantly higher than expected.

The results of the present experiment agree qualitatively with this pattern: no evidence of line structure, flux levels that were generally higher than expected, and an increase in the flux level from 26 Å to 33 Å. Although these results were quite unexpected when the experiment was performed, it now seems clear that they are at least qualitatively consistent with the results from every attempt to measure the solar spectrum between 26 and 34 Å with scanning spectrometers.

The failure to give clear evidence of any line structure in the solar spectrum and the generally high flux values are apparently common to the results from both scanning and fixed station spectrometers designed by different experimental groups. Probably the most significant result from the stearate stations of this experiment is that these data are the first crystal spectrometer measurements in this wavelength region for which it can be definitely

shown, from the experimental data, that scattered, long wavelength ultraviolet light did not contribute to the observed fluxes. If this consistent failure to observe the expected line structure in the solar spectrum is due to some fault of the experimental technique, then the difficulty is more subtle than the problem of scattered ultraviolet light.

It is also interesting to compare the results of the number 100 stations of the present experiment to other measurements of the intensity of the C VI Lyman- α line made with curved crystal spectrometers. The rocket packages flown in 1964 by Argo, Bergey, Henke, and Montgomery (10) were referred to briefly in the introduction. Three packages were flown, and each package contained eight nonscanning, curved crystal spectrometers. One of the stearate spectrometers in each package was focused for the C VI Lyman- α line at 33.74 Å. The intensities measured on the three flights for this line were 46, 58, and 63×10^6 photons/cm²-sec. These are in excellent agreement with the values of 80 and 58×10^6 photons/cm²-sec measured in the present experiment. Also, in November, 1966, three rockets carrying packages identical to those flown in 1964 were launched from southern Brazil on the day of the total eclipse (26). One launch was made before the eclipse began and the measured intensity of the C VI Lyman- α line was 43×10^6 photons/cm²-sec. Thus the measurements of the intensity of the C VI Lyman- α line made with six different curved stearate crystal spectrometers over a time interval of two years

all agree within an accuracy better than the expected experimental uncertainty.

The one other result that has an important bearing on the following discussion is the discrepancy between the calculated mass absorption coefficient of air and the atmospheric absorption curves for the different stearate stations. This discrepancy was present in the data from both flights of this experiment and was also present in the data obtained from the Brazil experiments (26). This result could be explained in principle by an error in the calculated absorption coefficient of air, shown in Fig. 27. As was discussed earlier, this curve was calculated for a "standard" atmospheric composition (17) using the mass absorption coefficients of nitrogen, oxygen, and argon recently measured by Henke (8).

It is also important to emphasize one aspect of the discussion of Part III. It was concluded in that section that long wavelength ultraviolet photons did not cause any significant error in the observed fluxes. However, it was also stated that the exact x-ray wavelength being measured by any of the stations could not be determined from the absorption data. The possibility that all of the stearate stations were measuring x-rays of a wavelength well outside the calculated resolution of the spectrometers cannot be excluded by the absorption data. In particular, it should be noted that the absorption coefficient curve shown in Fig. 27 is double-valued. X-rays in the wavelength region 10-31 Å have the same absorption coefficient as x-rays in the region 31-100 Å. The

possibility must be considered that the spectral window of the stearate stations was considerably broader than 1 Å.

It is clear that the data from the stearate stations are subject to a variety of interpretations, depending on which set of assumptions one chooses to make. However, if the assumption is made that Fig. 27 gives accurate values for the absorption of air, only one conclusion can be drawn from the data.

It was shown in Part III that if the flux measured by any one of stations 200, 300, or 700 was monochromatic, then the flux measured by all the stearate stations, including station 100, was monochromatic. But if the calculated absorption coefficient of air is correct, then all of the stations could not have been measuring monochromatic fluxes of the expected wavelength. The only remaining possibility is that none of the stations was measuring monochromatic fluxes. (The possibility that station 100 was measuring a monochromatic flux but of a wavelength different from 33.74 Å is considered completely negligible.) Since this is the only interpretation that is consistent with all of the data, an effort was made to obtain additional laboratory information relating to this possibility. Two possible sources of trouble were considered, and are described below.

If the natural widths of the crystals were considerably broader than was indicated by the measurements made with the single Bragg spectrometer, then the results might be explained. The resolution of the flight spectrometers would have been broader than

1 Å and the measured fluxes would represent an integral over a wide spectral region. For a sufficiently broad resolution, each of the stations 200, 300, and 700 would have been sensitive to wavelengths above the nitrogen absorption edge. Also, the flux measured by station 100 could have contained a component in the wavelength region shorter than the nitrogen edge. Such a situation would certainly confuse the absorption data. There was no evidence from the large amount of laboratory work done with the crystals to indicate that the crystal half-widths were any different than had been assumed in the calculations of spectrometer resolution. It was considered essential, however, to confirm the earlier results by measuring the crystal rocking curves with a double crystal spectrometer.

The other possibility considered was that specular reflection of longer wavelength x-rays might have resulted in a broad specular response. Total specular reflection is a well-known effect that occurs at small glancing angles because the index of refraction of x-rays is smaller in a material medium than in air. For x-ray wavelengths shorter than a few angstroms the critical angle for total reflection is very small (fractions of a degree). The critical angle increases with wavelength and is roughly proportional to λ . If absorption in the reflecting medium is negligible, the critical angle is sharply defined: for angles less than θ_c total reflection occurs and for angles greater than θ_c reflection is negligible. When absorption is an important effect, the situation is considerably

different. The step-function curve that describes the situation for zero absorption becomes a smoothly varying function of angle and has an appreciable tail that extends well beyond the critical angle (15). Whether or not specular reflection was a problem for the present experiment depended on the exact shape of this extended tail of the curve. No precise data were available on the specular reflection of long wavelength x-rays from lead stearate. As with the crystal rocking curves, precise data require the use of a double crystal spectrometer.

These two problems were discussed with Dr. Robert Liefeld of New Mexico State University. He very kindly offered his assistance and the use of his double crystal vacuum spectrometer to make the necessary measurements. A lead stearate crystal that had been made at the same time as the flight crystals was picked for examination. Rocking curves in the (1,-1) position were measured at wavelengths of 44.74 \AA (C_K) and 67.8 \AA (B_K). The results were in excellent agreement with the earlier measurements of the crystal widths. This almost certainly eliminated the possibility of unexpectedly poor crystal resolution.

The next step was to measure the efficiency for specular reflection. A lead stearate crystal was used in the first position as a monochromator. The stearate crystal in the second position was rotated step-wise from a glancing angle of 5 deg to a glancing angle equal to the Bragg angle, and measurements were made at each angle of the reflected intensity. The results were then normalized to a direct beam intensity of unity. The measurements were made for

carbon-K and boron-K radiation.

The carbon results are shown in Fig. 30. The diffraction peak is shown at 26.5 deg. The boron measurements were considerably more difficult. A boron anode was prepared by rubbing boron nitride powder onto the surface of the carbon anode. To avoid any question of confusion by carbon or nitrogen radiation, the x-ray tube was operated at 280 V, below the minimum voltage necessary to excite carbon-K radiation. An excitation curve of boron was measured to insure that the observed radiation was in fact the boron-K line. The very low excitation voltage and the double crystal geometry gave a low counting rate in the detector. The results that were obtained are shown in Fig. 31. For angles between 15 deg and the Bragg angle at 42.6 deg the counting rates were too low to be reliable. The strong similarity between the carbon and boron curves made it possible to extrapolate the boron results to somewhat larger angles with fair confidence.

The data of Figs. 30 and 31 were then used to calculate a spectral response curve for two of the flight spectrometers: station 100 and 700. The Bragg angles for these stations were about 20 deg and 15 deg respectively. These stations were chosen to represent the "best" and "worst" cases. Station 100 had the largest Bragg angle of the stearate stations and was focused on a strong line. Both facts tend to minimize the problem of specular reflection. Station 700 was measuring continuum and had the smallest Bragg angle of the four stearate stations.

In Fig. 32 the specular reflection data are plotted as a function of wavelength for the two glancing angles, 15 and 20 deg. The experimental data give only the two points at 44.7 and 67.8 Å. Advantage was taken of the strong similarity of the relative shapes of the boron and carbon curves and the expected variation of specular reflection with wavelength to estimate the points at 100 Å. This estimate should not be wrong by more than a factor of two.

In Fig. 33 the relative transmission of the counter windows is plotted against wavelength for stations 100 and 700. Counter windows and ultraviolet filters having a total of $80 \mu\text{g}/\text{cm}^2$ of aluminum and $90 \mu\text{g}/\text{cm}^2$ of Formvar were assumed. The shape of these curves at long wavelengths is quite sensitive to the thickness of aluminum.

From the data in Figs. 32 and 33, the spectral response of stations 100 and 700 were calculated for the wavelength region out to 120 Å. The results are shown in Fig. 34. This curve is believed to be quite accurate for wavelengths up to 80 Å, and within a factor of two beyond 100 Å.

To determine the relative contribution from the entire spectral region, it was necessary to integrate the curve of Fig. 34 against an assumed solar spectrum. If $f(\lambda)$ is taken as the differential flux at λ , then the count rate produced by the flux in the interval from λ to $\lambda + d\lambda$ is

$$dC = f(\lambda) \xi(\lambda) T(\lambda) d\lambda,$$

Fig. 30.-Specular reflection of 44.74 Å x-rays from lead stearate soap film analyzers.

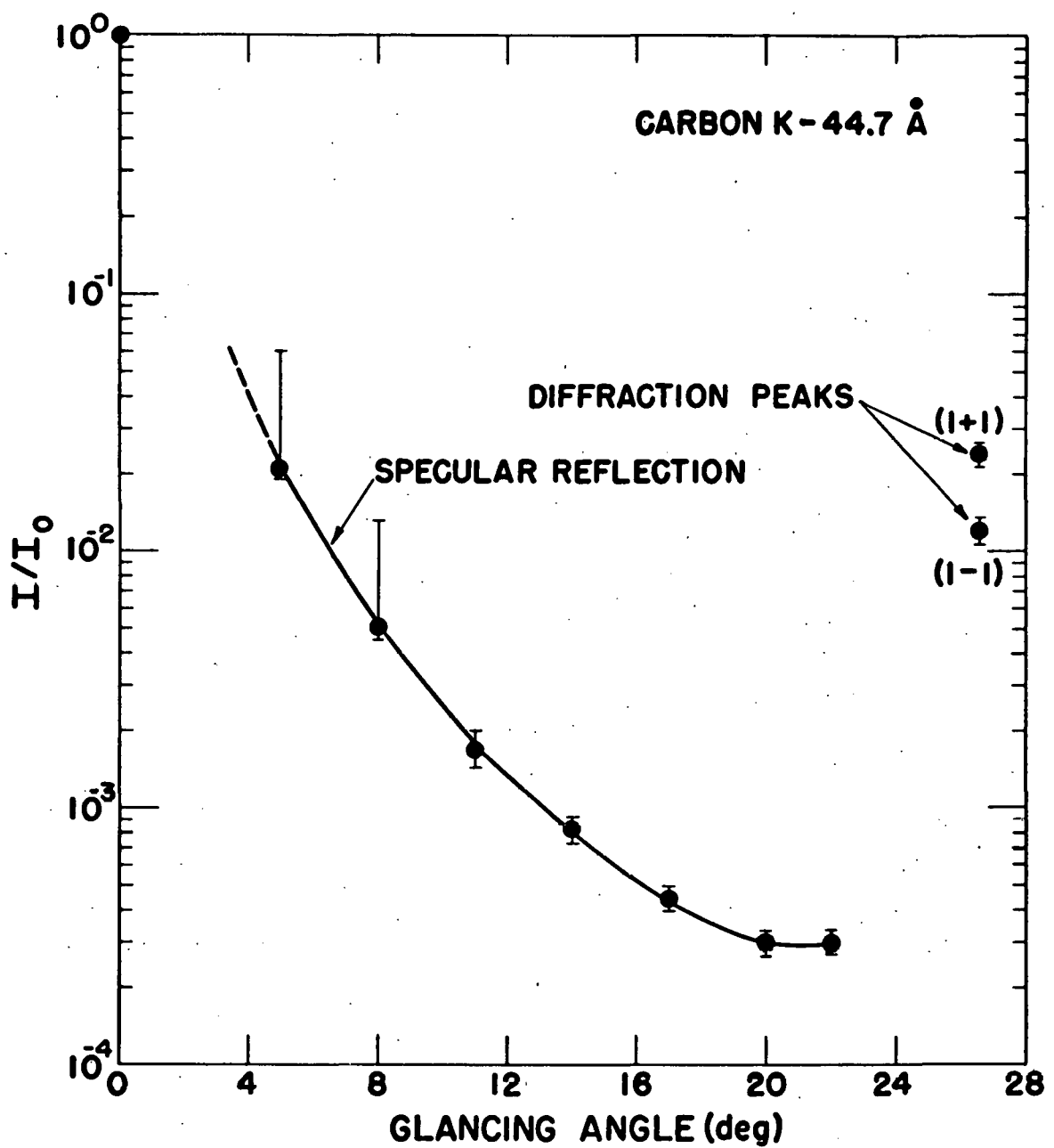


Fig. 31.-Specular reflection of 67.8 Å x-rays from lead stearate soap film analyzers.

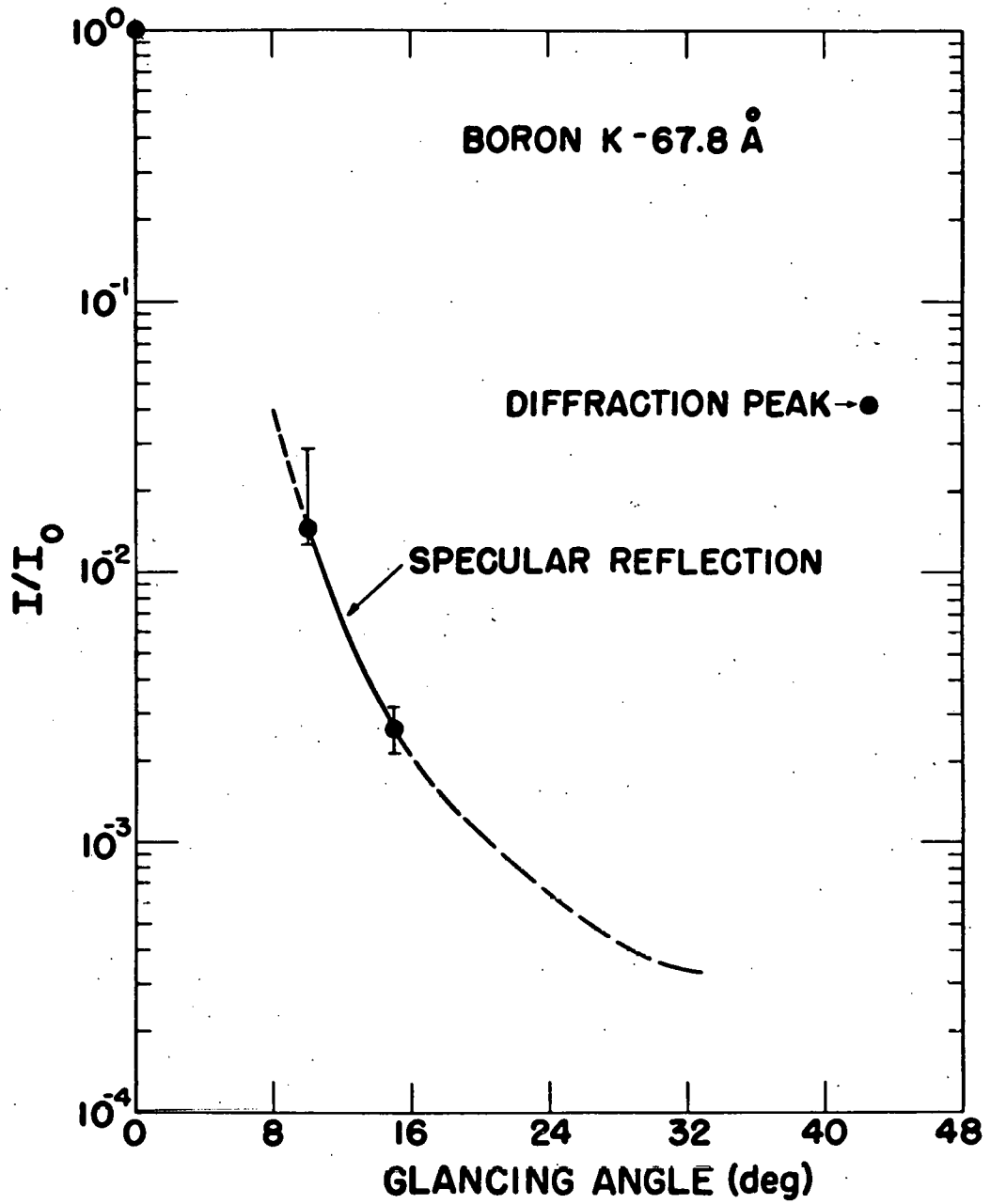


Fig. 32.-Specular reflection efficiency from a lead stearate soap film analyzer as a function of x-ray wavelength.

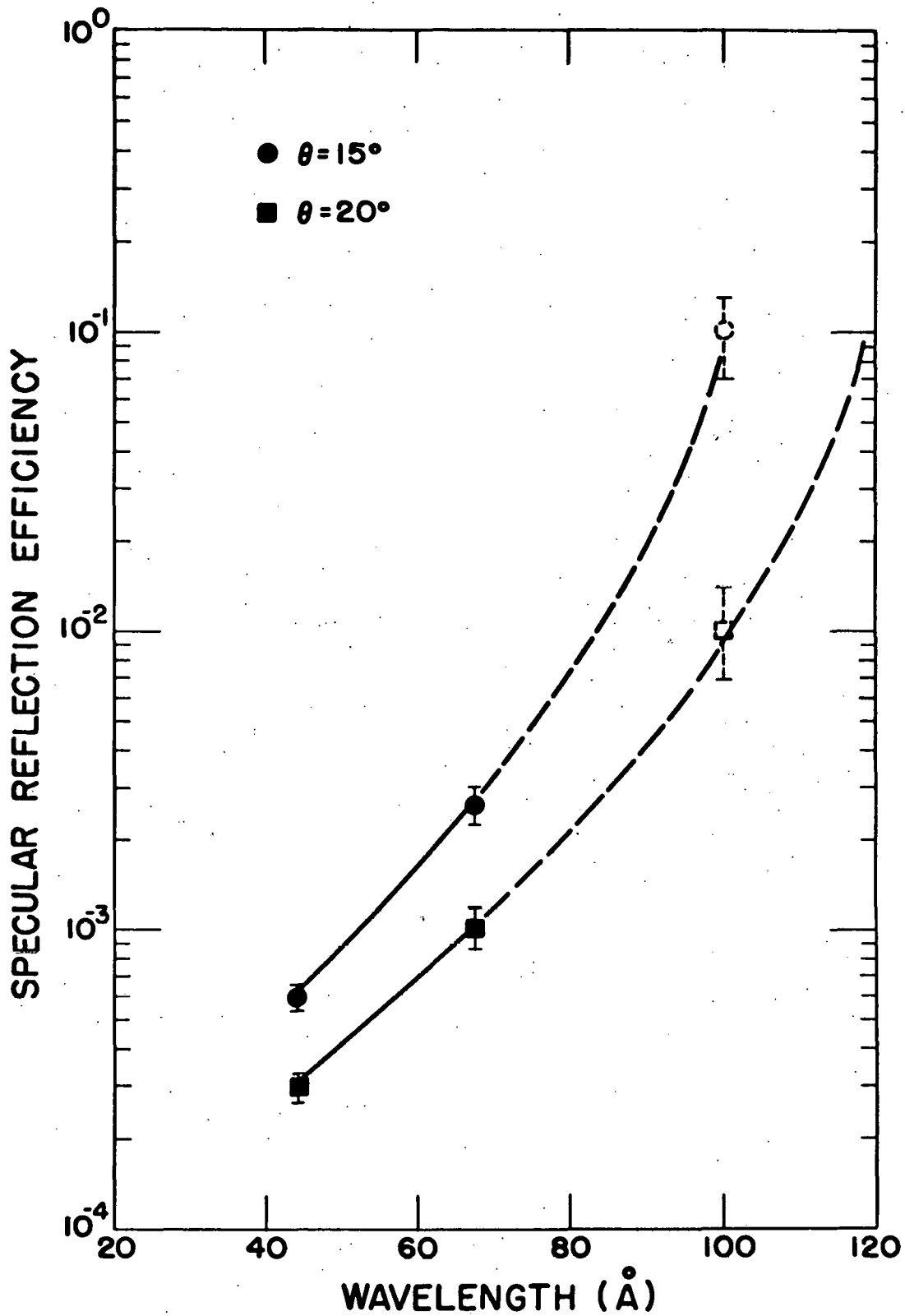


Fig. 33.-Relative counter window transmission of stations
100 and 700 as a function of x-ray wavelength.

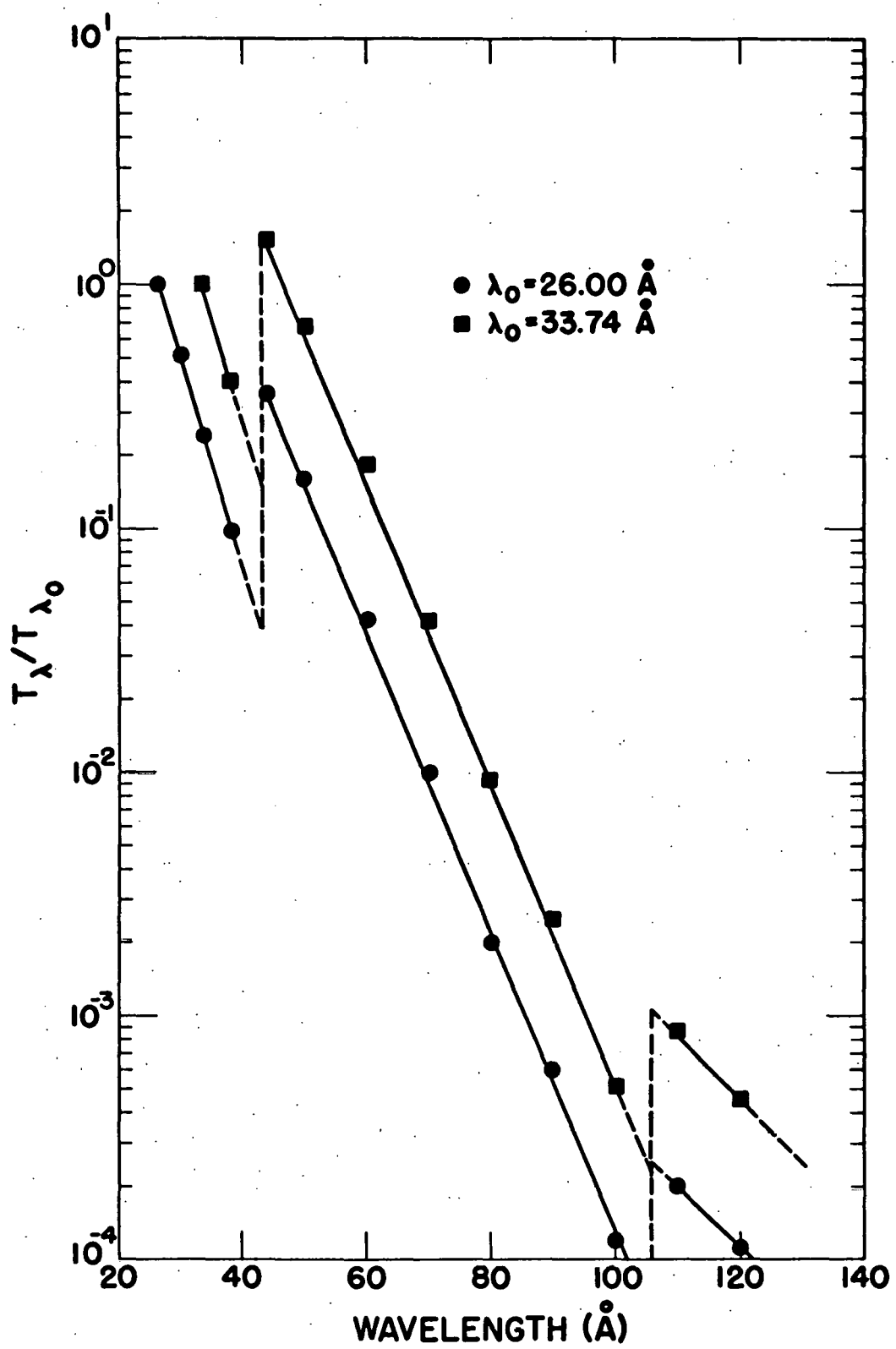
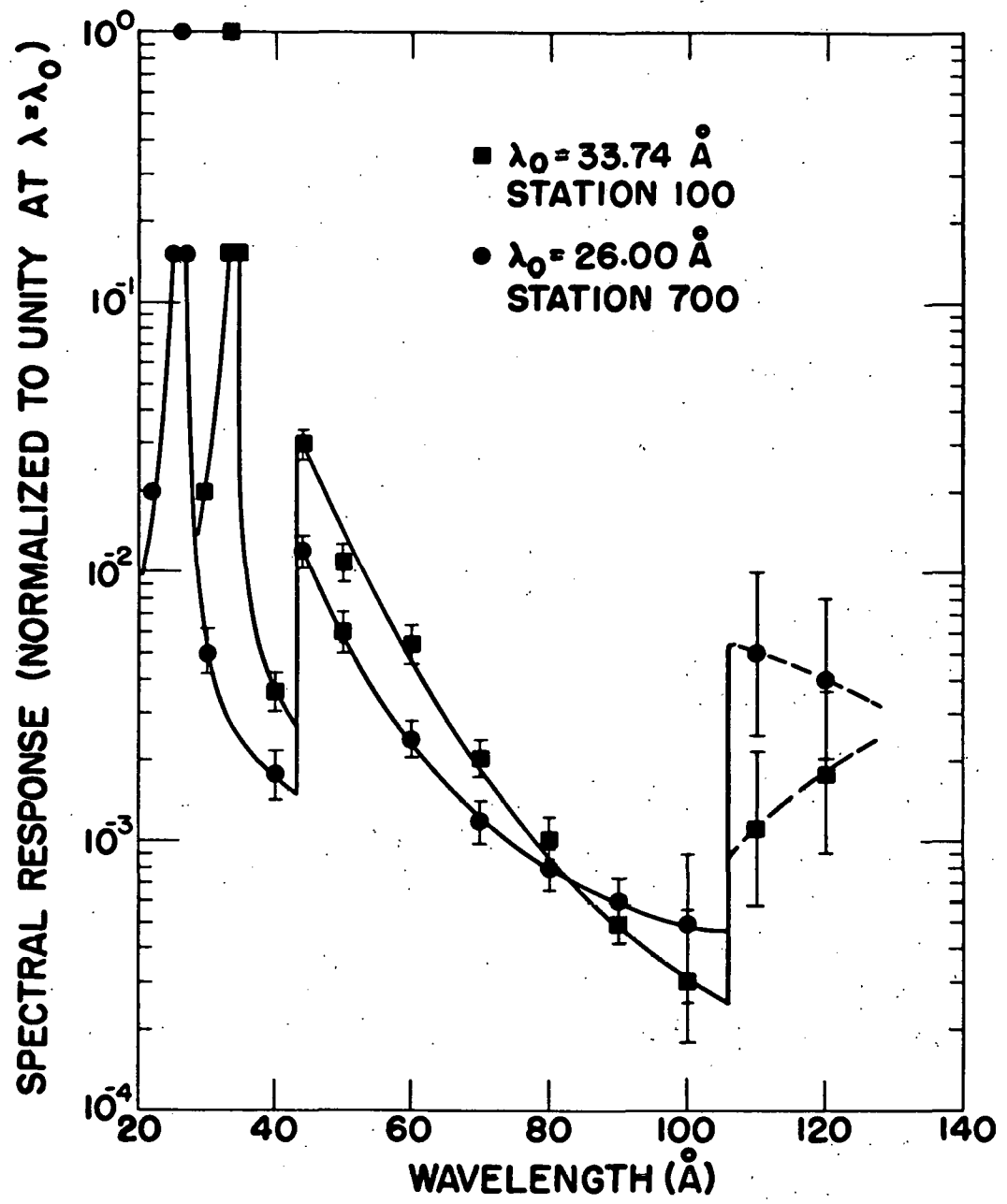


Fig. 34.-Spectral response of stations 100 and 700.



where $\xi(\lambda)$ = reflection (or diffraction) efficiency of the crystal
and $T(\lambda)$ = window and ultraviolet filter transmission.

The calculation was done numerically by replacing the differentials by finite differences. Then

$$\Delta C_i = f_i \xi_i T_i \Delta \lambda_i = F_i \xi_i T_i ,$$

where $F_i = f_i \Delta \lambda_i$.

The total count rate is

$$C = \sum_{i=1}^n F_i \xi_i T_i . \quad [48]$$

If we express the count rate resulting from the flux in the 1 \AA region, for which the spectrometer was focused as

$$C_k = F_k \xi_k T_k \quad [49]$$

then the ratio between the total count rate C and the count rate C_k can be written as

$$\frac{C}{C_k} = 1 + \sum_{\substack{i=1 \\ i \neq k}}^n \frac{F_i \xi_i T_i}{F_k \xi_k T_k} = 1 + \sum_{\substack{i=1 \\ i \neq k}}^n \Delta_i \quad [50]$$

where $\Delta_i = \frac{F_i \xi_i T_i}{F_k \xi_k T_k}$

The average values of the ratio $\xi_i T_i / \xi_k T_k$ were taken directly from Fig. 34. The solar spectrum used in the calculation was the continuum spectrum of Elwert (27) for a temperature of 1.5 million degrees. This spectrum gives the smallest contribution from specular

reflection of several assumed spectra considered. Using this spectrum and assuming a 1 Å effective width for the spectrometer, the values of Δ_i were calculated for stations 100 and 700. The results are shown in Table 11.

TABLE 11

RELATIVE CONTRIBUTIONS OF SPECULAR REFLECTION TO THE OBSERVED COUNT RATE OF STATION 100 AND 700 IN TEN ANGSTROM INTERVALS FROM THE SPECTRAL REGION 30-100 Å

$\Delta\lambda_i$ (Å)	Δ_i	
	Station 700	Station 100
30-40	0.06	---
40-50	0.15	0.14
50-60	0.20	0.20
60-70	0.09	0.10
70-80	0.06	0.05
80-90	0.04	0.02
90-100	0.03	0.01
100-110	0.08	0.01
110-120	0.16	0.03
120-130	<u>0.10</u>	<u>0.03</u>
Total	0.97	0.59

The results of Table 11 are considered minimum values since the contribution of the lines to the solar spectrum was not included. If the very rough estimate is made that the lines in each of the

wavelength intervals contain as much flux as the continuum, then the values of Δ_i in Table II should be multiplied by two.

The contribution of the properly diffracted continuum radiation at the Bragg angle is not included in the table. Its contribution is unity as defined in equation [50]. For station 100 the values of Δ_i give the contribution of the specularly reflected radiation relative to the contribution of the true continuum. The effect of the strong Lyman- α line is not included. The total intensity measured by station 100 is then

$$I_t = I_\alpha + I_c(1 + \sum \Delta_i) , \quad [51]$$

where I_t = total measured intensity

I_α = intensity of the Lyman- α line

I_c = contribution of the true continuum.

The product $I_c \sum \Delta_i$ is the contribution of the specularly reflected radiation. Station 700 is not focused on a line and for this station

$$I_t = I_c(1 + \sum \Delta_i) . \quad [52]$$

The above calculation is admittedly only approximate, but it seems almost certain that the long wavelength x-rays were responsible for a significant fraction of the observed count rates in stations 200, 300, and 700. The effect for station 100 was less important, but still large enough to influence the absorption data.

Of the different possible interpretations of the stearate results, this explanation seems by far the most likely. If the

numbers given in the above table are assumed to be approximately correct, then the results of several experiments, including the present measurements, can be explained. The generally observed lack of line structure could easily be caused by the fact that specular reflection produces an apparent continuum that is comparable in intensity to all but the strongest lines. The observed spectrum is "filled in" in regions where no lines exist. A thinner aluminum filter than was assumed in the calculation would result in a stronger contribution from the region 90-130 Å. For any scanning instrument using a filter that contains carbon, the relative contribution to the apparent continuum from the spectral region 40-80 Å increases continually as the scan moves from 25 Å toward the carbon absorption edge at 43.6 Å. The relative transmission of the filter gets more unfavorable as the absorption edge is approached. This could account for the observed increase in the flux levels from 25 Å toward longer wavelengths. For scans above 43.6 Å, the relative contribution from the spectral region 40-80 Å is very greatly reduced. This could certainly account for the sudden appearance of lines in Dr. Neupert's data for wavelengths above 43.6 Å.

If the Δ_i values in Table II are multiplied by two to account for lines, then the resulting sum of the Δ_i 's for station 700 is equal to about two. This means that two thirds of the observed count rate was due to x-rays outside the resolution "window." If the remaining one third is interpreted as the true continuum at 26 Å,

the resulting intensity for August 8 is 6×10^{-3} erg/cm²-sec-Å. This is in remarkably good agreement with the value of 5×10^{-3} erg/cm²-sec-Å obtained from station 600 at 19.83 Å. If the value of 6×10^{-3} erg/cm²-sec-Å is taken for the continuum intensity at 26 Å, then for the same assumed spectrum the continuum at 33.74 Å is 8.4×10^{-3} erg/cm²-sec-Å. The apparent continuum for station 100 is $I_c(1 + \sum \Delta_i)$, and is equal to 18×10^{-3} erg/cm²-sec-Å. If this is subtracted from the total measured intensity of station 100 on August 8, (see equation [51]) the resulting intensity for the Lyman-α line is 2.9×10^{-2} erg/cm²-sec. The corresponding number for August 11 is 2.2×10^{-2} erg/cm²-sec. This compares with a value of 3.3×10^{-2} calculated by Elwert (24). If a beam with the spectral distribution determined from the data in Table 11 is assumed for stations 100 and 700 then the average absorption coefficient for these stations would have been about 5×10^3 and 22×10^3 cm²/gm respectively. The ratio of the station 100 to the station 700 coefficient is 4.4 compared to the value of 3.3 determined from the atmospheric absorption data. (The atmospheric absorption data indicated an error of a factor of 3 in an expected ratio of 10.) The fact that the relative shapes of the absorption curves for stations 100 and 700 were very similar is not surprising since the contribution to station 700 from the region around 100 Å had approximately the same absorption coefficient as the 26 Å radiation, and the other component in each station was from the same region between 40 and 70 Å.

Considering the assumptions that were made in calculating the numbers in Table 11, the excellent agreements discussed in the above paragraph must be considered as at least partly accidental. There can be little doubt, however, that the effects of specular reflection in the very soft x-ray region had been seriously underestimated by the author and probably by other experimenters.

Summary

The stated purpose of this experiment was to measure the intensities of the first three lines of the Lyman series of C VI and N VII. This purpose was only partly satisfied. The intensities of the N VII Lyman- α and - β lines were measured, and the Lyman- γ line was shown to be low compared to the measured continuum at 19.83 Å. For the carbon series, only the intensity of the Lyman- α line could be determined. However, the absorption data obtained during the reentry portion of the flights led to a very important explanation of why the attempted measurements of the Lyman- β and - γ lines were unsuccessful. The possible explanation of scattered, long wavelength ultraviolet light was eliminated. The relative shapes of atmospheric absorption curves indicated that if any of the stations measured a monochromatic flux, then all of the stations measured a monochromatic flux. But this was clearly inconsistent with the calculated absorption coefficient of air. This reasoning led to a consideration of the problem of specular reflection. To evaluate the importance of this effect it was necessary to make laboratory measurements of the specular reflection of x-rays from

lead stearate crystals. The laboratory data indicated that this was certainly the most likely explanation for the carbon results of this experiment and possibly for the unexplained results of several other experiments.

Shown in Table 12 are the x-ray flux values from this experiment that are considered reliable. In the third column are calculated intensities. The fourth and fifth columns contain results from earlier measurements of the solar spectrum.

TABLE 12
SUMMARY OF EXPERIMENTAL RESULTS

	<u>Present Experiment</u> August 8	<u>Experiment</u> August 11	Elwert (24)	Blake, et al. (9)	Widing (11)
C VI Lyman- α (erg/cm ² -sec)	2.9×10^{-2}	2.2×10^{-2}	3.3×10^{-2}		6×10^{-3}
N VII Lyman- α (erg/cm ² -sec)	1.8×10^{-3}		4×10^{-3}	4.5×10^{-4}	
N VII Lyman- β (erg/cm ² -sec)	5×10^{-4}			$<1.5 \times 10^{-4}$	
Continuum at 26 Å (erg/cm ² -sec-Å)	6×10^{-3}	4×10^{-3}			
Continuum at 19.83 Å (erg/cm ² -sec-Å)	5×10^{-3}				

A summary of the conclusions from this experiment are listed below:

1. There is a significant x-ray continuum from the sun at 19.83 Å and 26 Å. The intensity is about 5×10^{-3} erg/cm²-sec-Å.
2. The nitrogen VII Lyman-γ line is too weak to measure above this continuum with an instrument having 0.1 Å resolution.
3. The N VII Lyman-α to -β ratio is smaller than is predicted by theory. This result has been observed in earlier measurement of the solar spectrum and in measurements of the spectrum from a laboratory plasma.
4. The intensity of the N VII Lyman-α line is less than predicted by theory.
5. The intensity of the C VI Lyman-α line agrees very well with the theoretical prediction for $T = 1.6 \times 10^6$ °K.
6. The most probable reason for the anomalous results obtained from the stearate stations was the specular reflection of x-rays from the 30-120 Å region into the detector.

In any future experiments where crystals are used to make measurements of the solar spectrum for wavelengths above 25 Å, the effects of specular reflection must be considered. The improvements that can be obtained by different choices of filter materials are limited. The use of crystals having 2d spacings more nearly equal to the wavelengths being measured would almost certainly give a decided improvement.

LIST OF REFERENCES

1. Tousey, R., Quart. J. Roy. Astron. Soc. 5, 123 (1964).
2. Edlén, B., Z. Astrophys. 22, 30 (1943).
3. Aller, L. H., The Atmosphere of the Sun and Stars, 2nd ed., (The Ronald Press Co., New York, 1963).
4. Allen, C. W., Astrophysical Quantities, (The Athlone Press, University of London, 1955).
5. Moore, C. E., Atomic Energy Levels, Circular of the National Bureau of Standards 467, Vol. I, (U. S. Govt. Printing Office, Washington, D. C., 1952).
6. Fawcett, B. C., Gabriel, A. H., Jones, B. B., and Peacock, N. J., Proc. Phys. Soc. London 84, 257 (1964).
7. Blodgett, K. B., and Langmuir, I., Phys. Rev. 51, 964 (1937).
8. Henke, B. L., unpublished material, Pomona College, Claremont, California.
9. Blake, R. L., Chubb, T. A., Friedman, H., and Unzicker, A. E., Astrophys. J. 142, 1 (1965).
10. Argo, H. V., Bergey, J. A., Henke, B. L., and Montgomery, M. D., Trans. Am. Geophys. Union 45, 625 (1964).
11. Widing, K. G., Astrophys. J. 143, 606 (1966).
12. Johann, H. H., Z. Physik 69, 185 (1931).
13. Ditsman, S. A., Akademiiia Nauk SSSR, Izvestiia, Seriia Fizicheskai (Eng. Trans.) 24, 390 (1960).
14. Dumond, J. W. M., and Kirkpatrick, H. A., Rev. Sci. Instr. 1, 88 (1930).
15. Compton, A. H. and Allison, S. K., X-Rays in Theory and Experiment, 2nd ed., (D. Van Nostrand Co., Inc., Princeton, 1935).
16. Conner, J. P., private communication.

17. U. S. Standard Atmosphere, 1962, Prepared under sponsorship of National Aeronautics and Space Administration, United States Air Force, and United States Weather Bureau, (U. S. Govt. Printing Office, Washington, D. C., 1962).
18. Unsöld, A., Physik der Sternatmosphären, (Springer-Verlag, Berlin, 1955).
19. Shklovskii, I. S., Physics of the Solar Corona, 2nd ed., Trans. by L. A. Fenn, (Pergamon Press, London, 1965).
20. McWhirter, R. W. P., and Hearn, A. G., Proc. Phys. Soc. London 82, 641 (1963).
21. Griem, H. R., Plasma Spectroscopy, (McGraw-Hill, New York, 1964).
22. Seaton, M. J., Mon. Not. R. Astr. Soc. 119, 90 (1959).
23. Jahoda, F. C., Ribe, F. L., Sawyer, G. A., and McWhirter, R. W. P., Proceedings of the Sixth International Conference on Ionization Phenomena in Gases, Vol. 3, ed. P. Hubert and E. Cremieu-Alcan (S.E.R.M.A., Paris) p. 347.
24. Elwert, G., Proceedings of the Seventh International Space Science Symposium, Vol. 2, ed. R. L. Smith-Rose and J. W. King (North-Holland Pub. Co., Amsterdam, 1967) p. 1287.
25. Burgess, A., Astrophys. J. 139, 776 (1964).
26. Argo, H. V., Bergey, J. A., Evans, W. D., and Singer, S., unpublished material, Los Alamos Scientific Laboratory, Los Alamos, New Mexico.
27. Elwert, G., J. Geophys. Res. 66, 391 (1961).